Discrete Fiber Raman Amplifiers for Agile All-Photonic Networks

Johann Gest

Photonic Systems Group, Department of Electrical and Computer Engineering

McGill University
Montreal, Quebec, Canada
September 27, 2007

A thesis submitted to McGill University in partial fulfillment of the requirements of the degree of degree of Doctor in Philosophy

Your file Votre référence
ISBN: 978-0-494-38590-6
Our file Notre référence
ISBN: 978-0-494-38590-6

DEDICATION

To my wife, Athina.

ACKNOWLEDGEMENTS

First, I would like to thank my supervisor, Prof. Lawrence R. Chen for his continuous encouragement, help and support throughout the research work and the thesis writing. It was an amazing experience and an honour to be part of his team. Prof. Chen is the most dedicated professor I have met and he will be an inspiration to me in my professional life.

I would like to give a special word of thanks to Chris Rolston who continuously improved our working conditions.

I would also like to thank people who directly or indirectly helped me: Nikolaos Gryspolakis, Dominic Pudo, Nicolas Bélanger, Jacques Laniel, Bing Xia and Patricia Greig.

A special thank to AAPN who financed this project.

Finally, I would like to thank my wife, my parents and my brother for their encouragement and love.

TABLE OF CONTENTS

LIST OF TABLES

LIST OF FIGURES

LIST OF ABBREVIATIONS

AAPN: Agile All-Photonic Network
AOGC: all-optical gain-clamping
APA: average power analysis
ASE: amplified spontaneous emission
DCF: dispersion compensating fiber
DSF: dispersion shifted fiber
DFRA: discrete fiber Raman amplifier
DRS: double Rayleigh scattering
EDFA: Erbium doped fiber amplifier
FBG: fiber Bragg grating
FOPA: fiber optical parametric amplifier
FRA: fiber Raman amplifier
GC-DFRA: gain-clamped DFRA
HFA: hybrid fiber amplifier
HNLF: highly nonlinear fiber
O-E-O: optical-to-electronic-to-optical
RIN: relative intensity noise
RK4: fourth order Runge-Kutta
SMF: single mode fiber
SNR: signal-to-noise ratio
SOA: semiconductor optical amplifiers
SRS: stimulated Raman scattering
TDFA: Thulium-doped fiber amplifier
TDM: time division multiplexing
WDM: wavelength division multiplexing
YDFA: Ytterbium-doped fiber amplifier

ABSTRACT

This thesis is dedicated to the study of gain transients of discrete fiber Raman amplifiers and to the all-optical gain-clamping technique which is used to mitigate those transients.

First, we study the standing-wave and the traveling-wave gain-clamping techniques when applied to a single discrete fiber Raman amplifier in the context of WDM channel add and drop. We take into account the operational regime of the amplifier and the location of the surviving channel in the amplification band. We demonstrate that the gain-clamped amplifier has to be operated in a regime below the critical regime to ensure that gain-clamping will be in effect. The efficiency of gain-clamping also depends on the feedback level of the lasing signal and on the implementation.

Next, we investigate the dynamic behaviour of a single discrete fiber Raman amplifier fed by multi-channel packet traffic. Our study shows that the efficiency of the gain-clamping technique to reduce the gain transients is dependent upon the operational regime of the amplifier and the packet duration. However, we also demonstrate that gain-clamping is not required to control the gain transients as the gain variations of the unclamped amplifier are small enough to be neglected.

We then theoretically analyse the dynamic response of cascades of discrete fiber Raman amplifiers subject to WDM channel add and drop. We consider cascades of mixed unclamped and gain-clamped amplifiers, varying the number and the position of the gain-clamped amplifiers in the cascade and taking into account the location of the surviving channel and the operational regime of the amplifiers. Our results show that the location of the gain-clamped amplifiers in a mixed cascade affects the transient

characteristics and that it is possible to control the transients within tolerable limits.

Finally, we investigate the gain transients that occur in hybrid amplifiers in the presence of channel add and drop. We demonstrate that the gain-clamping technique can be used to mitigate the gain transients in hybrid amplifiers and that the surviving channel location does not influence the transient characteristics, contrary to the case of single and cascaded fiber Raman amplifiers.

ABRÉGÉ

Cette thèse est dédiée à l'étude des effets transitoires de gain dans les amplificateurs à fibre Raman ainsi qu'à la technique de contrôle de gain tout-optique qui permet d'atténuer les effets transitoires.

Nous comparons la technique de contrôle de gain par onde stationnaire à celle par onde circulatoire lorsqu'elles sont appliquées à un unique amplificateur Raman discret dans le contexte d'addition et de coupures de signaux WDM. Nous tenons compte du régime opératoire de l'amplificateur ainsi que de la localisation du signal survivant dans la bande d'amplification. Nous démontrons que l'amplificateur clampé doit être opéré dans un régime sous le régime critique afin d'assurer l'efficacité du contrôle de gain . Lorsque le contrôle de gain est effectif, son efficacité dépend du niveau de rétroaction du signal lasant.

De plus, nous investiguons aussi le comportement dynamique d'uniques amplificateurs Raman discrets lorsqu'ils sont alimentés par un trafic paquetisé à multiples longueurs d'onde. Notre étude montre que l'aptitude du contrôle de gain à réduire les effets transitoires dépend du régime opératoire et de la durée des paquets. Cependant, nous démontrons aussi que le contrôle de gain n'est pas requis pour contrôler les effets transitoires car les variations de gain de l'amplificateur non-clampé sont suffisamment petites pour être négligées.

Nous analysons théoriquement la réponse dynamique d'amplificateurs Raman discrets en cascade lorsqu'ils font face à une addition et coupure de signaux. Nous considérons des cascades mixtes qui incluent des amplificateurs clampés ou non. Nous varions le nombre et la position des amplificateurs clampés dans la cascade et nous tenons compte de la localisation du signal survivant ainsi que du régime opératoires des

amplificateurs. Nos résultats montrent que la localisation des amplificateurs clampés dans une cascade mixte affecte les caractéristiques des effets transitoires et qu'il est possible de les maintenir en deçà de limites acceptables.

Finalement, nous examinons les effets transitoires qui prennent place dans des amplificateurs hybrides soumis à l'addition et à la coupure de signaux. Nous démontrons que le contrôle de gain peut être employé afin de réduire les effets transitoires dans les amplificateurs hybrides et que la localisation du signal survivant n'influence pas leurs caractéristiques, contrairement au cas des amplificateurs Raman uniques ou en cascade.

Chapter 1: Overview and motivation

1.1 Introduction to dynamic networks and gain transients

The telecommunications domain has profoundly evolved during the last decades. As the voice traffic used to be the major kind of traffic, the telecommunications networks had to change with the arrival of the Internet. Starting from that point, the traffic of data continuously grew up and finally exceeded the voice traffic in volume. The telecommunications had to face this new reality and the introduction of optical networks permitted to increase the transmission capacity. Such networks are used for trans-oceanic and long-haul communications. As the Internet led the explosive increasing capacity demand, technologies such as Wavelength Division Multiplexing (WDM) and Time Division Multiplexing (TDM) were introduced to benefit from the entire transmission capacity of optical networks.

However, the demand will certainly grow up again with the arrival of technologies such as telemedicine or video conferencing. Dynamic optical networks offer an answer to this challenge [1-4]. They enable optical channels to be dynamically routed, switched, provisioned, protected and restored all within the fiber optic layer. A dynamic optical network provides network flexibility and eliminates the costly and bandwidth limiting optical-to-electronic-to-optical (O-E-O) conversion processes inherent in today's optical networking systems.

This project is a part of what is called the Agile All-Photonic Network (AAPN) Research Program led by Professor David V. Plant at McGill University and funded by the Natural Sciences and Engineering Research

Council of Canada. Such a network which will cumulate dynamic WDM and TDM will be agile and robust. The major characteristics of AAPN are the following [5-6]:

- rapidly reconfigurable all-optical space-switching in the core;
- agility - namely the ability to perform time domain multiplexing to dynamically allocate bandwidth to traffic flows as the demand varies;
- control and routing functionality concentrated at the edge switches that surround the photonic core.

The WDM systems require high output power and low noise figure amplifiers. In addition to high performance, the implementation of new features such as dynamic wavelength routing can lead to optical power transients. As the WDM channels can follow different paths in the network before being gathered together in a link, they can present different input powers at an amplifier input as the attenuation and gain experienced by each channel can depend on the followed path. This difference in input power will lead to gain transients.

The phenomenon of gain (or power) transients is illustrated in Fig. 1, which presents the input and output power of a signal launched in a fiber amplifier: the overshoot at the leading edge of the output signal is caused by the unsaturated gain that the signal experiences when it is first turned on. The strong power of the signal in the front depletes the pump (e. g. in Raman amplifiers) or the population inversion (e. g. in doped fiber amplifiers). As a result, the remaining signal pulse does not experience the same high gain as the leading edge of the signal. Depletion of the pump or population inversion is the strongest when the signal front reaches the output of the fiber, which produces a gain that is smaller than the steady-state saturated gain. This causes the small undershoot in the signal power.

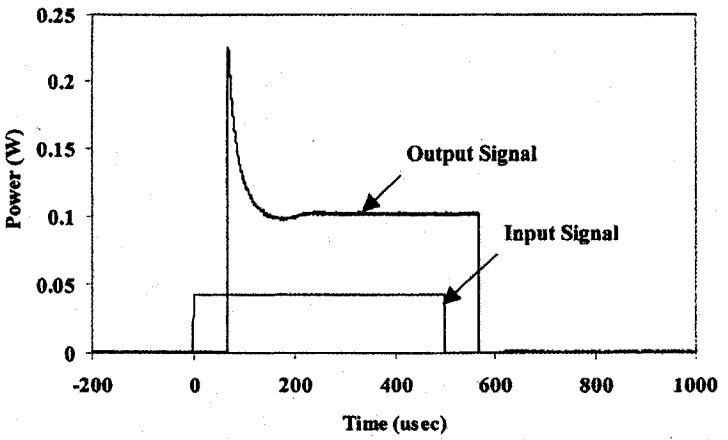

Fig. 1-1: Illustration of power transients in a fiber amplifier.

These transients also occur when the number of channels loaded in the amplifier varies. Because fiber amplifiers saturate on the basis of total power, addition or removal of channels in a multi-access wavelength-routed network will tend to perturb channels at other wavelengths, which share all or part of the route. These signal transients can compromise the flexibility of network architecture and impact system performance.

The quality of surviving channels can be degraded through four distinct mechanisms when the channel-loading conditions change. First, optical nonlinear effects in fiber will occur if the power excursions of the surviving channels are large enough due to the cut or removal of signal channels. Second, when channels are being added, the optical power can decrease during the transient period, which in turn can lead to eye-closure and degradation of bit-error rate. Third, optical signal-to-noise ratio (SNR) can deteriorate due to the change in gain spectrum during the transience. Finally, as the power at the receiver fluctuates, the threshold of the receiver must continuously be optimized at a very high speed - a potential problem for certain receivers.

1.2 Optical amplifiers

1.2.1 Erbium doped fiber amplifiers

An Erbium-Doped Fiber Amplifier (EDFA) consists of a pump and a length of silica fiber whose core is doped with ionized atoms, Er^{3+}, of the rare earth element Erbium. This fiber is pumped using a laser, typically at a wavelength of 980 nm or 1480 nm. This laser excites Er^{3+} atoms which amplify signals of around 1550 nm by stimulated emission. Although doped-fiber amplifiers were studied as early as the sixties, their use became practical fifteen years ago, after the techniques for fabrication and characterization of low-loss doped fibers were perfected and after the development of 980 nm and 1480 nm semiconductor pump lasers. EDFAs cumulate many advantages: low electrical consumption, high gain, large signal bandwidth, the fact that it is an all-fiber device (making it independent to polarization and decreasing the insertion losses), low crosstalk, low noise and a compact component.

The dynamics of the EDFAs were extensively studied in hundreds of papers. It was shown that gain dynamics have long saturation and recovery time constants (~200 μs- 3 ms) [7]. Thus, EDFAs are immune to patterning and crosstalk effects at typically considered data rates. One potential issue, however, is the change of the number of channels loaded in the amplifier. For example, when one, four or seven out of eight channels are cut, the surviving channels present large power excursions in less than 10 μs [8]. In order to limit power transients, three techniques are used: pump control, signal control and gain-clamping. First, the pump control method consists in adjusting the pump power during the transient in order to eliminate the signal power variations [9-11]. This technique is very fast (the response time can be as low as 0.5 μs) and it reduces power

transients from 3 dB to 0.3 dB [10]. Second, the signal control represents another dynamic technique which minimizes the transient response. This method uses a control signal in addition to the channels loaded in the amplifier; the power of this control signal is adjusted to compensate for the addition or removal of channels [12]. Finally, a passive technique called gain-clamping can also be used. The principle of the operation consists of a lasing signal generated at a wavelength outside of the channels bandwidth. In a laser, the gain is equal to the losses of the laser/amplifier cavity and since the losses are fixed, the gain is clamped; thereby a lasing signal clamps the gain of the entire amplifier. Optical gain-clamping can be achieved in two different ways: with a feedback loop in a traveling-wave configuration [13-15] or in a standing-wave configuration using fiber Bragg gratings (FBGs) [16-19].

Generally, in-line amplifiers are used in cascade in order to reduce the number of costly repeaters. However, the speed of power transients is dependent upon the number of amplifiers in the route. The time varying output of the first amplifier appears as an input to the second one, which has time-dependant gain and therefore the output power of the second amplifier changes at a faster rate. Therefore, even if power transients are generally thought to have slow gain dynamics, which is a key advantage, it is not the case for a cascaded configuration. Gain transients in cascaded EDFAs have been reported in [20-24]. Two different techniques are usually used to mitigate such power transients. The first one consists in using gain-clamping or pump-control at each amplifier of the cascade [22-23]. The second one is to optically gain-clamp the first amplifier and to let the lasing signal propagate to the other amplifiers as a control signal [24].

1.2.2 Fiber Raman amplifiers

As the demand for capacity on the Internet keeps growing, the EDFA-based transmission technology may eventually hit the upper limit of transmission capacity. Fiber Raman Amplifiers (FRAs) are studied as a solution for increasing the spectral efficiency and bandwidth. A FRA uses stimulated Raman scattering (SRS) occurring in silica fibers when an intense pump beam propagates through it. The Stokes shift for silica fibers is approximately 13 THz with a 3 dB bandwidth of about 5 THz. Broader gain spectra may be obtained by the use of multi-wavelength pump sources, a technique applicable only for Raman amplifiers. Even though the Raman effect in silica fiber has been known for a long time, it was only recently with the arrival of high power laser diodes that practical FRAs were built. The use of FRAs permitted to expand the transmission capacity of telecommunications networks over very long transmission length and to achieve high bit rate [25-30].

Two types of FRAs currently exist (Fig 1-2): the distributed FRA, in which the amplification occurs gradually and directly in the transmission fiber, and the discrete (or lumped) FRA (DFRA), which provides gain at a localized point of the transmission fiber. The principal advantages of FRAs over EDFAs are the flexibility to provide gain bandwidths not usually available in doped-fiber amplifiers with the provision of suitable pump sources, the possibility to have wider amplification bandwidth by using multiple pumps at different wavelengths and the fact that the amplification can be achieved in any silica fiber. Particular attention must be given to the design of the FRAs because of the non-linear interactions between the pumps and the signals [31] and of course, because FRAs are also sensitive to power transients.

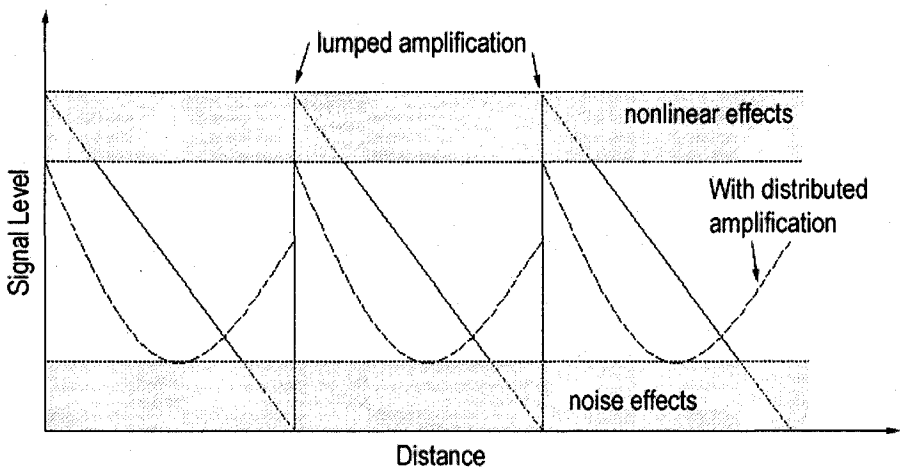

Fig. 1-2: Operational modes of a FRA.

Contrary to EDFAs for which the gain transients have been extensively studied, the gain transients that occur in both discrete and distributed FRAs are less known. This thesis concentrates on the theory and the gain transients of FRAs.

1.3 Motivation and objectives

FRAs will probably be used in the new long-haul and ultralong-haul optical telecommunication networks. Dynamic networks will not be exempt from this trend. However, before implementing this new technology in a dynamic network, it is essential to know the dynamic behaviour of a FRA. The prior art on the dynamics of FRAs is incomplete and often does not reflect reality as previous studies usually focus on only a small number of channels.

Our main objective is to determine whether DFRAs can be deployed in dynamic networks such as AAPN. For this reason, we propose to study DFRAs in a real WDM situation and in the worst possible case of transience. We study all-optical gain-clamping (AOGC) as a passive

technique to determine if this technique is efficient in mitigating the gain transients occurring in DFRAs. We also consider the case of cascaded DFRAs and look at the impact the cascade has on the gain transients. Finally, we consider the association of a DFRA and an EDFA (denoted as a hybrid amplifier) in order to determine if DFRAs can be deployed in systems that already contain EDFAs.

1.4 Contributions of the thesis

The contributions of this work are the following:

- study of gain transients in DFRAs in a real WDM environment and in the worst possible case of transient;
- study of the impact of the surviving channel location on the gain transient characteristics of DFRAs;
- comparison of the standing-wave vs. traveling wave configurations for the gain-clamped DFRAs;
- statistical study of DFRAs subject to packet-like traffic variations;
- study of cascaded DFRAs in the worst possible case;
- study of the gain transients of hybrid amplifiers.

This thesis has resulted in the following peer-reviewed articles and conference proceedings:

J. Gest and L. R. Chen, "Comparison of two all-optical gain-clamping techniques for discrete fiber Raman amplifiers," *Queen's University 22nd Biennial Symposium on Communications*, pp. 51-53, 2004.

J. Gest and L. R. Chen, "Performance analysis of all-optical gain-clamped discrete fiber Raman amplifiers," *Lasers and Electro-Optics Society Annual Meeting*, vol. 2, no. 7-11, pp. 925-926, 2004.

J. Gest and L. R. Chen, "Analysis of gain transients in cascades of discrete fiber Raman amplifiers," *Photonics North*, paper 5970B-72, 2005.

J. Gest and L. R. Chen, "Dynamic response of discrete fiber Raman amplifiers to multi-channel randomly variable packet traffic," *Progress in Electromagnetics Research Symposium* (PIERS'07), 1P3b, 2007.

J. Gest and L. R. Chen, "Impact of the all-optical gain-clamping technique on the transience characteristics of cascaded discrete fiber Raman amplifiers," *Optics Communications*, vol. 273, no. 1, pp. 138-148, 2007.

J. Gest and L. R. Chen, "Dynamic gain variation in discrete fiber Raman amplifiers subject to multi-channel packet traffic," submitted to *Optics Communications*, April 2007.

J. Gest and L. R. Chen, "Analysis of gain transients in hybrid Raman/Erbium doped fiber amplifiers," to be submitted.

The remainder of this thesis is organized as follows. In Chapter 2, a background of the physical processes involved in FRAs and of the gain-clamping techniques are given. Chapters 3 and 4 concentrate on single DFRAs. In Chapter 3, the efficiency of the AOGC is analysed in the context of the addition and cut of WDM channels. In Chapter 4, we investigate the gain transients that occur in single DFRAs subject to packet-like traffic variations. Chapters 5 and 6 deal with gain transients in multiple amplifiers subject to the addition and cut of WDM channels. In Chapter 5, we analyse the gain transients that occur in cascaded DFRAs. The dynamic behaviour of hybrid amplifiers (DFRA / EDFA) is investigated in Chapter 6. In Chapter 7, a summary is given and the future work is outlined.

Chapter 2: Fiber Raman amplifiers

In this chapter, we introduce the Raman scattering phenomenon responsible for Raman amplification. We also present the various characteristics of FRAs including their advantages over EDFAs. Furthermore, we discuss the gain transients that occur in FRAs and we introduce the different techniques used to mitigate them. Finally, we present the mathematical equations governing the amplification in a FRA and two numerical techniques used to simulate the propagation of signals.

2.1 Raman amplification

2.1.1 Spontaneous Raman effect

When light is scattered from an atom or molecule, photons are either elastically scattered (Rayleigh scattering) or inelastically scattered (Raman scattering or effect). Figure 2-1 presents the three possible scattering mechanisms (Brillouin scattering is not considered).

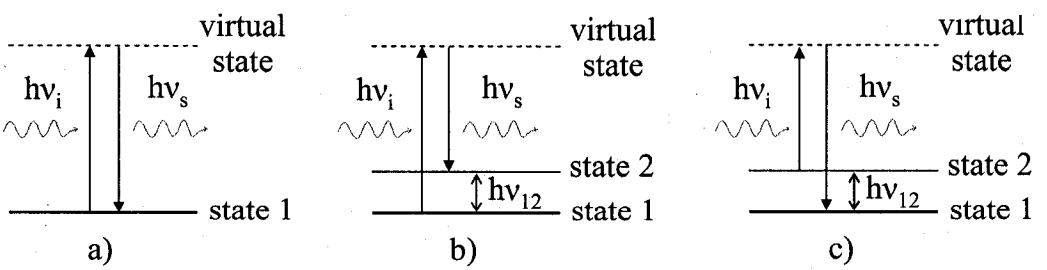

Fig. 2-1: Energy levels and photon scattering mechanisms.

Figure 2-1 a) illustrates the case of the Rayleigh scattering in which no energy is exchanged between the atom and the incident photon. The atom absorbs the incident photon, reaches the virtual state and then emits a photon of same energy as the incident photon. In Fig. 2-1 b), an atom (or molecule) in a certain vibrational, rotational or electronic state, say state 1, absorbs a photon with energy $h\nu_i$. The atom raises to the virtual state and undergoes immediately a transition of energy $h\nu_s$, which brings the atom to the excited state, say state 2. The atom has now an energy of $h\nu_{12}$ greater than that of the atom before absorbing the incident photon. $h\nu_{12}$ corresponds to the difference of energy between the incident photon and the emitted photon. An energy transition in which the emitted photon has lower energy than the incident photon is called a Stokes transition. Figure 2-1 c) presents the scattering mechanism when the atom is initially in the excited state (state 2). By absorbing the incident photon of energy $h\nu_i$, the atom reaches the virtual energy state. After emitting a photon of energy $h\nu_s$, the atom comes back to the ground state (state 1). An energy transition in which the emitted photon has higher energy than the incident photon is called an anti-Stokes transition. Both of these phenomena are called Raman scattering. Even if the response time of the Raman scattering is fast (on the order of 10 fs), this phenomenon enables vibrational modes of the material, known as the optical phonons. In crystals, only specific phonons are allowed due to the underlying periodic structure, thus Raman scattering can only appear at certain frequencies. For amorphous materials like glasses, more vibrational staes are supported and thereby the discrete spectral lines are not discrete anymore.

The Raman effect was first reported by Chandrasekhara Vankata Raman in 1928, who later received the Nobel Prize in 1930 for his work on the scattering of light.

2.1.2 Stimulated Raman scattering

Raman amplification is based on the SRS phenomenon, presented in Fig. 2-2. A 'signal' photon of energy $h\nu_s$ induces the inelastic scattering of a 'pump' photon of energy $h\nu_p$ in an optical medium in the nonlinear regime. As a result, another 'signal' photon of energy $h\nu_s$ is produced, in addition to an optical phonon.

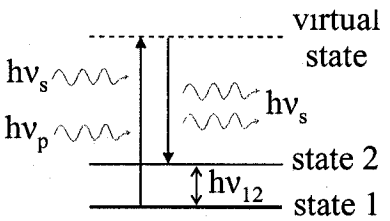

Fig. 2-2: Stimulated Raman scattering.

The Stokes shift for silica fibers is approximately 13 THz with a 3 dB bandwidth of about 5 THz as presented in Fig. 2-3. We notice that the anti-Stokes transition is neglected in silica fibers as the lifetime of the molecules in the excited state (state 2) is so short that the probability of having a 'pump' photon and a 'signal' photon encountering a phonon is almost nil.

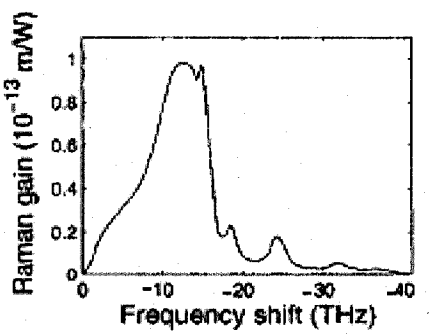

Fig. 2-3: Typical Raman gain spectrum in a silica fiber.

Even if Raman amplification can be achieved in any silica fibers, one prefers fibers presenting a high Raman coefficient gain as they require less pump power along with smaller fiber lengths. The fibers usually used for Raman amplification include dispersion compensating fibers (DCF), dispersion shifted fibers (DSF), germanium-doped fibers and highly nonlinear fibers (HNLF). Figure 2-4 a) presents the Raman gain profile for three fibers: Single Mode Fiber (SMF), DSF and DCF. The SMF has the lowest Raman gain coefficient as this fiber presents the least dopant in the core with respect to the other fibers. As the dopant concentration is increased in the core, the Raman gain coefficient increases. However, using Fig. 2-4 b) that presents the normalized Raman gain profile for the same fibers, we notice that the shape of the Raman gain vs. frequency is not affected by the dopant.

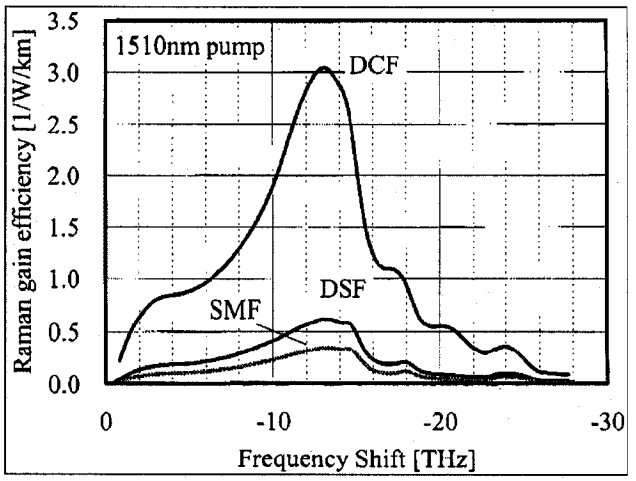

a

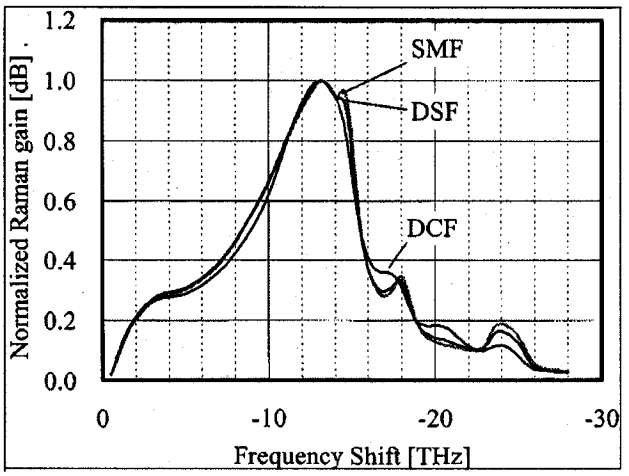

b

Fig. 2-4: Raman gain spectra (a) and normalized Raman gain spectra (b) for three fibers [32].

2.2 Fiber Raman amplifiers

A FRA is a simple means to amplify optical signals using SRS. Figure 2-5 presents a simple schematic of a FRA. The pump and the signal to be amplified are coupled into the fiber using a WDM coupler. As the pump and the signal propagate along the fiber, the pump power is transferred to the signal through SRS. At the end of the FRA, a WDM coupler separates the amplified signal from the depleted pump.

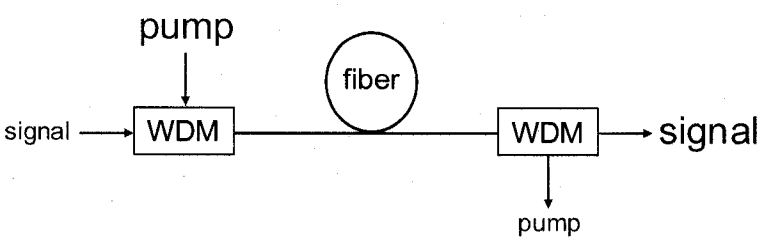

Fig. 2-5: Schematic of a FRA.

The principal advantages of FRAs over EDFAs are the following:

- the flexibility to provide gain bandwidths not usually available in doped-fiber amplifiers with the provision of suitable pump sources;
- the possibility to have wider amplification bandwidth by using multiple pumps at different wavelengths;
- the possibility to flatten the gain without the use of an external bandpass filter when multiple pumps are used;
- the possibility to achieve the amplification in any silica fiber;
- the possibility for lower noise; and
- the possibility for distributed amplification directly into the transmission fiber.

As a result, FRAs offer the possibility to open new telecommunications wavelength windows, as for example in the ultra-long wavelength band (1600 nm to 1670 nm) as in [32]. By combining multiple pumps at different wavelengths, amplification bandwidths of 100 nm and more can be easily achieved [33-36]. However, FRAs are more complex to design than EDFAs and particular attention must be given to nonlinear interactions between the pumps and the signals.

As presented in section 1.2.2, FRAs also present the advantage of two operational modes: distributed and discrete (or lumped). The distributed FRAs present better noise performance but the pump power is more

severely affected by the code format [37]. On the other hand, DFRAs are more flexible in their use (pre-amplifier, in-line amplifier or booster amplifier).

Even if FRAs can be co- or counter-pumped, the co-pumped scheme is rarely used. The Raman gain coefficient has the drawback of a strong polarization dependence. In fact, the Raman gain coefficient can be up to 10 times higher when the signal and pump polarization states are parallel rather than perpendicular in the case of a co-pumped FRA [38]. Counter-propagating the pump in a FRA reduces the correlation between the states of polarization of the pumps and signals and the Raman gain coefficient becomes insensitive to polarization, as illustrated in Fig. 2-6 [39].

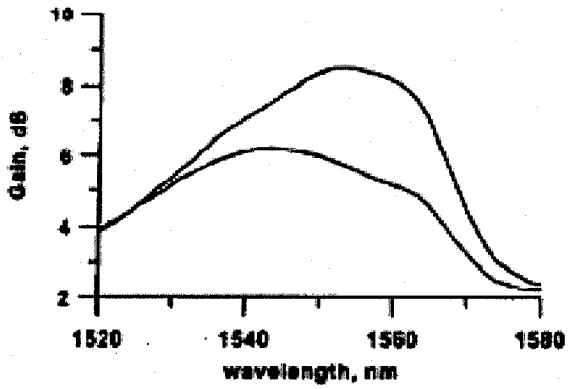

a

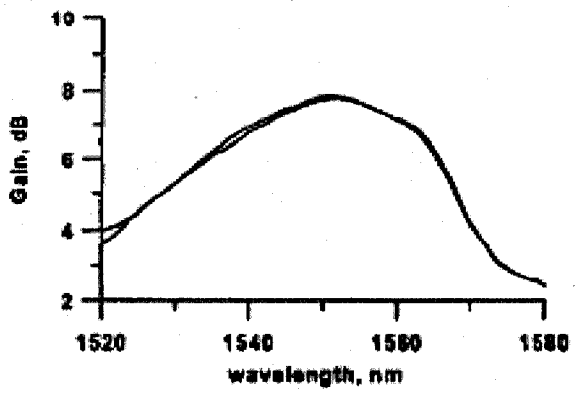

b

Fig. 2-6: Polarization dependence of the Raman gain in DCF for forward propagating pump (a) and backward propagating pump (b). The two curves represent orthogonal pump polarizations [39].

There are four primary sources of noise in Raman amplifiers. The first is the usual amplified spontaneous emission (ASE). In FRAs, signal–ASE beating noise dominates over ASE–ASE beating noise. Fortunately, Raman amplifiers have an inherently low noise from signal–ASE beating. However, when the pump power is high, the backward ASE is reflected in the other direction and experiences gain, increasing the noise. In distributed FRAs with high gains, Rayleigh backscattering increases the signal–ASE beating and can limit the noise performance improvement compared to EDFAs [40]. Concerning DFRAs, noise figures as low as 4.2 dB have been reported [41].

The second noise source is the double Rayleigh scattering (DRS). The ASE traveling in the backward direction is reflected in the forward direction by DRS and experiences gain due to SRS. It results in the degradation of the SNR due to interference between the signal itself and the double Rayleigh scattered signal [42]. As both signals occupy the same spectral region, DRS cannot be filtered. One solution consists in using multiple stages of amplification with isolators between them. For example, a 30-dB discrete Raman amplifier has been demonstrated with two stages of amplification and a noise figure less than 5.5 dB [43].

The third source of noise arises from the short upper-state lifetime of Raman scattering process. Because of this virtually instantaneous response time, pump power fluctuations are transferred to the signal power. This, in turn, results in the deterioration of the relative intensity noise (RIN) on the signals compared to the RIN on the pumps sources. The usual way of avoiding this coupling is to counterpropagate the pumps with respect to the signals. Another way to reduce the RIN on signals uses a design based on counterpropagating Fabry–Pérot laser diodes instead of grating-stabilized laser diodes [44].

Finally, the last source of noise arises from a phonon-stimulated optical noise created when the wavelength of the signals to be amplified is close to pump wavelengths. An increase in noise figure of up to 3 dB has been reported for signals spectrally located close to the pump wavelength [45-46].

2.3 Gain transients and gain-control techniques

2.3.1 Gain transients

In 2001, for the first time, Chen *et al.* observed power transients in FRAs comparable to those in EDFAs [47]. Their simple set-up was a length of DCF and a 1454.7 nm pump source. Then a modulated signal located at 1545.3 nm was launched into the counter-pumped FRA. The signal power was large enough to saturate the FRA, enabling the observation of power transients. They also verified that the observed transient was in agreement with the theoretical model. Figure 2-7 a) presents the measured signal power (i) in time at the output of the DFRA and the input signal power (ii). The measured output power is in very good agreement with the simulated output power [Fig. 2-7 (b)].

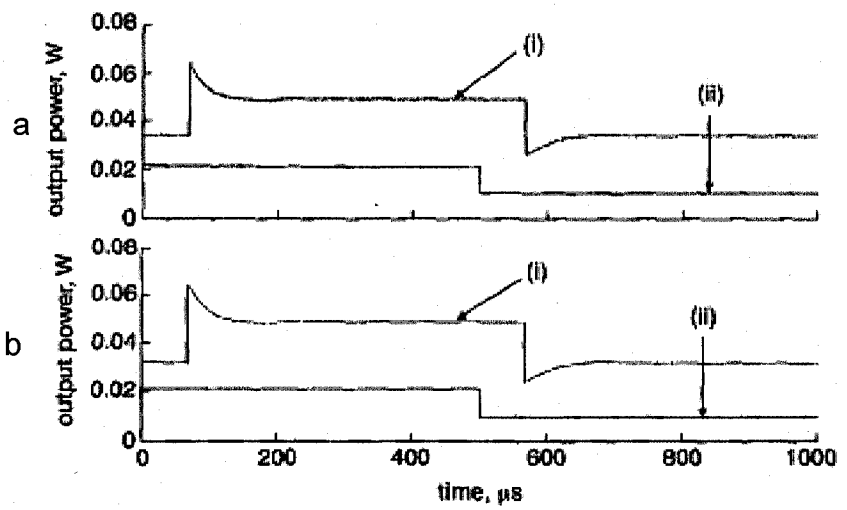

Fig. 2-7: Measured (a) and simulated (b) Raman transient effect with 50% amplitude modulation on input signal to simulate partial channel addition and drop (i-output, ii-input ×10) [47].

In [48], Wang *et al.* studied the gain transients occurring in FRAs as a function of operating parameters such as signal input power, fiber type and surviving signal wavelength. They demonstrated that co-pumped

FRAs present stronger gain transients than counter-pumped FRAs, which is consistent with the greater pump depletion effect in the co-pumping case.

Tong *et al.* also investigated the transient response to slowly varying input power waveforms in a counter-pumped FRA [49]. They concluded that in a multi-channel case, a gradually changed input waveform can eliminate the abrupt power fluctuation due to instantaneous signal-to-signal Raman interactions.

2.3.2 Gain-control techniques

In order to mitigate the power transients that occur in EDFAs, different mitigation techniques have been developed. These techniques, which can be separated in two groups, have also been successfully applied to FRAs. In this section, we first look at the active gain control technique, i.e. the pump control, and we then consider the passive all-optical gain-clamping (AOGC) technique.

2.3.2.1 Pump control

The pump control technique consists in adjusting the pump power launched into the FRA in order to ensure that the signal gain is constant in time. The pump control is much more difficult to implement for FRAs compared to EDFAs because of the nonlinear pump-to-pump, pump-to-signal and signal-to-signal interactions, especially for multi-pumped schemes. The simplest way to achieve the pump control is to select one of the signals to be amplified as a probe channel and to adjust the pump power as a function of the time evolution of this probe signal. The probe signal power is measured by a power detector and converted into an electrical signal. The electrical probe signal is then sent to the pump

controller which adjusts the pump power, following a certain algorithm. As a FRA saturates on a total input power basis and as nonlinear interactions govern the FRA behaviour, a change in a single signal power at the input of FRA affects the gain of all signals at the output of the FRA. If the gain of the probe signal increases (or decreases), the pump controller decreases (or increases) the amount of pump power launched into the FRA.

The pump control was applied to FRA for the first time by Chen *et al.* in 2001 [50]. Figure 2-8 presents the experimental set-up built to control the gain transients. Channels 1 to 4 are modulated to simulate addition and drop operations and channels 5 to 8 act as surviving channels.

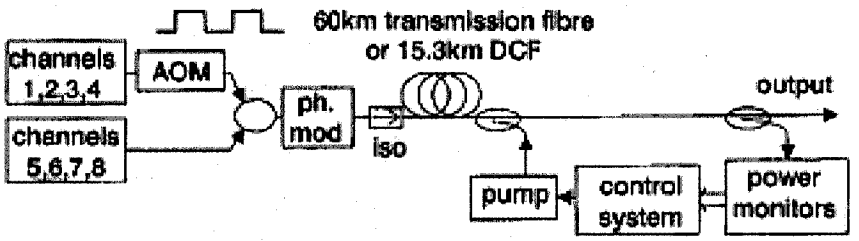

Fig. 2-8: Experimental set-up to observe and control Raman transient effects [50].

The control circuit was implemented to vary the counter-directional pump power and the control signal was derived either from the surviving channel output power, or from the both the surviving and total output power. When the control was off, Raman gain fluctuations on the surviving channels ranged from 0.35 to 1.2 dB as the drop/total ratios ranged from 4/8 to 20/24 in the distributed FRA. On the other hand, the use of the control algorithm kept gain fluctuations on the surviving channels constant to within ± 0.06 dB. Figure 2-9 a) presents the gain variation in time of a surviving channel when the gain control is off (i) and on (ii); Fig. 2-9 b) shows the corresponding pump power fluctuation when the gain control is on.

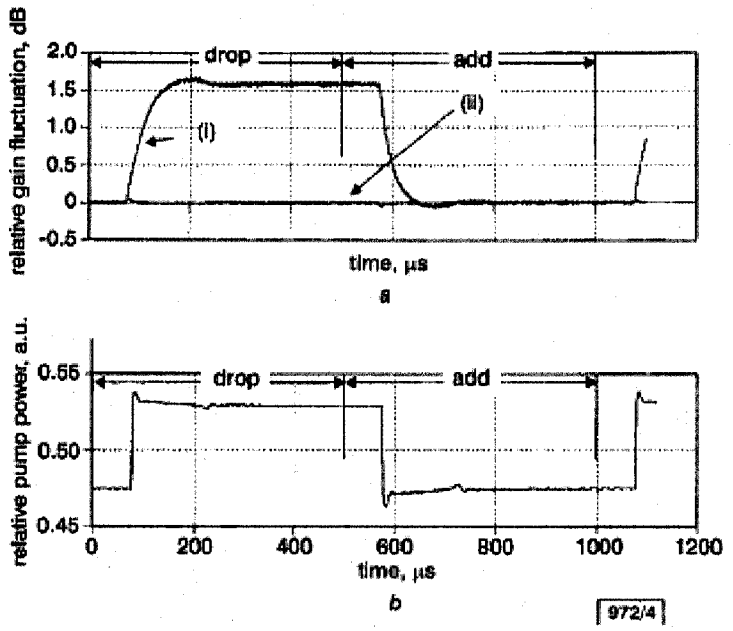

Fig. 2-9: Signal gain fluctuation in time (a) and corresponding pump power waveform generated by control circuit (b) [50].

The key point of this control technique lies in the control circuit and several studies have concentrated on improving the technique for both forward- and backward-pumped FRAs [51-55]. Pump control has recently been demonstrated for multi-pumped FRAs [56].

2.3.2.2 All-optical gain-clamping

The second gain control technique used to mitigate gain transients in FRAs is the passive AOGC. The AOGC consists in introducing a lasing signal generated inside the amplifier at a wavelength outside the channel bandwidth. This lasing signal then acts as a feedback control signal. When the power of the signals to be amplified varies at the FRA input, the power of the lasing signal adjusts along the FRA so that the gain of the signals remains unchanged. AOGC presents the advantage of not requiring expensive optoelectronic devices and its response time is not limited by the electronic circuits. However, the response time of the AOGC depends on the length of the lasing signal cavity as this response time is directly

related to the time it takes for the lasing signal to re-establish its steady-state. Thus, reducing the length of the DFRA enables the reduction of the response time.

The AOGC can be realized in two different configurations: the traveling-wave and the standing-wave configurations.

2.3.2.2.1 Traveling-wave AOGC

The traveling-wave configuration consists in building the lasing signal with a ring cavity [Fig. 2-10]. An optical coupler extracts a small amount of power out of the amplifier which propagates through the loop and is re-introduced into the amplifier by the second optical coupler. Usually, a bandpass filter is added in the loop to isolate the lasing signal wavelength and to reduce the amount of noise re-introduced into the amplifier. As in a laser, the gain is equal to the losses and since the losses are fixed, the gain is clamped. This lasing signal makes the amplifier gain-clamped. Adding an optical attenuator in the ring allows for the variation of the losses of the ring cavity, thereby adjusting the degree of gain-clamping for the amplifier. The losses of the ring are equal to the losses of all of its components: optical couplers, fiber, bandpass filter and optical attenuator.

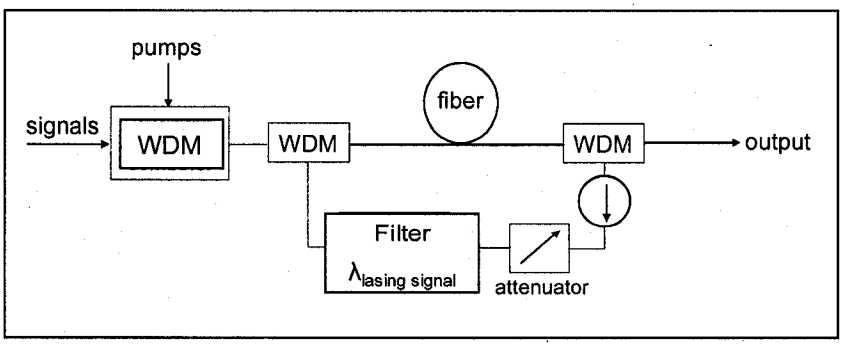

Fig. 2-10: Travelling-wave AOGC configuration.

This configuration presents two major advantages: it is possible to vary the wavelength of the lasing signal by using an adjustable bandpass filter and to vary the losses of the ring cavity. However, it also presents drawbacks. Optical couplers extracts part of the WDM signals power which results in a less efficient amplifier. As the bandpass filter cannot completely eliminate the noise circulating in the ring, this noise is re-injected into the amplifier and amplified. It results in a degradation of the noise performance of this configuration in comparison to others.

The first application of the traveling-wave AOGC was to realize a static study of gain-clamped FRAs, i.e. the variation of the signal gain vs. the signal input power [57-58]. These studies demonstrate the efficiency of the traveling-wave AOGC to maintain the signal gain constant over a certain range of input power with the drawback of degraded noise performance in comparison to an unclamped amplifier. This gain-clamping configuration was also applied to mitigate the power transients in FRA [59-60]. In particular, in [59], Karásek *et al.* investigated theoretically and experimentally the gain transients in a lumped FRA in the context of channels addition and drop. They noticed that the amplitude of the remaining power transients that occured when channels were added and dropped is about 8 times lower than the steady-state power excursions of the unclamped amplifier.

2.3.2.2.2 Standing-wave AOGC

The standing-wave AOGC configuration uses a pair of FBGs to create the lasing signal cavity [Fig. 2-11]. The noise corresponding to the reflection wavelength of the FBGs is reflected back and forth by the FBGs and amplified each time it enters the FRA until this signal lases. In this configuration, the losses of the lasing cavity are fixed largely by the FBG reflection coefficients. As for the traveling-wave configuration, it is possible

to adjust the wavelength of the lasing signal and the losses of the cavity by straining or compressing the FBGs. This configuration presents the advantage of neither affecting the WDM signals, nor increasing the noise.

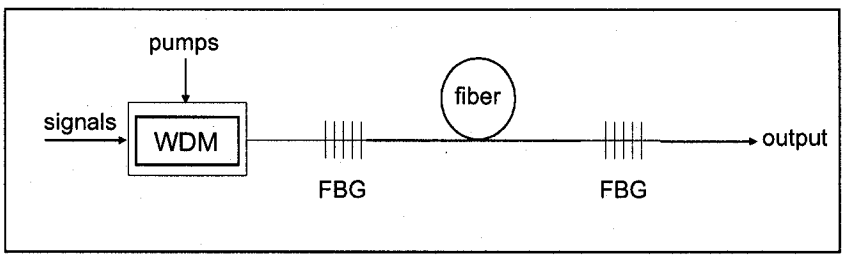

Fig. 2-11: Standing-wave AOGC configuration.

Only one article focuses on the standing-wave AOGC configuration [61]. The authors carry out a static study of a standing-wave AOGC DFRA. A stable signal gain is obtained for a signal input range of 30 dB. The gain variation is kept below 0.17 dB and the noise figure is flattened at the same time. Up to now, no studies on the mitigation of gain transients by standing-wave AOGC have been reported.

A major drawback of gain-clamping is the degradation of the noise figure [58]. The noise figure relates the amount of ASE noise that is added to the signal relative to amount of gain. When the amplifier is gain-clamped, the power of the Raman ASE is considerably increased. At the same time, the gain remains roughly the same as the unclamped case, which results in a higher noise figure. The problems usually encountered in lasers, such as the intermodal beat noise in the case of multiple longitudinal modes lasers, are also to be considered in the case of gain-clamped amplifiers. One problem with multiple longitudinal modes in continuous wave lasers is the modes can beat together producing noise at the beat frequencies. Noise can also be produced by a phenomenon called "mode-locking." Although the longitudinal modes of a laser oscillator normally oscillate independently, their phases can be locked together by an external mechanism. For example, one such external mechanism could be

absorption centers in the fiber in the region in which the light propagates. When the mode phases are locked together, the mode amplitudes combine to generate pulses in the output which appear as noise in a multiple longitudinal mode laser.

2.3.3 Gain transients in cascades of DFRAs

The phenomenon of gain transients has also been studied in cascaded FRAs. The first study was undertaken by Zhang *et al.* in 2001 [62]. They demonstrated that both the power excursions and recovery times increase dramatically when several FRAs are cascaded. In order to reduce the gain transients, they applied the pump control to each amplifier of the cascade of 8 DFRAs and they succeed in keeping gain transients of the surviving channel below 0.5 dB. In [63] and [64], Bolognini and Di Pasquale applied the traveling-wave AOGC to reduce the gain transients following the addition and drop of 15 channels amongst 16 in a cascade of ten DFRAs. The use of AOGC enables to reduce the power excursion following the drop of 15 channels at the output of the cascade from 13.8 dB for a cascade of 10 unclamped cascades to 8 dB when each amplifier of the cascade is gain-clamped.

In [65], Karásek *et al.* used a different technique to control the gain transients in a cascade of three DFRAs. Only the first DFRA of the cascade is gain controlled with the traveling-wave AOGC and the lasing signal is allowed to propagate through the next two DFRAs. Two WDM signals are amplified by the cascade of which one is modulated to simulate the addition and drop operations. It was found that when sufficient lasing in the first amplifier of the gain-controlled cascade is allowed, steady-state power fluctuations observed in an unclamped cascade are eliminated completely. The amplitude of the remaining power

transients that occur when channels are switched off is about eight times lower than the steady-state power excursion of the unclamped cascade.

2.4 Numerical models

In this section, we present numerical models that govern the propagation and the amplification of optical signals in time in a FRA. We also introduce two numerical methods used to solve the propagation equations.

2.4.1 Equations

2.4.1.1 Complete model

In order to analyze accurately the dynamic behaviour of a FRA, we need a model which can accommodate multiple pumps, WDM signals, ASE noise and lasing signals. For simplicity, the model assumes that the pumps, the WDM signals and the lasing signals have an infinitesimally narrow bandwidth, while the ASE noise signals have a defined bandwidth or resolution $\Delta\nu$.

The complete model includes all physical effects assumed to be important. This model takes into account the following effects:

- Rayleigh scattering including multiple reflections;
- SRS (with a fiber dependent Raman coefficient);
- spontaneous Raman emission and its temperature dependence;
- amplification of the above;
- time dependence;
- wavelength dependent loss of the fiber;

- arbitrary interactions between unlimited number of pumps and signals independently of their direction (pump-to-pump, pump-to-signal and signal-to-signal interactions);
- forward or backward propagating pumps;
- gain-clamping using Bragg gratings (standing-wave AOGC) or feedback loop (traveling-wave), when applicable.

The effects excluded are the anti-Stokes generation, the polarization effects (concerning WDM signals) and the nonlinear index effects.

Equation (2.1) represents the propagation equation of the backward and forward signals $P^{+}(z,t,\nu)$ and $P^{-}(z,t,\nu)$ describing their evolution in time and space [66]:

$$\begin{aligned}
&\frac{\partial P^{\pm}(z,t,\nu)}{\partial z} \mp \frac{1}{\upsilon_g(\nu)} \frac{\partial P^{\pm}(z,t,\nu)}{\partial t} \\
&= \mp\alpha(\nu)P^{\pm}(z,t,\nu) \pm \gamma(\nu)P^{\mp}(z,t,\nu) \\
&\pm P^{\pm}(z,t,\nu)\sum_{\mu>\nu}\frac{g_R(\nu-\mu)}{K_{eff}A_{eff}}[P^{\pm}(z,t,\mu)+P^{\mp}(z,t,\mu)] \\
&\mp P^{\pm}(z,t,\nu)\sum_{\mu<\nu}\frac{\nu}{\mu}\frac{g_R(\mu-\nu)}{K_{eff}A_{eff}}\times[P^{\pm}(z,t,\mu)+P^{\mp}(z,t,\mu)] \\
&\pm h\nu\sum_{\mu>\nu}\frac{g_R(\nu-\mu)}{K_{eff}A_{eff}}[P^{\pm}(z,t,\mu)+P^{\mp}(z,t,\mu)][1+\frac{1}{e^{h(\mu-\nu)/kT}-1}]\Delta\nu \\
&\mp 2h\nu P^{\pm}(z,t,\mu)\sum_{\mu<\nu}\frac{g_R(\mu-\nu)}{K_{eff}A_{eff}}[1+\frac{1}{e^{h(\nu-\mu)/kT}-1}]\Delta\mu
\end{aligned}$$

Equation 2.1

where $u_g(\nu)$ is the group velocity, $\alpha(\nu)$ is the fiber loss coefficient, $\gamma(\nu)$ is the Rayleigh scattering coefficient, K_{eff} is the polarization factor for noise signals, A_{eff} is the fiber effective area, g_R is the Raman gain coefficient of the fiber, h is Planck's constant, k is Boltzman's constant and T is the temperature. The Rayleigh backscattering coefficient is assumed constant

for all wavelengths and equal to 1×10^{-7} m^{-1}. The temperature is set to 300 °K. Appendix A presents the loss coefficient $\alpha(v)$ and the effective Raman gain coefficient of the HNLF used in this thesis.

When the amplifier is gain-clamped, specific boundary conditions apply depending on the AOGC type. Equation (2.2) presents the boundary conditions on the lasing signal when the traveling-wave AOGC is utilized.

$$P^{+}(0,t,v) = F \times P^{+}(L,t,v)$$
$$P^{-}(L,t,v) = 0 \qquad \textbf{Equation 2.2}$$

where (1-F) represents the total losses (F is denoted as the feedback level) in the resonator ring. If the standing wave AOGC is applied to the amplifier, Eq. (2.3) describes the boundary conditions of the lasing signal.

$$P^{+}(0,t,v) = R_1 \times P^{-}(0,t,v)$$
$$P^{-}(L,t,v) = R_2 \times P^{+}(L,t,v) \qquad \textbf{Equation 2.3}$$

where R_1 and R_2 are the reflection coefficients of the Bragg gratings at $z = 0$ and $z = L$, respectively.

The two configurations of gain-clamping can be designed to have the same feedback level for the lasing signal and, in this case, we have the following relation:

$$F = \sqrt{R_1 \times R_2} \qquad \textbf{Equation 2.4}$$

2.4.1.2 Simplified model

The model described in Eq. (2.1) describes the propagation in time and the amplification of all signals including the ASE signals. However, taking

into account the noise requires extensive computation times. Usually, a simpler model is adopted by researchers to simulate the dynamics of a FRA. Equation (2.5) presents the simpler model in which all phenomena participating to the creation or amplification of noise have been excluded.

$$\frac{\partial P^{\pm}(z,t,\nu)}{\partial z} \mp \frac{1}{\upsilon_g(\nu)} \frac{\partial P^{\pm}(z,t,\nu)}{\partial t}$$

$$= \mp\alpha(\nu)P^{\pm}(z,t,\nu)$$

$$\pm P^{\pm}(z,t,\nu)\sum_{\mu>\nu} \frac{g_R(\nu-\mu)}{K_{eff}A_{eff}}[P^{\pm}(z,t,\mu)+P^{\mp}(z,t,\mu)] \qquad \textbf{Equation 2.5}$$

$$\mp P^{\pm}(z,t,\nu)\sum_{\mu<\nu} \frac{\nu}{\mu}\frac{g_R(\mu-\nu)}{K_{eff}A_{eff}} \times [P^{\pm}(z,t,\mu)+P^{\mp}(z,t,\mu)]$$

When a gain-clamped FRA has to be simulated, Eq. (2.5) can be used to simulate the propagation of the pump and WDM signals, but Eq. (2.1) has to be applied to the propagation of the lasing signal for both the traveling-wave and the standing-wave configurations.

2.4.2 Runge-Kutta method

Equations (2.1) and (2.5) can easily be solved using the fourth order Runge-Kutta method (denoted as RK4) [67].

2.4.3 Average power analysis

As fiber amplifiers use long fiber lengths and wide bandwidths, the corresponding increase in the required computation times makes the simulation process nonpractical. The challenges associated with accurate simulations of FRAs have been addressed and resolved through the average power analysis (APA) model for the performance evaluations of semiconductor optical amplifiers (SOAs) and EDFAs [68], [69].

The APA has been applied to static Raman amplifiers by Min *et al.* [70]. Considerable reduction in computation time by over two to three orders of magnitude was achieved. The same approach was successfully applied to simulate dynamic FRAs by Karásek *et al.* with a substantial computational time reduction and an equal accuracy [71].

We applied the APA for all simulations in this thesis except for those in section 2.1. The time-domain APA is presented in Appendix B. It is the first time that the time-domain APA is applied to gain-clamped FRAs. This time-domain APA method produces results within 2% of the direct RK4 method while reducing the computation time by more than one order of magnitude.

2.5. Summary

In this chapter, after introducing the SRS responsible for the amplification in FRAs, we presented some generalities about FRAs including the polarization effects, their advantages and their noise performances. We also introduced the gain transients occurring in FRAs and the different gain-control techniques that can be used to mitigate them. We finally presented the complete and simplified numerical models to simulate FRAs and two numerical methods to solve the system of equations.

Chapter 3: Traveling-wave and standing-wave gain-clamping configurations for single DFRAs

3.1 Introduction

This chapter is dedicated to the study of gain transients of single gain-clamped DFRAs (GC-DFRAs). More precisely, we compare the dynamic characteristics of a standing-wave GC-DFRA to those of a traveling-wave GC-DFRA in the context of WDM channel add and drop. This study takes into account the operational modes of the amplifiers and the location of the surviving channel in the amplification band. We demonstrate that the efficiency of AOGC in DFRAs is dependent on the operational mode of the amplifier and that the location of the surviving signal affects the gain transient characteristics.

3.2 Simulations conditions

In the following studies, unless otherwise stated, we consider a backward-pumped DFRA comprising 5 km of highly non-linear fiber (HNLF) (see Appendix A) and three pumps located at 1435 nm, 1450 nm and 1480 nm with corresponding pump powers of 0.2 W, 0.2 W and 0.3 W. We consider 32 WDM channels operating in the L band and spaced by 100 GHz from 1560 nm to 1585.6 nm input to the amplifier. The lasing signal wavelength is set at 1625 nm, which induces the least gain tilt as a function of the input signals power [72]. To simulate addition and drop operations, 31 of the 32 signals are cut or added as shown in Fig. 3-1. We analyze the transient response for different surviving channel wavelengths, i.e. at the

shortest wavelength (λ_s = 1560.0 nm), at midband (λ_m = 1572.3 nm), and at the longest wavelength (λ_l = 1585.6 nm).

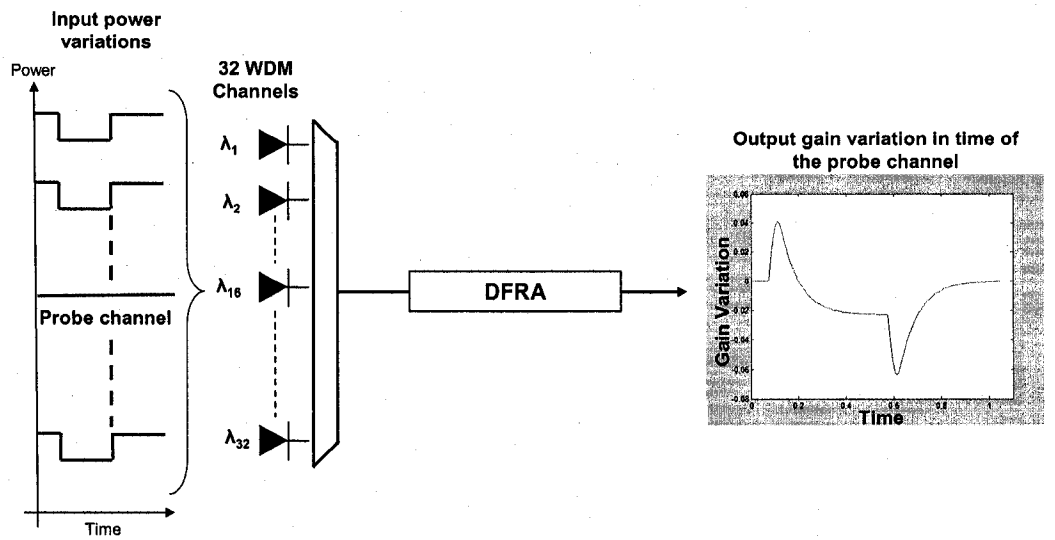

Fig. 3-1: Schematic of the system under study.

For both amplifier configurations, we use two feedback levels:

- (1) F = 0.245;
- (2) F = 0.5.

These values are chosen to permit an efficient gain-clamping over a large dynamic input power range while offering a high on-off gain.

In the case of the standing-wave GC-DFRA, we analyze three different configurations when the feedback level is 0.245:

- (a) R_1 = 0.2, R_2 = 0.3;
- (b) R_1 = R_2 = 0.245;
- (c) R_1 = 0.3, R_2 = 0.2.

For a feedback level of 0.5, we only study the case where R_1 and R_2 are both equal to 0.5.

In order to evaluate the gain-clamping effect, we define the critical power P_{crit} as a performance metric. The critical input power is the signal input

power to the amplifier which causes the gain to decrease by 0.5 dB from its value in the small signal regime. When the signal input power is equal to P_{crit}, the amplifier is said to be operated in critical regime. When the input signal power exceeds P_{crit}, gain-clamping starts to fail. In the saturation regime, the total input signal power corresponds to the saturation power P_{sat}, i.e. the input signal power necessary to achieve a gain equal to the small-signal gain minus 3 dB. Both travelling-wave and standing-wave GC-DFRAs are operated in the small-signal, the critical and the saturation regimes.

In order to compare both gain-clamping techniques, we use the following parameters: steady-state gain variation ΔG, peak gain excursions (i.e. overshoot and undershoot), rise time following an undershoot and fall time following an overshoot, see Fig. 3-2 for an illustration of these parameters. The steady-state gain variation ΔG is the difference between the gain of the surviving channel in the case where all channels are input to the amplifier and the case where the surviving channel is the only input signal. The peak gain excursion is defined as the difference (in dB) between the gain at the peak following the drop (overshoot) or the addition (undershoot) of channels and the gain of the next steady-state. The fall and rise times represent the time taken to pass between the 10% and 90% values of the gain excursions that follow the drop or addition of channels, respectively. The time at which the 31 WDM signals are cut and added depend on the operational regime and on the gain-clamping configurations and they are specified in each section.

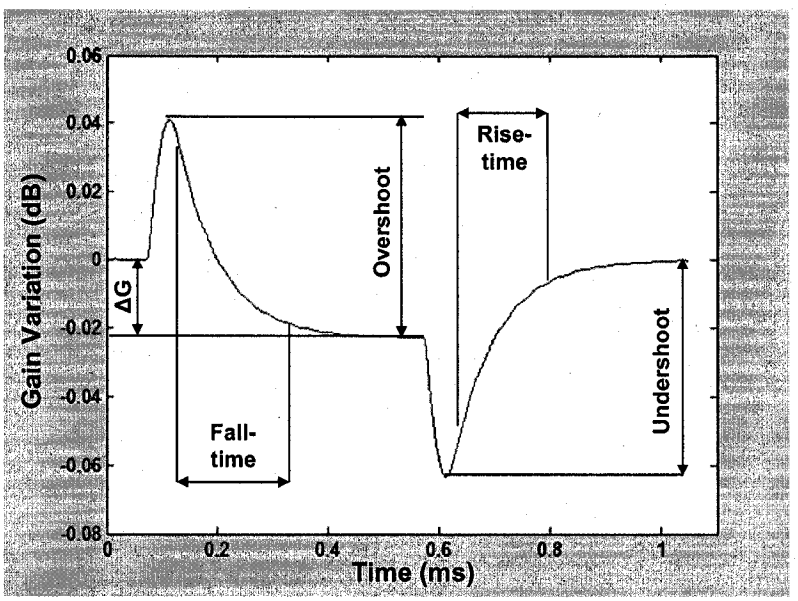

Fig. 3-2: Output gain variation and transient comparison parameters.

It can happen that AOGC is inefficient to control the gain transients. When all of the WDM channels are loaded in the amplifier, the pump power can be insufficient to create the lasing signal. In that case, the cut of WDM channels at the entry of the amplifier releases additional pump power to create the lasing signal. However, it takes a very long time for the lasing signal to achieve its steady-state and consequently, the fall time of the surviving channel is much longer than that observed in a GC-DFRA where AOGC is efficient. In the remainder of the thesis, we consider that AOGC is not in effect when there is no lasing signal in the presence of all of the WDM channels into the amplifier. Such GC-DFRAs are characterized by long fall and rise times for the surviving channel following the addition and drop of the other WDM channels.

3.3 Traveling-wave configuration

In this section, we present the transient characteristics of the traveling-wave GC-DFRA under the small-signal, the critical and the saturation regimes.

3.3.1 In the small-signal regime

Figure 3-3 presents the on-off gain of the amplifier when the 32 signals are launched with a -40 dBm per channel input power into the amplifier. We notice that the on-off gain decreases as the feedback level of the lasing signal increases. When the feedback level increases, the ring cavity losses increase. As a result, more pump power is required for the control signal to lase and consequently, less is available to amplify the WDM channels resulting in a much lower on-off gain.

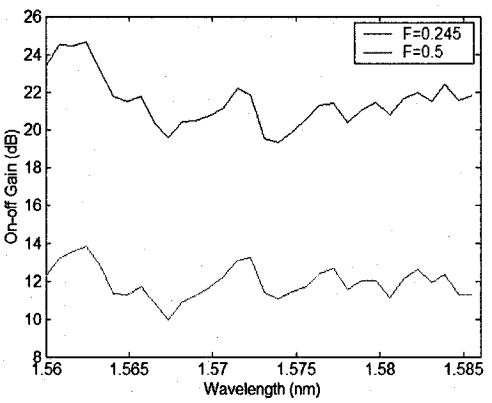

Fig. 3-3: On-off gain of the travelling-wave GC-DFRA with two feedback levels in the small-signal regime.

The time-domain gain variation of the probe channel at the output of the amplifier is presented in Fig. 3-4 for three different wavelengths. Figures 3-4 (a) and (b) show the results for a feedback level of 0.245 and 0.5, respectively. The drop of 31 WDM channels occurs at t = 50 μs and the channels are added again at t = 550 μs. In both cases, the surviving

channel experiences an overshoot after the cut of channels and an undershoot after the addition of channels. The cut and addition of channels are followed by transient periods corresponding to the time required by the lasing channel to stabilize. For both feedback levels, the traveling-wave gain-clamping configuration is efficient in mitigating the gain transients. We also notice a slight difference in the surviving channel gain variation in function of the location of this channel in the amplification band.

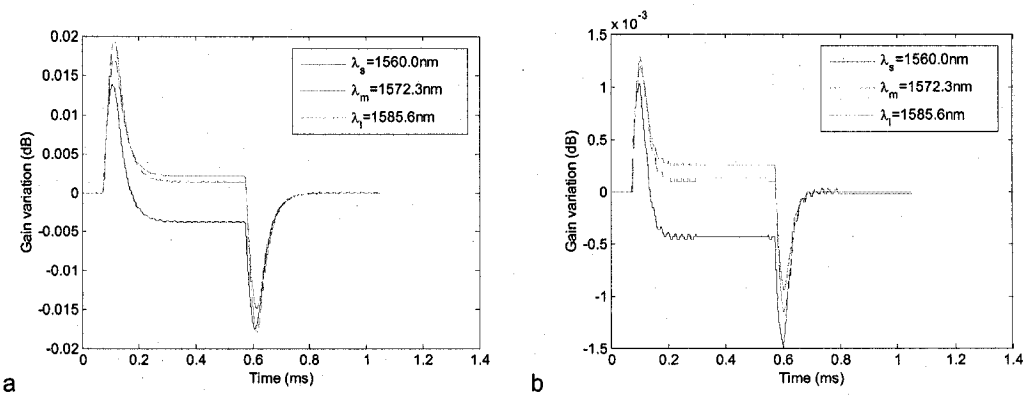

Fig. 3-4: Surviving channel gain variation in time for three probe channel location with F = 0.245 (a) and F = 0.5 (b) in the small-signal regime.

Figure 3-5 presents the lasing signal in time at the output of the standing-wave GC-DFRA with F = 0.245 under the small-signal regime when the surviving channel is set at the shortest wavelength (λ_s = 1560.0 nm). The time evolution of the lasing signal has the same behaviour than that of the surviving channel. The lasing signal power increases after the cut of channels as more pump power is available and it comes back to its initial value when the channels are added. The cut and the addition of channels are followed by oscillations for the lasing signal power.

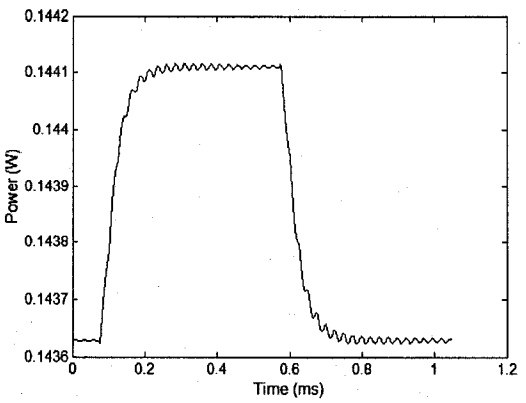

Fig. 3-5: Time evolution of the lasing signal at the output of the standing-wave GC-DFRA operated in the small-signal regime with F = 0.245 when the surviving channel is set at the shortest wavelength (λ_s = 1560.0 nm).

The gain transient parameters are summarized in Table 3-1. From these results, we notice that the over- and undershoots and ΔG are reduced by one order of magnitude when the feedback level increases from 0.245 to 0.5. The fall and rise times are similar and they approximately equal to 80 μs for F = 0.245 and 50 μs for F = 0.5. We see that increasing the feedback level also reduces the fall and rise times. Table 3-1 also shows that the dynamic response of the traveling-wave GC-DFRAs depends on the location of the surviving channel. The transients are worse if the surviving channel is at either extreme of the amplification band, i.e. at 1560 or 1585.6 nm. On the other hand, when the surviving channel is located at midband (λ_m = 1572.3 nm), the transients are less significant because the power it receives from the lower wavelength channels is compensated by the power it gives to the higher wavelength channels.

Feedback level	Surviving channel λ (nm)	Overshoot (10^{-3}dB)	Fall time (μs)	Gain variation (10^{-3}dB)	Undershoot (10^{-3}dB)	Rise time (μs)
F = 0.245	1560.0	17.52	79	-3.72	17.50	81
	1572.3	14.96	78	2.14	14.90	79
	1585.6	17.91	77	1.39	17.80	79
F = 0.5	1560.0	1.47	50	-0.44	1.47	50
	1572.3	0.98	48	0.25	0.98	48
	1585.6	1.21	50	0.13	1.21	50

Tab. 3-1: Transient characteristics of the surviving channel for three probe channel location with F = 0.245 and F = 0.5 in the small-signal regime.

3.3.2 In the critical regime

Here, the traveling-wave GC-DFRAs are operated in the critical regime and the corresponding on-off gains are presented in Fig. 3-6 for both feedback levels.

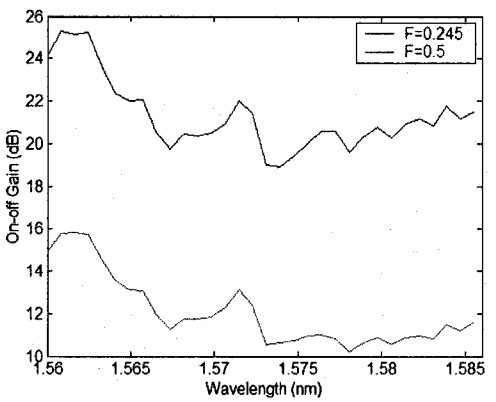

Fig. 3-6: On-off gain of the travelling-wave GC-DFRA with two feedback levels in the critical regime.

Figure 3-7 depicts the surviving channel gain variation during the addition and drop of channels. The cut of WDM channels occurs at t = 50 μs for both feedback levels and the addition of channels happens at t = 2 ms for

F = 0.245 and t = 750 µs for F = 0.5. We observe that the amplifiers have very different behaviour depending on the feedback level value. With F = 0.245 [Fig. 3-7 (a)], the surviving channel reaches its steady-state right after the cut of channels which means that the amplifier is gain-clamped. For F = 0.5, the cut of channels is followed by an oscillation period and a drop of power to achieve a steady-state. In that scenario, gain-clamping is not fully in effect since there is not enough pump power to sustain the lasing signal when all of the channels are loaded in the amplifier. However, by cutting the channels, the pumps become less depleted which leaves enough power to create the lasing signal. As the laser power increases (feedback signal grows), the surviving channel power progressively decreases until a steady-state is reached after a long time.

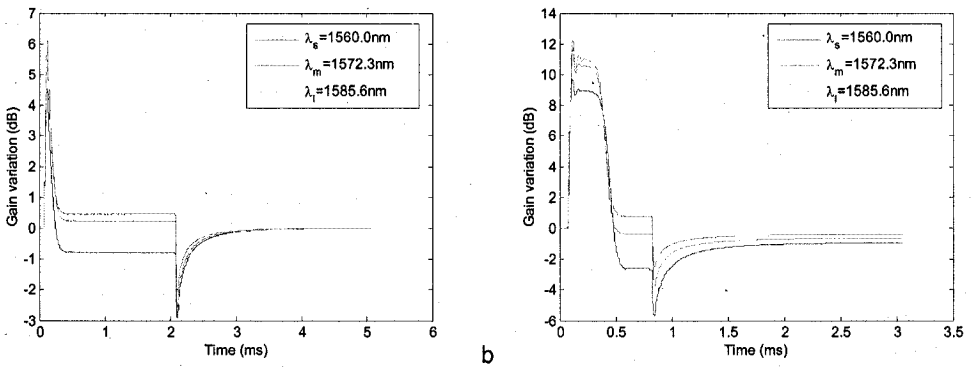

Fig. 3-7: Surviving channel gain variation in time for three probe channel location with F = 0.245 (a) and F = 0.5 (b) in the critical regime.

Figure 3-8 presents the lasing signal in time at the output of the standing-wave GC-DFRA with F = 0.5 under the critical regime when the surviving channel is set at the shortest wavelength (λ_s = 1560.0 nm). The time evolution of the lasing signal has a different behaviour than that presented in Fig. 3-5. We note that the lasing signal power is close to zero when all of the channels are loaded in the amplifier (t = 0). We also notice that the cut of channels is not instantly followed by an increase of the lasing signal power. It takes a long time to create the lasing signal and as this lasing

signal power increases, the surviving channel power decreases until both signals reach a steady-state. The lasing signal comes back to its initial value when the channels are added.

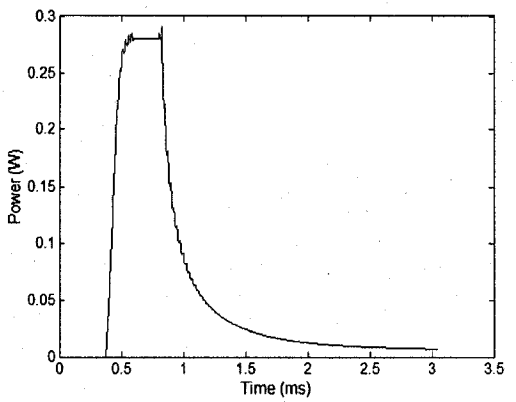

Fig. 3-8: Time evolution of the lasing signal at the output of the GC-DFRA operated in the critical regime with F = 0.5 when the surviving channel is set at the shortest wavelength (λ_s = 1560.0 nm).

Table 3-2 reports the gain transient parameters which confirm the previous observations. We notice that all of the comparison parameters are higher for the high feedback level. This is due to the fact that gain-clamping is not in effect for F = 0.5. Approximately, we note that the overshoot doubles and the fall time triples as the feedback level is increased. The undershoot, the rise time and ΔG increase less drastically with the feedback level, especially in the case of the rise time. A similar observation as in the small-signal regime can be made with respect to the impact of the surviving channel location on the gain transients: the transients are worse if the surviving channel is at either extreme of the amplification band.

Configuration	Surviving channel λ (nm)	Overshoot (dB)	Fall time (μs)	Gain variation (dB)	Undershoot (dB)	Rise time (μs)
$F = 0.245$	1560.0	5.34	110	-0.78	2.92	629
	1572.3	5.07	103	0.45	2.06	542
	1585.6	5.91	105	0.24	2.57	602
$F = 0.5$	1560.0	12.63	337	-2.61	5.68	644
	1572.3	10.94	299	0.78	2.52	573
	1585.6	12.33	296	-0.34	3.76	609

Tab. 3-2: Transient characteristics of the surviving channel for three probe channel location with $F = 0.245$ and $F = 0.5$ in the critical regime.

3.3.3 In the saturation regime

The last operational regime under study is the saturation regime. The on-off gains of the GC-DFRAs are reported in Fig. 3-9.

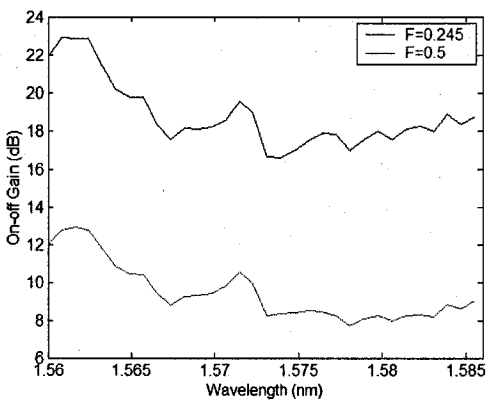

Fig. 3-9: On-off gain of the travelling-wave GC-DFRA with two feedback levels in the saturation regime.

As the operational regime of the amplifiers reaches the saturation regime, we note that the gain-clamping is not in effect independently of the feedback level as shown in Fig. 3-10. In both cases, the behaviour of the surviving channel gain variation in time is the same as that of the

traveling-wave GC-DFRA operated under the critical regime with F = 0.5. The cut of WDM channels is followed by an overshoot and oscillation and it takes a long time to the amplifier to reach the steady-state.

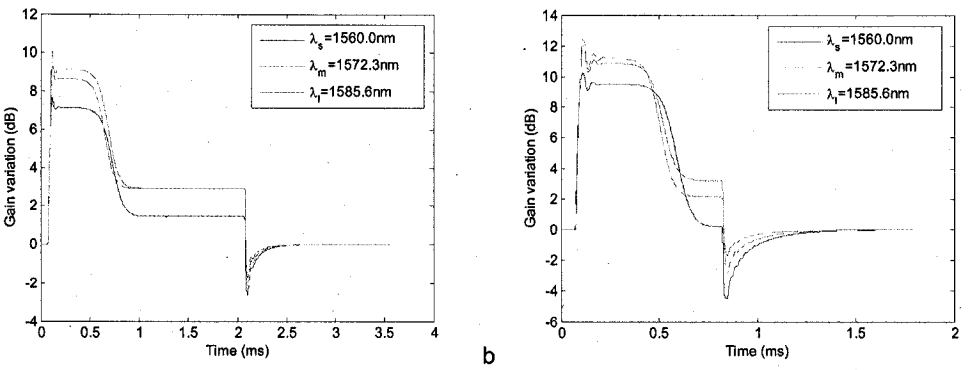

Fig. 3-10: Surviving channel gain variation in time for three probe channel location with F = 0.245 (a) and F = 0.5 (b) in the saturation regime.

From Table 3-3, we observe that the best transient performances are now shared between both configurations. As the GC-DFRA operated with F = 0.245 offers the lowest overshoots, undershoots and rise times, it also present the worst fall times in comparison to the GC-DFRA operated with F = 0.5. As in the small-signal and the critical regimes, the lowest transients are observed when the surviving channel is located at midband.

Configuration	Surviving channel λ (nm)	Overshoot (dB)	Fall time (μs)	Gain variation (dB)	Undershoot (dB)	Rise time (μs)
F = 0.245	1560.0	6.23	668	1.43	2.62	244
	1572.3	6.43	578	2.90	1.71	215
	1585.6	4.74	616	2.92	2.21	223
F = 0.5	1560.0	10.05	498	0.22	4.47	347
	1572.3	8.84	410	3.18	1.71	269
	1585.6	10.32	429	2.15	2.83	322

Tab. 3-3: Transient characteristics of the surviving channel for three probe channel location with F = 0.245 and F = 0.5 in the saturation regime.

3.4 Standing-wave configuration

In this section, we analyze the transient characteristics of a standing-wave GC-DFRA operated in the small-signal, the critical and the saturation regimes. As for the traveling-wave GC-DFRA, the same two feedback levels are applied to the amplifier, i.e. F = 0.245 and 0.5. In the case of F = 0.245, three FBGs reflection coefficients configurations are studied, i.e. R_1 = 0.2, R_2 = 0.3; R_1 = R_2 = 0.245; R_1 = 0.3, R_2 = 0.2. For F = 0.5, we only chose to study one configuration, i.e. R_1 = R_2 = 0.5.

3.4.1 In the small-signal regime

Figure 3-11 presents the on-off gain of the four standing-wave GC-DFRAs operated in the small-signal regime. As for the traveling-wave GC-DFRA, we note that increasing the feedback level decreases the gain. We also notice that the FBGs configuration does not affect significantly the on-off gain.

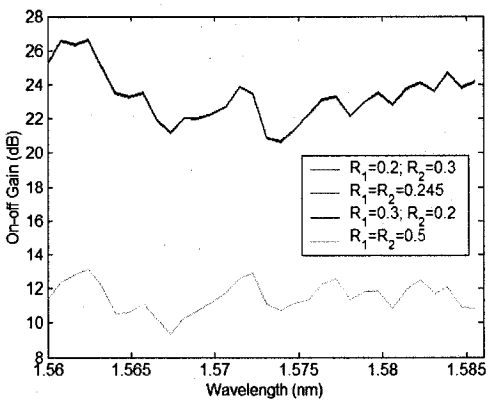

Fig. 3-11: On-off gain of the standing-wave GC-DFRA with four FBGs reflection coefficients configurations in the small-signal regime.

The gain variation of the surviving channel during the addition and drop of channels is reported in Fig. 3-12. As for the traveling-wave GC-DFRA, we note that the location of the surviving channel impacts the transients. The

31 WDM channels are cut at t = 50 µs and added again at t = 550 µs at the input of the amplifier. We observe that, with both feedback levels, gain-claming is in effect and that the GC-DFRA with the highest feedback level reaches the the steady-state following the cut of channels fastest [Fig. 3-12 (d)].

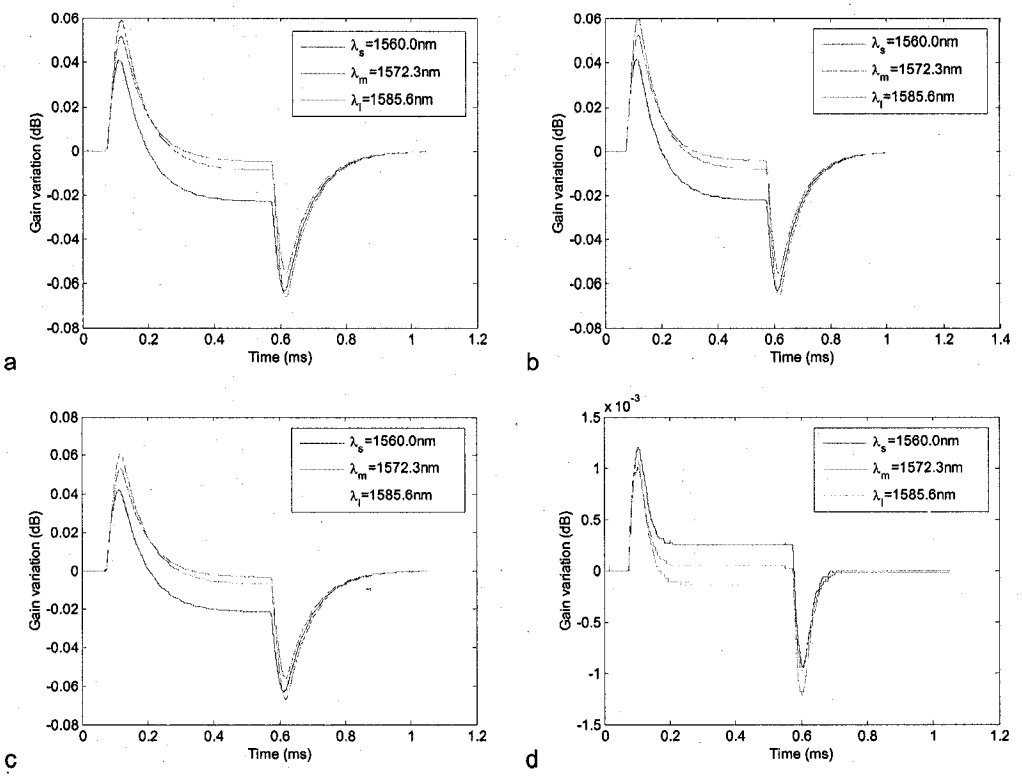

Fig. 3-12: Surviving channel gain variation in time for three probe channel location with R_1 = 0.2, R_2 = 0.3 (a); R_1 = R_2 = 0.245 (b); R_1 = 0.3, R_2 = 0.2 (c) and R_1 = R_2 = 0.5 (d) in the small-signal regime.

The transient characteristics of the four amplifiers are reported in Table 3-4. The same observation on the impact of the surviving channel wavelength can be made for the traveling-wave GC-DFRA: the surviving channel located at midband presents the lowest gain transients. This property will also be verified for the critical and the saturation regimes. In this operational regime, the GC-DFRA with F = 0.5 presents the best transient performances for each parameter. Increasing the feedback level

from 0.245 to 0.5 enables to reduce the over- and undershoots by 60 times and the fall and rise time by around 3 times. ΔG is also reduced and reaches a value below 10^{-3} dB.

Configuration	Surviving channel λ (nm)	Overshoot (10^{-3}dB)	Fall time (μs)	Gain variation (10^{-3}dB)	Undershoot (10^{-3}dB)	Rise time (μs)
$R_1 = 0.2$ $R_2 = 0.3$	1560.0	63.95	168	-22.87	63.34	174
	1572.3	56.13	167	-4.57	55.35	173
	1585.6	67.31	167	-8.32	66.37	173
$R_1 = 0.245$ $R_2 = 0.245$	1560.0	63.84	168	-22.22	63.35	175
	1572.3	56.39	167	-4.11	55.65	174
	1585.6	67.54	168	-7.75	66.68	175
$R_1 = 0.3$ $R_2 = 0.2$	1560.0	63.68	169	-21.41	63.15	175
	1572.3	56.58	168	-3.52	55.80	174
	1585.6	67.27	168	-7.01	66.82	174
$R_1 = R_2 = 0.5$	1560.0	0.95	62	0.25	0.95	57
	1572.3	0.94	55	0.05	0.95	54
	1585.6	1.16	62	-0.14	1.16	57

Tab. 3-4: Transient characteristics of the surviving channel for three probe channel location with $R_1 = 0.2$, $R_2 = 0.3$; $R_1 = R_2 = 0.245$; $R_1 = 0.3$, $R_2 = 0.2$ and $R_1 = R_2 = 0.5$ in the small-signal regime.

The transient performances of the three amplifiers having a feedback level of 0.245, are similar. However, we note that the amplifier having the highest reflection coefficient at the first FBG offers the lowest ΔG when the amplifier having the lowest reflection coefficient at the first FBG presents the lowest fall and rise times. The best performances in term of over- and undershot are shared between the three configurations.

3.4.2 In the critical regime

The standing-wave GC-DFRAs are now operated in the critical regime and the corresponding on-off gains are presented in Fig. 3-13 for both feedback levels.

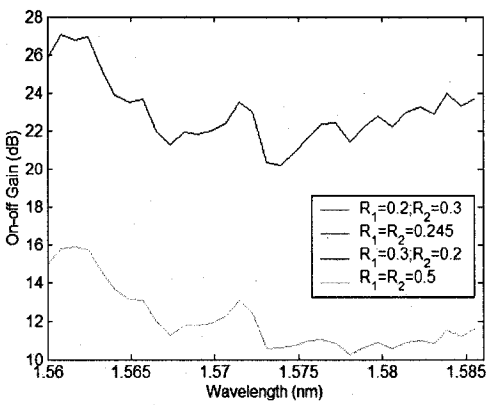

Fig. 3-13: On-off gain of the standing-wave GC-DFRA with four FBGs reflection coefficients configurations in the critical regime.

Figure 3-14 depicts the surviving channel gain variation during the addition and drop of channels. The cut of WDM channels occurs at t = 50 μs for both feedback levels and the addition of channels happens at t = 1.5 ms for F = 0.245 and t = 750 μs for F = 0.5. Contrary to the traveling-wave GC-DFRA case, where the gain-clamping is efficient in the critical regime with F = 0.245, gain-clamping is not in effect in the standing-wave GC-DFRA. The same situation occurs with F = 0.5.

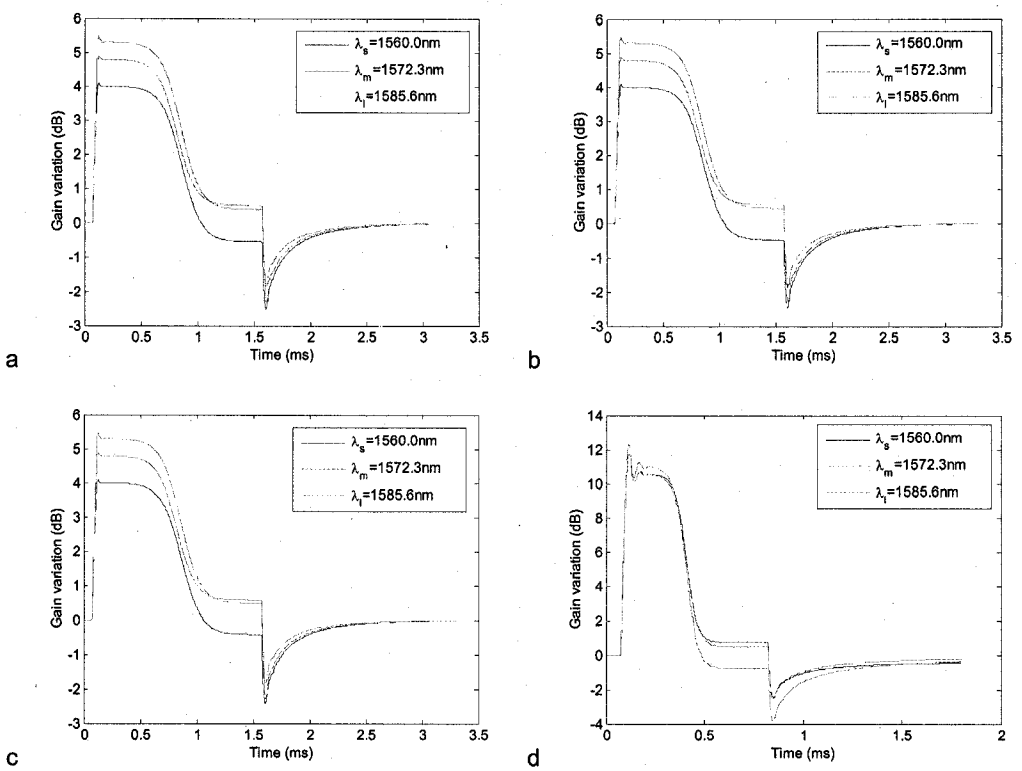

Fig. 3-14: Surviving channel gain variation in time for three probe channel location with $R_1 = 0.2$, $R_2 = 0.3$ (a); $R_1 = R_2 = 0.245$ (b); $R_1 = 0.3$, $R_2 = 0.2$ (c) and $R_1 = R_2 = 0.5$ (d) in the critical regime.

Table 3-5 reports the gain transient parameters which confirm the previous observations. We notice that all of the amplifiers have high over- and undershoots and fall and rise times. This is due to the fact that gain-clamping fails for both feedback levels. Increasing F from 0.245 to 0.5 almost doubles the overshoot and the rise time, slightly increases the undershoot in addition to decreasing the fall time, as ΔG stays comparable. The transient characteristics of the three configurations with a feedback level of 0.245 are similar. However, we note that the amplifier having the highest reflection coefficient at the first FBG ($R_1 = 0.3$, $R_2 = 0.2$) offers the lowest ΔG, overshoot, undershoot and rise time when the amplifier having the lowest reflection coefficient at the first FBG ($R_1 = 0.2$, $R_2 = 0.3$) presents the lowest fall time.

Configuration	Surviving channel λ (nm)	Overshoot (dB)	Fall time (μs)	Gain variation (dB)	Undershoot (dB)	Rise time (μs)
$R_1 = 0.2$ $R_2 = 0.3$	1560.0	4.65	414	-0.55	2.50	657
	1572.3	4.39	391	0.50	1.87	609
	1585.6	5.09	456	0.40	2.31	628
$R_1 = 0.245$ $R_2 = 0.245$	1560.0	4.58	418	-0.48	2.46	652
	1572.3	4.44	394	0.44	1.85	603
	1585.6	4.95	459	0.54	2.29	625
$R_1 = 0.3$ $R_2 = 0.2$	1560.0	4.52	418	-0.42	2.42	647
	1572.3	4.38	395	0.49	1.84	598
	1585.6	4.91	461	0.58	2.27	621
$R_1 = R_2 = 0.5$	1560.0	10.95	335	0.77	2.52	1434
	1572.3	11.24	299	0.48	2.49	1018
	1585.6	13.06	294	-0.77	3.83	1257

Tab. 3-5: Transient characteristics of the surviving channel for three probe channel location with $R_1 = 0.2$, $R_2 = 0.3$; $R_1 = R_2 = 0.245$; $R_1 = 0.3$, $R_2 = 0.2$ and $R_1 = R_2 = 0.5$ in the critical regime.

3.4.3 In the saturation regime

The last operational regime under study is the saturation regime. The on-off gains of the GC-DFRAs are reported in Fig. 3-15.

As illustrated in Fig. 3-16, we observe that gain-clamping is not in effect when the GC-DFRAs are operated in the saturation regime. In those figures, the drop of WDM channels occurs at t = 50 μs and the addition of channels occurs at t = 1.75 ms for F = 0.245 and at t = 750 μs for F = 0.5.

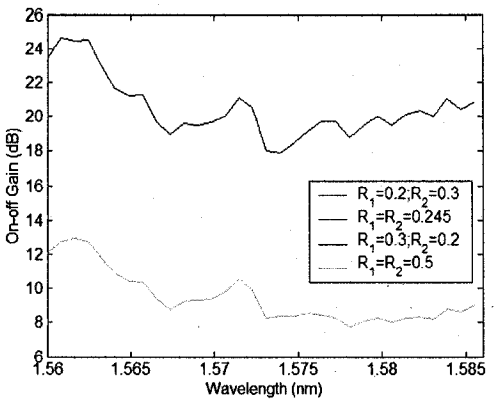

Fig. 3-15: On-off gain of the standing-wave GC-DFRA with four FBGs reflection coefficients configurations in the saturation regime.

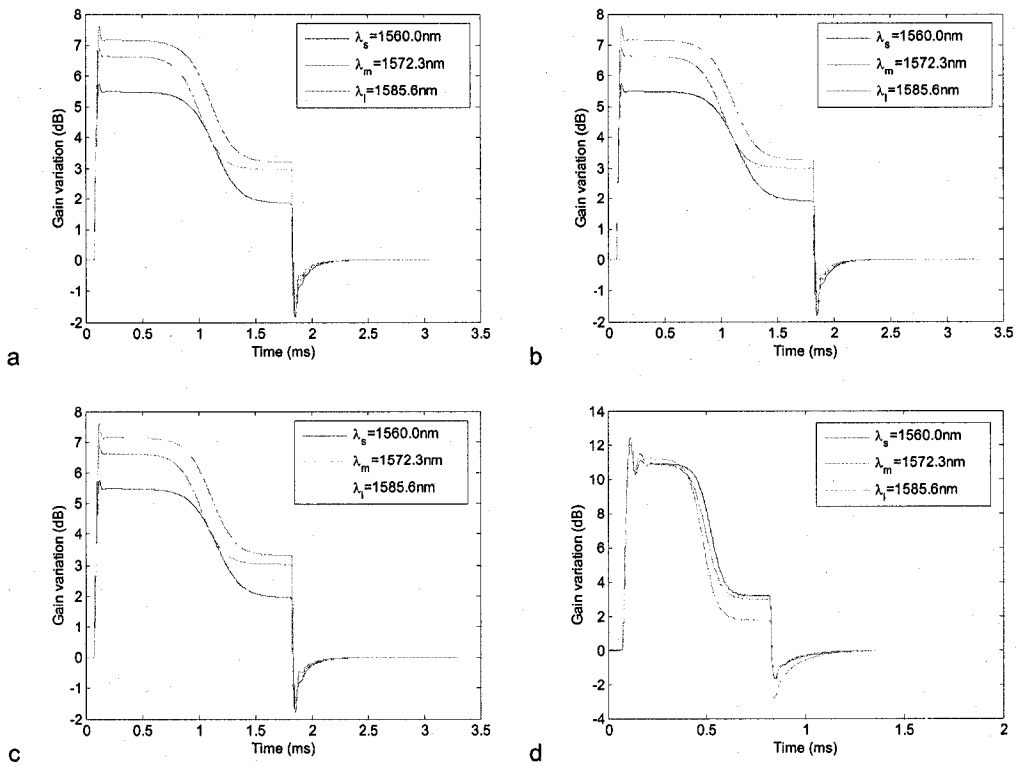

Fig.3-16: Surviving channel gain variation in time for three probe channel location with R_1 = 0.2, R_2 = 0.3 (a); R_1 = R_2 = 0.245 (b); R_1 = 0.3, R_2 = 0.2 (c) and R_1 = R_2 = 0.5 (d) in the saturation regime.

Configuration	Surviving channel λ (nm)	Overshoot (dB)	Fall time (µs)	Gain variation (dB)	Undershoot (dB)	Rise time (µs)
$R_1 = 0.2$ $R_2 = 0.3$	1560.0	3.91	1177	1.84	1.83	202
	1572.3	3.95	1020	2.95	1.37	178
	1585.6	4.42	1129	3.21	1.71	181
$R_1 = 0.245$ $R_2 = 0.245$	1560.0	3.85	1186	1.90	1.80	200
	1572.3	3.91	1025	2.99	1.36	177
	1585.6	4.37	1134	3.26	1.70	181
$R_1 = 0.3$ $R_2 = 0.2$	1560.0	3.80	1187	1.96	1.78	198
	1572.3	3.87	1026	3.03	1.36	176
	1585.6	4.33	1137	3.30	1.70	179
$R_1 = R_2 = 0.5$	1560.0	8.85	472	3.17	1.71	292
	1572.3	9.04	407	2.98	1.61	234
	1585.6	10.68	382	1.79	2.81	274

Tab. 3-6: Transient characteristics of the surviving channel for three probe channel location with $R_1 = 0.2$, $R_2 = 0.3$; $R_1 = R_2 = 0.245$; $R_1 = 0.3$, $R_2 = 0.2$ and $R_1 = R_2 = 0.5$ in the small-signal regime.

From Table 3-6, we observe that the best transient performances are shared between both configurations. As the GC-DFRAs operated with F = 0.245 offer the lowest overshoots, undershoots and rise times, they also present the worst fall times in comparison to the GC-DFRA operated with $F = 0.5$. As noted previously, the three configurations with a feedback level of 0.245 present similar transient performances and we notice that the amplifier having the highest reflection coefficient at the first FBG ($R_1 = 0.3$, $R_2 = 0.2$) offers the lowest ΔG, overshoot, undershoot and rise time when the amplifier having the lowest reflection coefficient at the first FBG (R_1 = 0.2, $R_2 = 0.3$) presents the lowest fall time.

One remark has to be made here: in the small-signal regime, the transient characteristics following the cut of channels have values comparable to

those following the addition of channels. As the operational regime is increased to the critical regime, we notice that the overshoots and the rise times become largely greater to the undershoots and the fall times, respectively. In the saturation regime, the increase of the overshoot over the undershoot is amplified but the fall times become now larger to the rise times. Those remarks are valid for both gain-clamping configurations.

3.5 Traveling-wave GC_DFRA vs. standing-wave GC_DFRA

In this section, we compare the transient performances of both gain-clamping configurations: traveling-wave GC-DFRA vs. standing-wave GC-DFRA.

In the small-signal regime, we note that the gain-clamping is efficient for both configurations and feedback levels. However, the performances depend on the feedback level applied to the lasing signal. If the traveling-wave GC-DFRA offers the best transient characteristics with F = 0.245, it is not the case when F is increased to 0.5. In that case, the best performances are shared between the two configurations. The standing-wave GC-DFRA has the lowest over- and undershoots when the traveling-wave presents the lowest fall and rise times.

In the critical regime, the behaviour of both configurations is drastically different in the case of F = 0.245. The gain-clamping is efficient to mitigate the transient for traveling-wave GC-DFRA but fails for the standing-wave GC-DFRA. Obviously, the traveling-wave presents the fastest fall and rise times as gain-clamping is in effect. When F is increased to 0.5, gain-clamping is not in effect for both gain-clamping configurations. The standing-wave GC-DFRA offers the lowest overshoots, undershoots and fall times but the worst rise times.

In the saturation regime, gain-clamping is inefficient to mitigate the gain transients for both configurations. When the feedback level is fixed to 0.245, the standing-wave GC-DFRA has the best performances in terms of over- and undershoots and rise times as the traveling-wave GC-DFRA presents the lowest fall times and ΔG. When *F* is increased to 0.5, the standing-wave GC-DFRA presents the best performances for all of the parameters except for ΔG.

3.6 Conclusion

In this chapter, we analyzed the characteristics of the gain transients occurring in GC-DFRAs subject to the worst possible case of WDM channels addition and drop. In particular, we analyzed the performances of two AOGC configurations. In this study, we took into account the operational regime of the amplifiers (i.e. we vary the per channel input power), the location of the surviving channel in the amplification band and the feedback level of the lasing signal.

The following conclusions can be drawn from our study:

- when the surviving channel is located at midband, the transients are less significant because the power it receives from the lower wavelength channels is compensated by the power it gives to the higher wavelength channels;
- when the gain-clamping is in effect, increasing the feedback level enables a better control of the transients but at the expense of a lower on-off gain;
- the efficiency of the all-optical gain clamping depends on the gain-clamping configuration, the feedback level and on the operational regime.

For the remainder of the thesis, we chose to study GC-DFRAs in the small-signal and in the critical minus 3 dB regimes in order to ensure the efficiency of the gain-clamping technique.

Chapter 4: Dynamic gain variations in DFRAs subject to multi-channel packet traffic

4.1 Introduction

In dynamic networks such as AAPN, the different packets at a given wavelength can propagate along different paths before being collected on a common link at the input of an amplifier. Since these packets will experience different amplification and loss, the multi-channel packets can exhibit randomly varying power levels at the input of the amplifier. While the gain transients and power excursions in EDFAs subject to burst-mode packet traffic has been studied in [73-75], no such studies exist for FRAs.

In this chapter, we study the behaviour of DFRAs fed by multi-channel packet traffic. More precisely, we apply the gain-clamping technique in order to determine whether it can reduce the gain transients occurring at the output of the amplifier. We study both unclamped and gain-clamped amplifiers in a realistic WDM situation using 64 WDM channels out which one is non-varying. We start by investigating the influence of the standard deviation of the input power Gaussian distribution when the amplifiers are operated in the small-signal regime. Next, we analyze the impact of the packet duration on the transients by using packet durations of 25 and 100 μs. Finally, by increasing the per channel input power, we study the impact of the operational regime on the gain transients characteristics.

4.2 Simulations conditions

4.2.1 Conditions on the amplifiers

In our investigation, we consider both unclamped and GC-DFRAs. Each amplifier comprises 5 km of HNLF and three pumps at 1435, 1450 and 1480 nm. The use of three pumps enables amplification over 25 nm (the amplifiers are not optimized to provide the broadest amplification bandwidth). We use backward pumping in order to avoid any polarization dependence of Raman gain.

The amplifiers are fed by 64 channels spaced by 50 GHz (from 1562.5 nm to 1588.2 nm) and are operated in the small-signal regime and in the critical minus 3 dB regime. Here, the small-signal per signal input power is set at -30 dBm and the critical minus 3 dB per signal input power at -17.9 dBm.

In the case of a gain-clamped amplifier, the location of the lasing signal wavelength is important as a gain tilt can occur in comparison to the unclamped amplifier gain. In our case, the best location of this signal is at 1625 nm [72]. In order to ensure a reasonable gain and a large dynamic range for gain-clamped operation, the reflection coefficients of the FBGs R_1 and R_2 are both set to 0.31.

In order to obtain the same on-off gain spectra in the small-signal regime for both unclamped and GC-DFRAs, the distribution of the three pump powers must be adapted for each case. The pump powers are fixed at 0.190, 0.135 and 0.195 W for the unclamped amplifier and at 0.25, 0.20 and 0.30 W for the GC-DFRA. Each amplifier is followed by a gain flattening filter in order to provide 16 dB gain for each channel when they

are operated in small-signal regime. Figure 4-1 presents the on-off gain of the unclamped and gain-clamped DFRAs before the gain flattening filter.

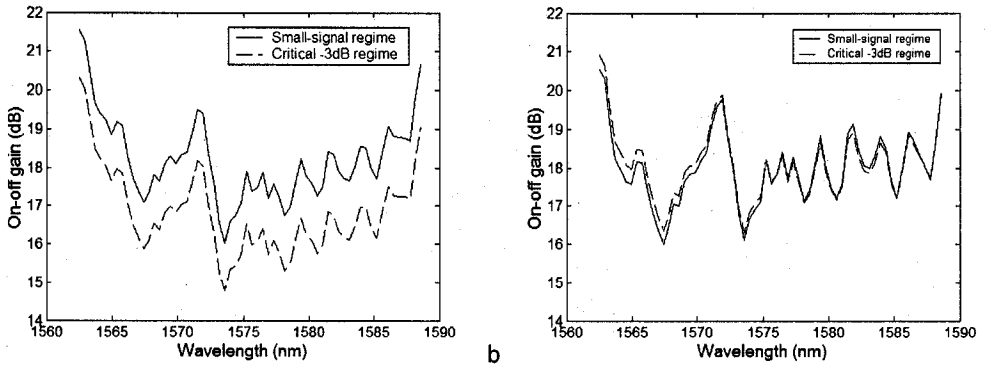

Fig. 4-1: On-off gain spectra of the unclamped DFRA (a) and the GC-DFRA (b) in the small-signal and the critical minus 3 dB regimes.

4.2.2 Framework of the simulations

Our main objective is to analyze the behaviour of a DFRA subject to multi-channel packet traffic. In this context, one of the 64 signals is set as a non-varying (in time) probe channel while the other 63 channels have randomly varying input powers; see Fig. 4-2 (a). We examine the gain transients for the probe channel located at midband (in this case, λ_m = 1575.2 nm). One simulation consists in the propagation of 5 packets, i.e. the input power of the 63 channels varies 5 times. We consider two different packet durations: 25 μs and 100 μs. In accordance with the AAPN architecture and bandwidth provisioning schemes described in [6], we assume that there is no dead time between packets. The input power of each of the 63 channels is changed randomly and independently of the others according to a Gaussian distribution. In order to perform a statistical study, we run 500 simulations for one DFRA (unclamped or gain-clamped) with a given operational regime (small-signal or critical minus 3 dB), a given input power Gaussian distribution (with specific mean and standard deviation), and a given packet duration.

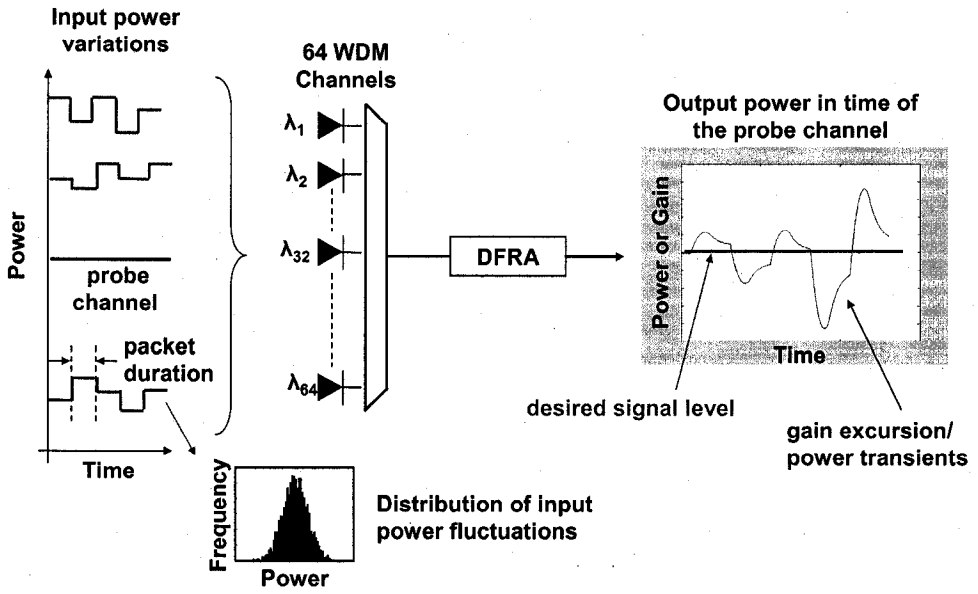

a)

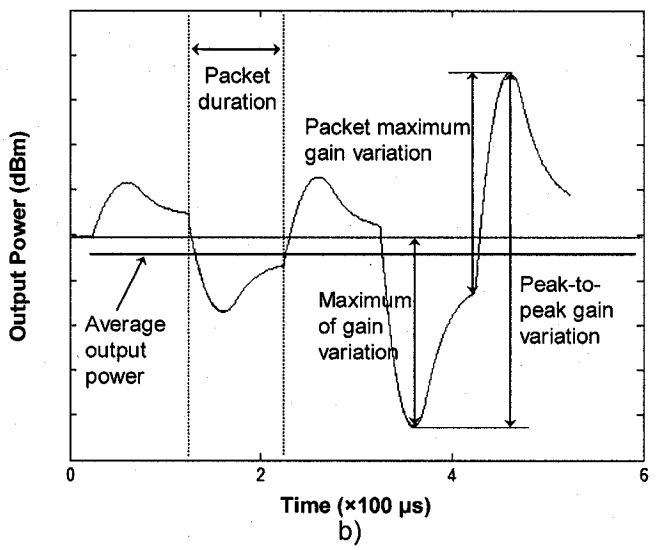

b)

Fig. 4.2: (a) Schematic of the system under study. (b) Output power of the probe channel in time

We use the following parameters illustrated in Fig. 4-2 (b) to evaluate the dynamic response of the amplifiers: the average output power (P_{avg}) and the three excursions i.e, the peak-to-peak gain variation (ΔG_{pp}), the maximum gain variation (ΔG_{max}), and the maximum gain variation occurring during a packet (referred to as the packet maximum gain variation, ΔG_{packet}). P_{avg} is the mean of the probe channel power during the

propagation of the 5 packets. In order to compare the amplifiers, we obtain the mean and variance of the distributions of these parameters.

4.3 Simulations results

We begin by examining the influence of the standard deviation of the input power Gaussian distribution when the DFRAs are operated in the small-signal regime with a packet duration of 25 μs. Next, we analyze the impact of the packet duration on the transients. Finally, by increasing the per channel input power, we investigate the importance of the operational regime.

4.3.1 Influence of the standard deviation of the input power Gaussian distribution and of the gain-clamping technique

In this section, we operate the unclamped and GC-DFRAs in the small-signal regime. The amplifiers are fed by packets whose duration is fixed to 25 μs. The input powers of the 63 time-varying channels are varied randomly for each packet according to a Gaussian distribution with a mean value of -30 dBm and an input standard deviation (σ_{in}) of 1, 5, 10, 25 or 50% of the mean value.

Figure 4-3 presents two examples of distributions for the output power and peak-to-peak gain variation in the probe channel for an unclamped amplifier in the small-signal regime.

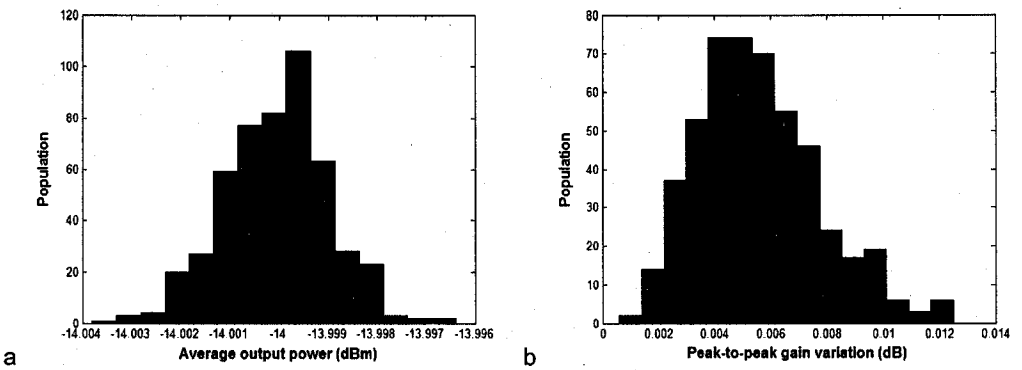

a b

Fig. 4-3: Distribution of the average output power (a) and of the peak-to-peak gain variation (b) for the probe channel in an unclamped amplifier operated in the small-signal regime and a packet duration of 25 µs.

Figure 4-4 presents the mean value and the variance of probe channel parameters distributions for the unclamped DFRA. For both amplifiers, the mean and the variance of all of the parameters increase with σ_{in}. The single exception is the mean of P_{avg} that is constant and equal to -14 dBm (which is the target value) for both amplifiers and independent of σ_{in}. We can also remark that ΔG_{pp} presents the highest gain variation and variance, followed by ΔG_{packet}. Statistically, ΔG_{packet} is superior to ΔG_{max} which corresponds to the difference between the maximum output power (in absolute value) and the initial output power (at t = 0, when all of the channels have the same input power). Thus, if we want to keep the various excursions below a certain value (1 dB for example), attention must only be paid to ΔG_{pp}.

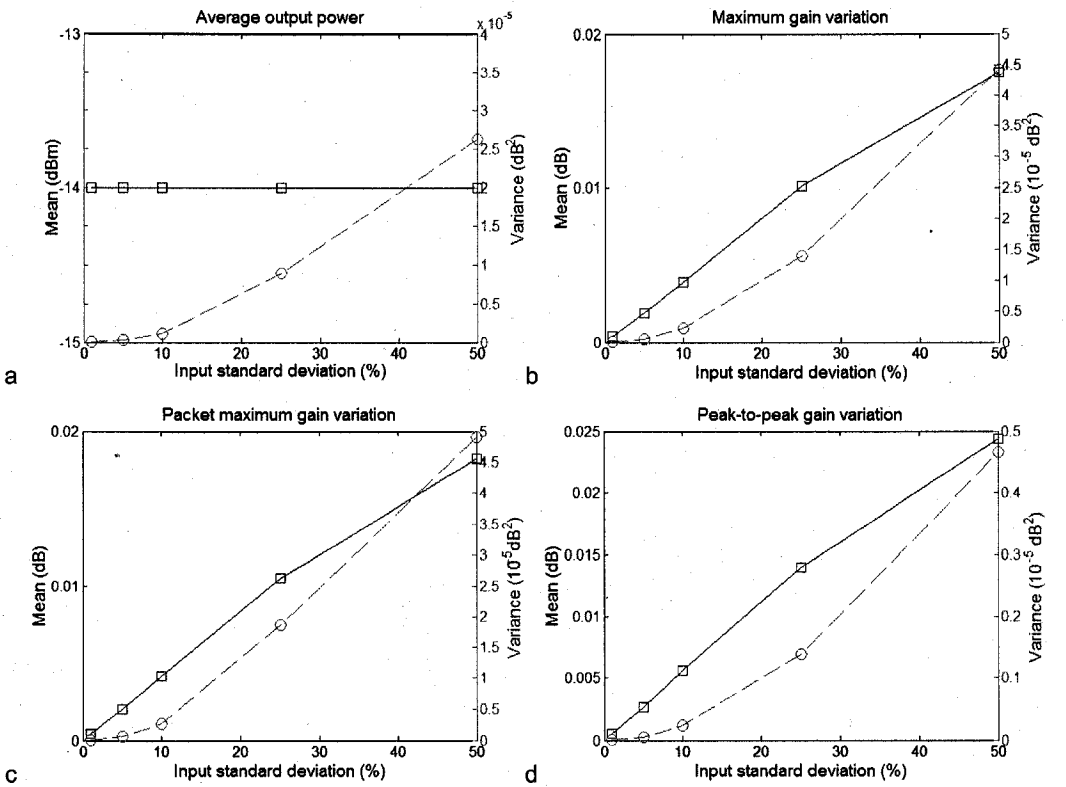

Fig. 4-4: Means (square) and variances (circle) of the comparison parameters as function of σ_{in} for the unclamped DFRA operated in the small-signal regime with packet duration of 25 µs.

The results of the GC-DFRAs are presented in Fig. 4-5. As for the unclamped DFRA, the mean of P_{avg} is constant and equal to -14 dBm and the other parameters increase with σ_{in} when the amplifier is gain-clamped. Note that the means of the different gain variations are lower when the amplifier is gain-clamped, which confirms its efficiency in mitigating the gain excursions. The gain-control technique also reduces the scattering of the different gain variations as their variance is reduced compared to the unclamped configuration, which is more notable as σ_{in} increases. If we consider the case ΔG_{pp}, using the gain-clamping technique reduces the mean by 0.005 dB compared to that of the unclamped DFRA when the σ_{in} is 50%.

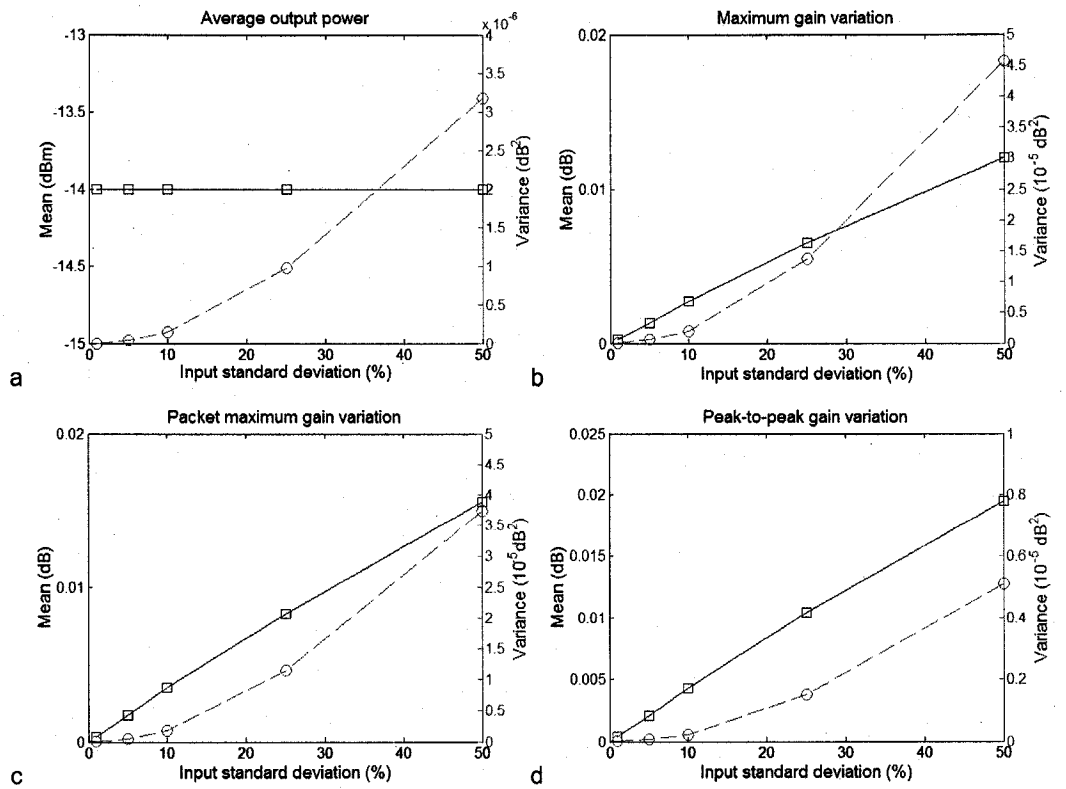

Fig. 4-5: Means (square) and variances (circle) of the comparison parameters as function of σ_{in} for the GC-DFRA operated in the small-signal regime with packet duration of 25 µs.

Although the gain-clamping technique is efficient to reduce the mean and the variance of the excursions, the differences in performance between the unclamped and gain-clamped amplifiers are very slight in absolute value. For the unclamped DFRA operated in the small-signal regime, the major gain variation is represented by ΔG_{pp} when σ_{in} is 50% and its value is only 0.0244 dB. The same observation can be made for the variance of the different gain variations.

We can conclude from the above observations that the unclamped DFRA operated in the small-signal regime is practically blind to the randomly variable packet traffic. Intuitively, we expect this kind of behaviour and the reasoning is as follows. At the entry of the DFRA, the power of some wavelengths is increased while that of other wavelengths is decreased. As a result, the total input power remains more or less constant on average

and the observed transient will be small (this is in contrast to the worst-case of scenarios considered in Chapters 3 and 5 following channel add and drop). Even if the gain-clamping technique reduces the various gain variations and their scattering, the application of this technique is useless in the small-signal regime as the unclamped DFRA is insensitive to the variable packet traffic.

4.3.2 Influence of the packet duration

In this section, we assess the impact of the packet duration on the gain variations.

Figure 4-6 presents the results when the packet duration is 100 µs and when the unclamped DFRA is operated in the small-signal regime. As with a packet duration of 25 µs, P_{avg} of the probe channel is equal to -14 dBm. We also notice that the packet duration does not influence the evolution of the parameters means and variances with σ_{in}. These observations are also valid for the GC-DFRA fed by packets 100 µs in duration [Fig. 4-7].

Except for the mean of P_{avg}, the mean and variance of all parameters are increased when the packet length is increased. For example, for an unclamped amplifier, the peak-to-peak gain variation increases from 0.0244 to 0.0368 dB (for σ_{in} = 50%) when the packet duration is increased from 25 to 100 µs. If the DFRA is gain-clamped, the peak-to-peak gain variation varies from 0.0195 to 0.0240 dB (for σ_{in} = 50%) when the packet duration is increased from 25 to 100 µs. Furthermore, the increase of the means and the variances with σ_{in} is also greater when the packet duration is increased.

Consequently, increasing the packet duration implies higher gain variations and it also scatters the distribution of those variations for both

the unclamped and GC-DFRAs. Only the mean of P_{avg} is not affected by the packet length in the small-signal regime.

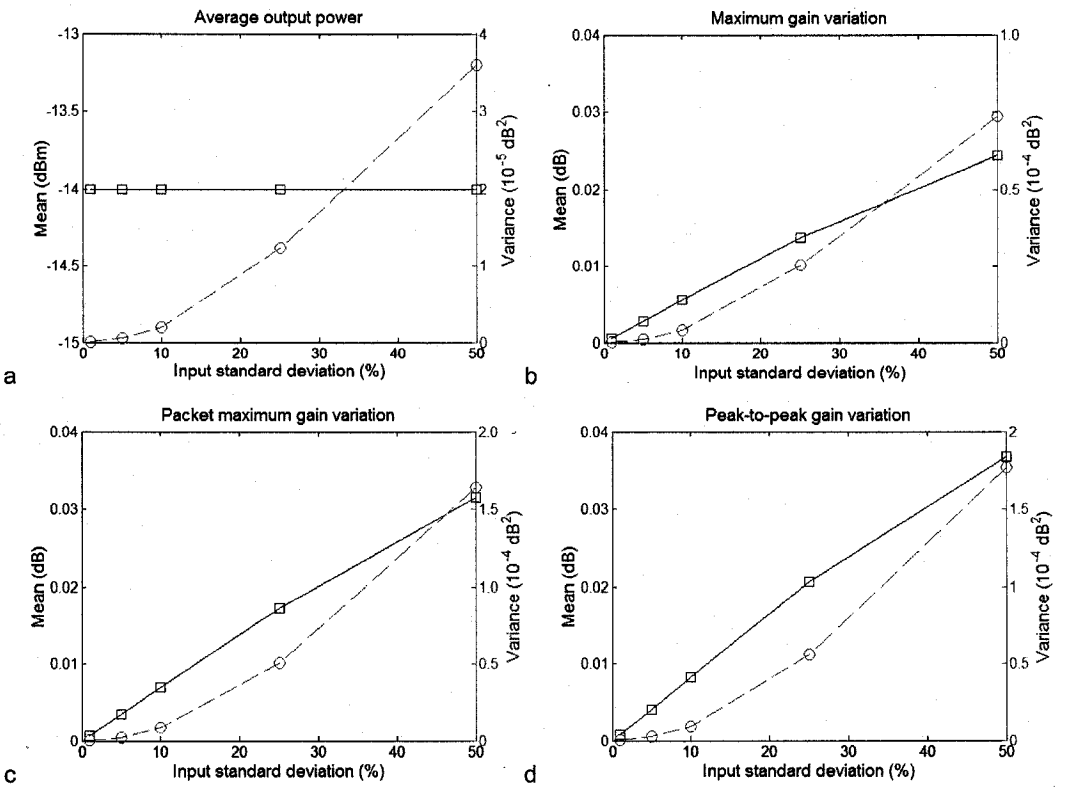

Fig. 4-6: Means (square) and variances (circle) of the comparison parameters as function of σ_{in} for the unclamped DFRA operated in the small-signal regime with packet duration of 100 µs.

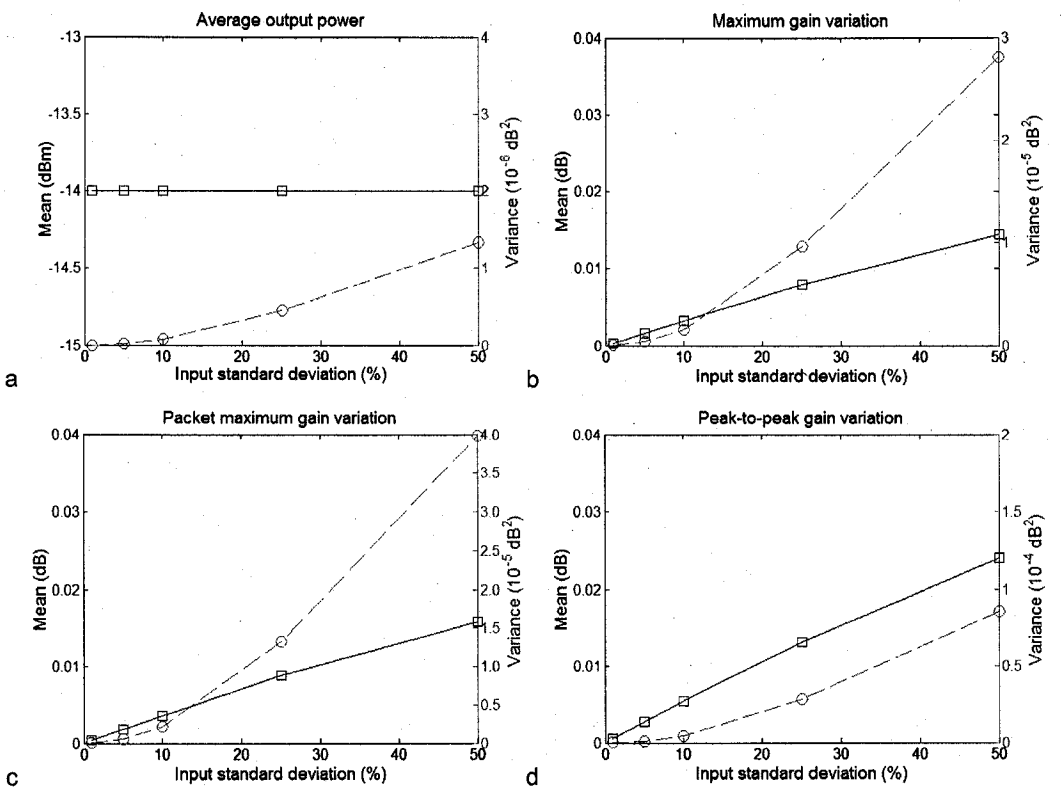

Fig. 4-7: Means (square) and variances (circle) of the comparison parameters as function of σ_{in} for the GC-DFRA operated in the small-signal regime with packet duration of 100 µs.

4.3.3 Influence of the operational mode of the amplifiers

In this section, we increase the operational regime of the DFRAs and we compare the results to those obtained in the two previous sections. The amplifiers are operated in the critical minus 3 dB regime i.e. the per signal input power is set at -20.7 dBm before launching the packets of varying powers. The Gaussian distribution for the input power of the packets has a mean value of -20.7 dBm and σ_{in} is varied from 1 to 50% of the mean value as before. We apply these conditions to the unclamped and gain-clamped DFRAs and Figs. 4-8 and 4-10 presents the means and the variances of the different comparison parameters distributions for the unclamped DFRA. The results of the GC-DFRA operated in the critical minus 3 dB regime are presented in Figs. 4-9 and 4-11.

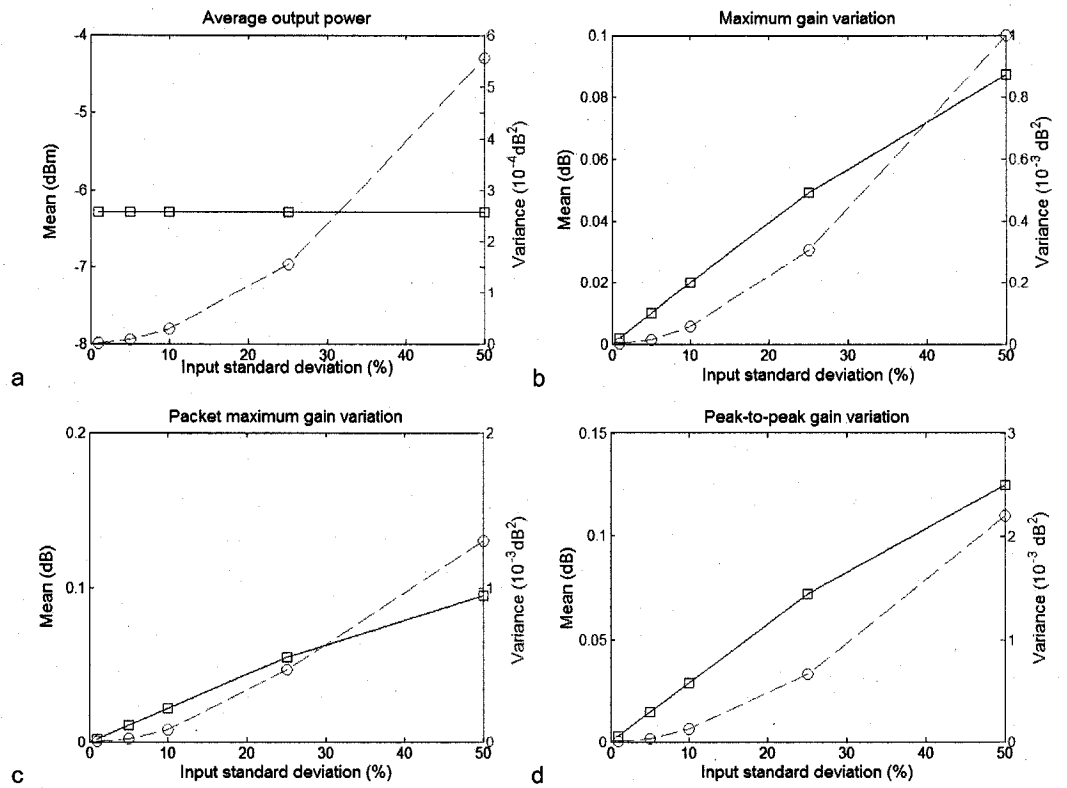

Fig. 4-8: Means (square) and variances (circle) of the comparison parameters as function of σ_{in} for the unclamped DFRA operated in the critical minus 3 dB regime with packet duration of 25 µs.

Figures 4-8 and 4-9 present the results when the packet length is 25 µs and when both amplifiers are operated in the critical minus 3 dB regime. The same general observations as those noticed for Figs. 4-4 and 4-5 can be made. The increase of the amplifiers operational mode results in an increase of the mean and variance of all of the comparison parameters. This increase can be estimated to be at least one order of magnitude. For example, when the DFRA is unclamped, the distribution of ΔG_{pp} has a mean of 0.0056 dB in the small-signal regime for σ_{in} = 10%. If the amplifier is operated in the critical minus 3 dB regime, ΔG_{pp} presents a mean of 0.0288 dB with the same conditions. The same behaviour is observed for the gain-clamped amplifier.

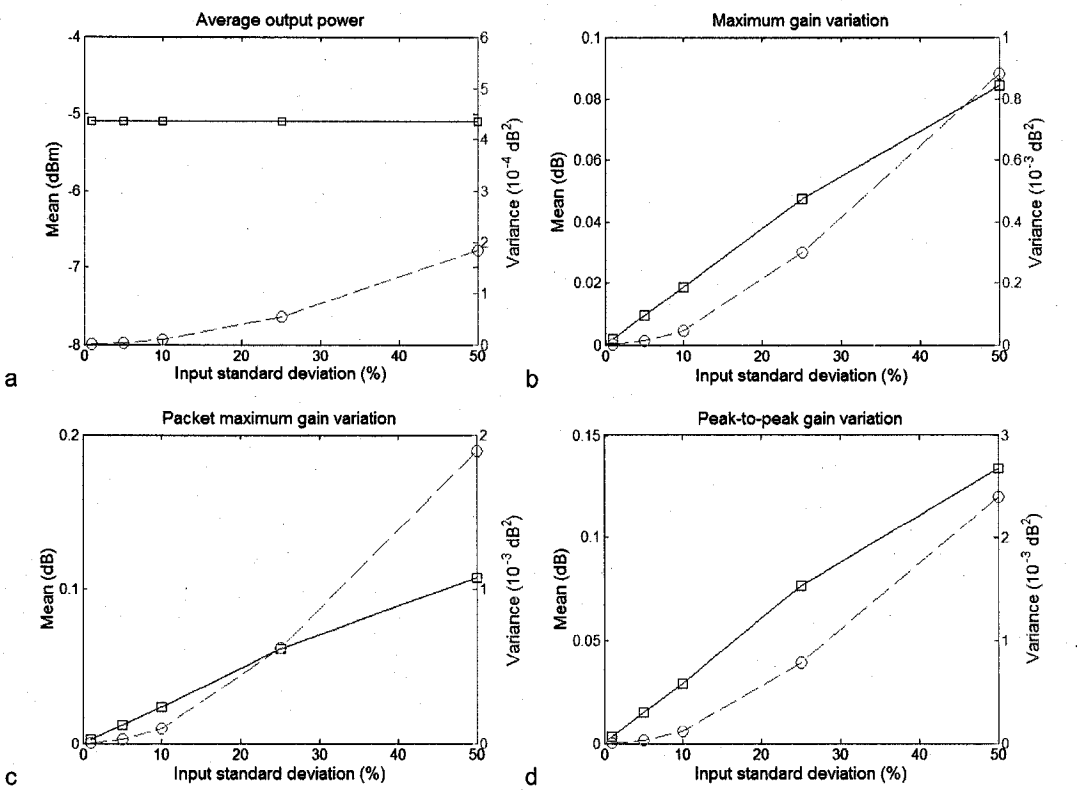

Fig. 4-9: Means (square) and variances (circle) of the comparison parameters as function of σ_{in} for the GC-DFRA operated in the critical minus 3 dB regime with packet duration of 25 μs.

However, some major behaviours are changed by increasing the operational regime of the amplifiers. The first notable observation is about the mean of P_{avg}. As in the small-signal regime, the gain-clamping technique has no effect on this parameter, in the critical minus 3 dB regime, the GC-DFRA presents a lower mean than that of the unclamped amplifier. The gain-control technique also reduces the scattering of P_{avg} as it reduces the variance of its distribution.

The second difference with the small-signal regime concerns the efficiency of the gain-clamping technique. As the GC-DFRA presents the smallest mean and variance for the different excursions in the small-signal regime, the situation is different when the operational regime is increased. When σ_{in} = 1%, the unclamped DFRA presents the lowest excursions and the

least scattering of those excursions. The GC-DFRA is totally inefficient in controlling the gain transients. When σ_{in} is increased to 5, 10, 25 or 50%, the same scenario is repeated for the distributions of ΔG_{pp} and ΔG_{packet}. However for those values of σ_{in}, the GC-DFRA presents the lowest mean and variance for ΔG_{max}. When the amplifier is gain-clamped, the mean of ΔG_{max} is 0.0095 dB and 0.0101 dB for σ_{in} of 5 and 10% respectively compared to 0.0185 dB and 0.0199 dB when the amplifier is unclamped. As far as gain variation is concerned, the scattering of the values is also reduced by the application of the gain-control technique.

Figures 4-10 and 4-11 present the means and the variances of the comparison parameters distributions when the packet duration is 100 µs and the amplifiers are operated in the critical minus 3 dB regime. Increasing the packet duration does not affect the mean of P_{avg} distribution. As for the 25 µs packet duration case, this value is -6.29 dBm when the DFRA is unclamped and -5.09 dBm when the amplifier is gain-clamped. All of the other parameters are increased when the packet duration is stretched. In comparison with the small-signal regime, all of the comparison parameters are increased by at least one order of magnitude and the mean of P_{avg} is different if the amplifier is gain-clamped or not.

In the critical minus 3 dB regime, the behaviour of both amplifiers depends on the packet duration time. When the packet duration is 25 µs, the gain-clamping technique is unable to control the gain transients. However, when the packet duration is increased to 100 µs, the GC-DFRA presents better transient performances in comparison to the unclamped DFRA. For σ_{in} = 1%, both gain-clamped and unclamped DFRAs present similar means of ΔG_{pp} and ΔG_{max} and the gain-clamped amplifier even offers a more scattered distribution of ΔG_{pp} as the variance is 1.90×10^{-6} dB^2 compared to 1.58×10^{-6} dB^2 for the unclamped amplifier. Nevertheless, when σ_{in} is increased to 5, 10, 25 and 50%, there is a clear difference

between the results of the unclamped and GC-DFRAs. In this situation, the gain-clamping technique is efficient to reduce the different gain variations and to reduce the scattering of those variations. However, the different excursions and their scattering that affect the unclamped DFRA operated in the critical minus 3 dB regime are low enough to be neglected. The worst gain variation is represented by ΔG_{pp} with σ_{in} equal to 50% and packet duration of 100 µs. In this case, the mean of ΔG_{pp} is 0.1699 dB, which is low enough to be neglected. The variance associated to ΔG_{pp} is the worst observed yet is still only 0.0039 dB^2.

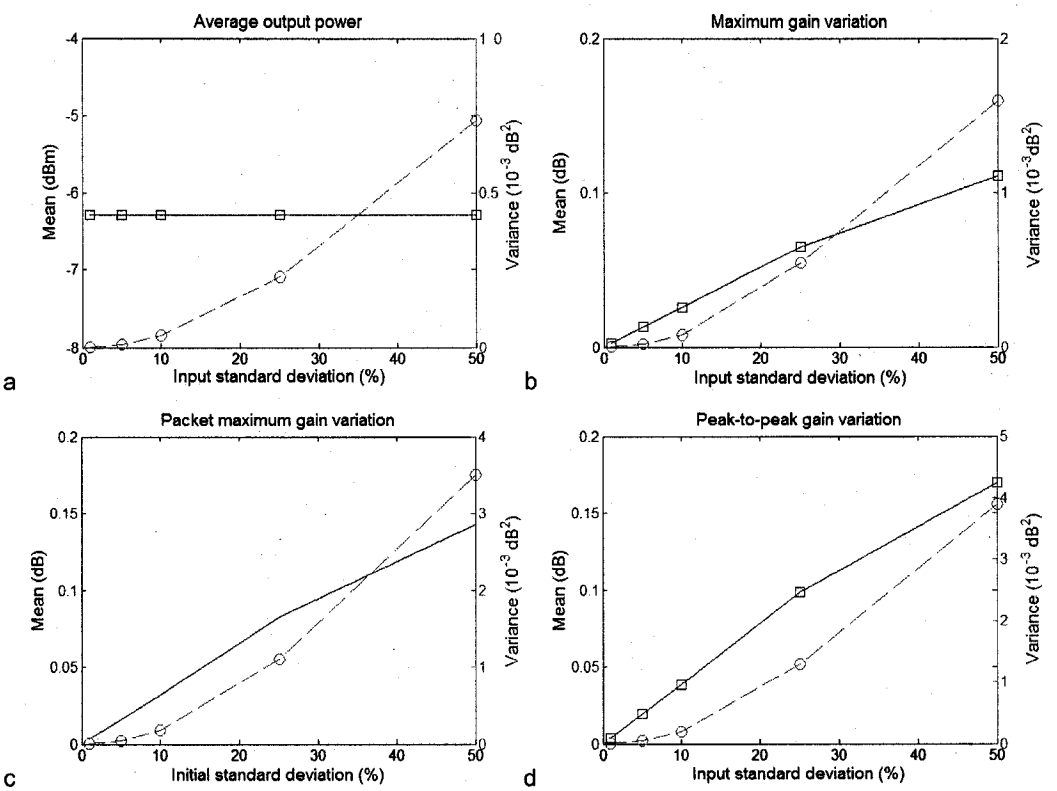

Fig. 4-10: Means (square) and variances (circle) of the comparison parameters as function of σ_{in} for the unclamped DFRA operated in the critical minus 3 dB regime with packet duration of 100 µs.

In the critical minus 3 dB regime, the gain-clamping technique is not a security of having the lowest gain variations contrary to the small-signal regime case. The efficiency of the AOGC in mitigating the gain transients

is dependent on the packet duration. For short packet duration, i.e. 25 µs, the unclamped DFRA presents the best performances in terms of gain variations. Otherwise, the evolution of parameters with the input standard deviation is the same than as in the small-signal regime and the low gain variations observed for the unclamped DFRA render unnecessary the use of the gain-clamping technique when it enables to mitigate the gain transients, i.e. when the packet duration is 100 µs,

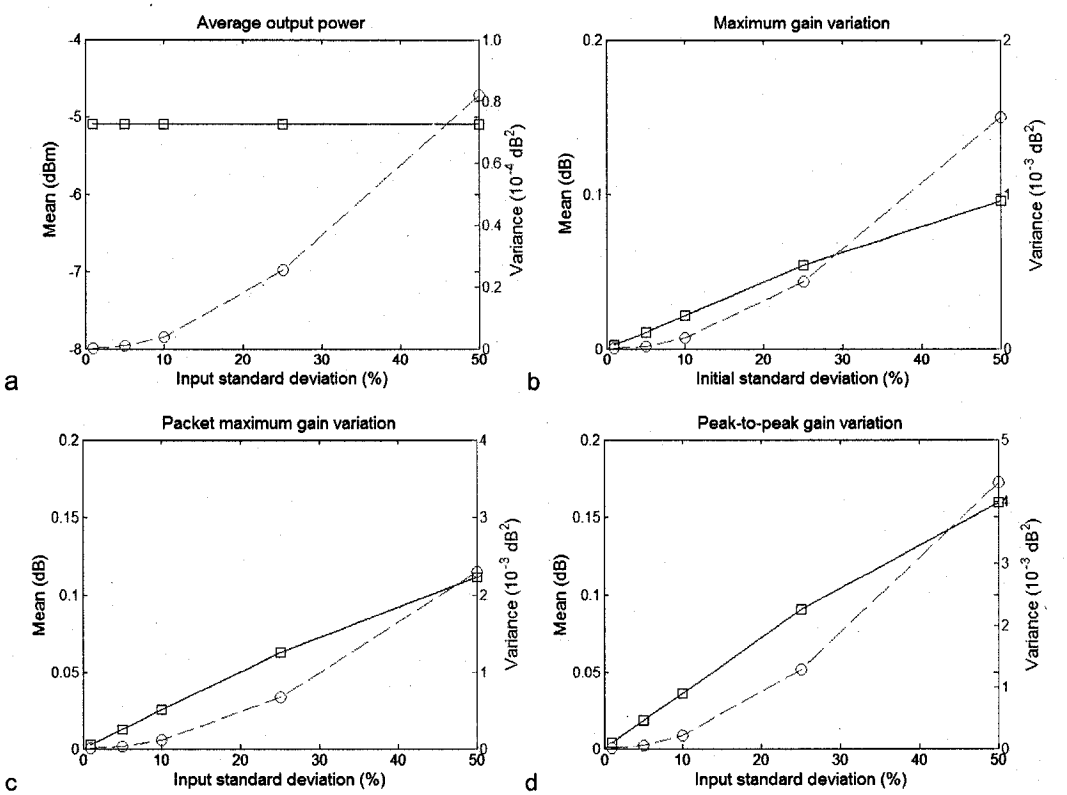

Fig. 4-11: Means (square) and variances (circle) of the comparison parameters as function of σ_{in} for the GC-DFRA operated in the critical minus 3 dB regime with packet duration of 100 µs.

4.4 Conclusion

In this chapter, we have studied the behaviour of DFRAs fed by multi-channel packet traffic. In particular, we considered at the influence of the

packet duration, the operational mode of the amplifier, and the input power distribution on the performance of both unclamped and gain-clamped amplifiers.

The results of our study show the following:

- the mean of P_{avg} is constant with the input standard deviation;
- the mean and the variance of the various excursions increase with the input standard deviation;
- in the small-signal regime, the gain-clamping technique is efficient to mitigate the gain transients and to reduce the scattering of the gain variations. However, as the different excursions and their scattering observed for the unclamped DFRA are low enough to be neglected, the gain-clamping technique is unnecessary;
- in the critical minus 3 dB regime, the efficiency of gain-clamping is dependent on the packet duration. As in the small-signal regime, even when the gain-clamping technique enables the mitigation of the gain transients, its use is not necessary as the gain variations of the unclamped DFRA are small enough to be neglected.

Our study shows that gain-clamping is not required to control the gain transients for single DFRAs fed by multi-channel packet traffic. However, in-line fiber amplifiers are usually used in cascades, which amplifies the gain transients [19] (this topic will also be addressed in the following chapter). Thus, we expect that the gain transients caused by multi-channel packet traffic will increase with the number of amplifiers in a cascade and will require some form of gain control.

Chapter 5: Transient characteristics of cascaded DFRAs

5.1 Introduction

In this chapter, we theoretically analyse the dynamic response of 9 different cascades of DFRAs. As the studies described in section 2.3.3 consider only 3 cases of cascades, i.e. a cascade of all unclamped DFRAs, a cascade of all GC-DFRAs, and a cascade where only the first DFRA is gain-clamped with the propagation of the lasing signal through the other DFRAs of the cascade—we consider cascades of mixed unclamped and GC-DFRAs. The gain-clamping is an efficient technique to mitigate the power transients but it presents the disadvantage of being pump power consuming. Thus, gain-clamping each amplifier of the cascade or gain-clamping the first amplifier and letting the lasing signal propagate through the cascade requires a lot of pump power. The results of our study are used to determine the important question of whether or not it is necessary to gain-clamp each DFRA of the cascade to control the transients within tolerable limits. The ability to control the transients using only a few properly placed GC-DFRAs would present the advantage of reducing the total pump power required in the cascade.

We consider a 64-channel system in which all of the channels except one are modulated to simulate channel addition and drop. We vary the number and the position of the GC-DFRAs in the cascade to determine whether a cascade in which only a few amplifiers are gain-clamped (referred to as a mixed cascade) can be as effective as a cascade comprising all gain-clamped amplifiers for controlling the power transients within tolerable limits (for example, 1 dB). We take into account the location of the surviving channel and the operational regime of the amplifiers. Our results

show that the location of the GC-DFRAs in a mixed cascade affects the transient characteristics and that it is possible to control the transients within tolerable limits.

5.2 Simulations conditions

5.2.1 Conditions on the amplifiers

The design of the unclamped and gain-clamped amplifiers is the same as those given in section 4.2.1: each DFRA comprises 5 km of HNLF and is backward pumped using three pumps at 1435 nm, 1450 nm, and 1480 nm, which is efficient to give amplification over 25 nm. In the case of gain-clamping, again we set the lasing signal at 1625 nm to induce the least gain tilt relative to the unclamped case. The reflection coefficients of the FBGs R_1 and R_2 are both set to 0.31, which gives a feedback level high enough to ensure a reasonable gain and a large dynamic range for gain-clamped operation.

The on-off gain of the unclamped amplifier operated in the small-signal and the critical minus 3 dB regimes is presented in Fig. 4-1 (a). When the DFRA is unclamped, the on-off gain decreases as the operational regime increases. For example, the gain at 1575.2 nm in the critical minus 3 dB regime is 1.40 dB smaller that that in the small-signal regime due to the DFRA saturation. Figure 4-1 (b) presents the on-off gain of the GC-DFRA under the small-signal and the critical minus 3 dB regimes. When gain-clamping is applied, the difference between the on-off gain in the small-signal regime and that in the critical minus 3 dB regime is reduced. For example, the gain at 1575.2 nm in the critical minus 3 dB regime is only 0.18 dB smaller than that in the small-signal regime compared to a difference of 1.40 dB when the amplifier is unclamped. Each amplifier is

followed by gain flattening filter, set to provide 16 dB gain for each WDM signal when the amplifier is operated in the small-signal regime (the filter is adapted to the kind of amplifier which precedes it, i.e. unclamped or gain-clamped).

5.2.2 Conditions on the cascades

Each cascade comprises five DFRAs and each amplifier can be either unclamped or gain-clamped (see Fig. 5-1). We place a variable optical attenuator between successive amplifiers in the cascade to ensure the same per signal input power in the small-signal regime. In our case, the attenuation is set to 16 dB, which corresponds to the loss of 80 km of single mode fiber with a typical loss coefficient of 0.2 dB/km (all WDM channels are assumed to have the same loss coefficient).

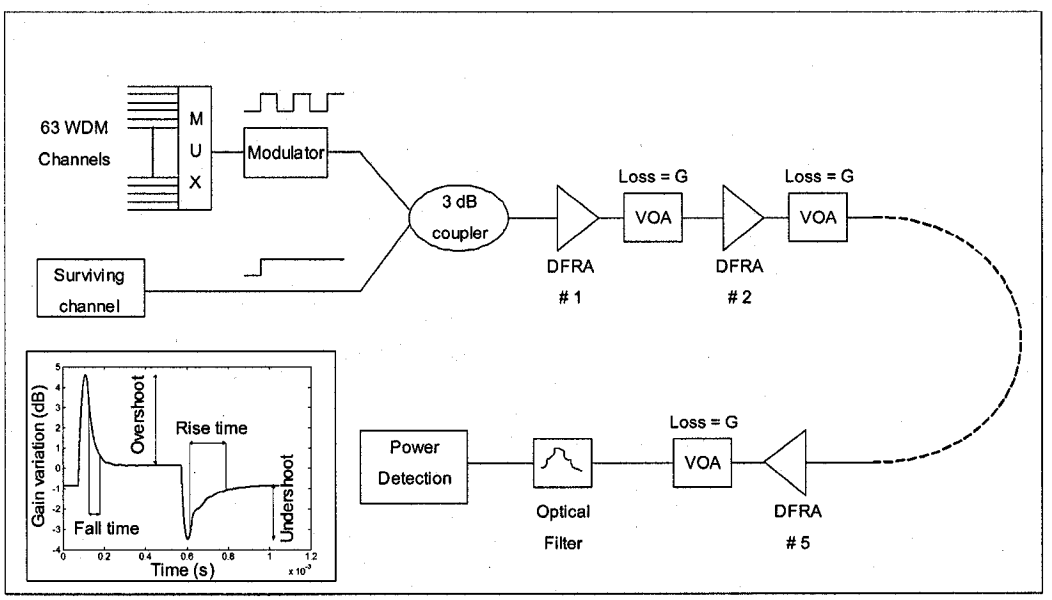

Fig. 5-1: Set-up of numerically simulated amplifier cascade. Each DFRA can be either unclamped or gain-clamped.

Since we want to determine the impact of gain-clamping in a cascade of DFRAs, we vary the number and the location of the gain-clamped

amplifiers. We successively apply gain-clamping to 1, 2, 3, and all 5 DFRAs in the cascade. The different configurations are summarized in Table 5-1.

Name	Description and order of amplifiers
Cascade 1 (all unclamped)	U-U-U-U-U
Cascade 2	U-U-U-U-**C**
Cascade3	**C**-U-U-U-U
Cascade 4	U-U-U-**C**-**C**
Cascade 5	**C**-**C**-U-U-U
Cascade 6	U-U-**C**-**C**-**C**
Cascade 7	**C**-**C**-**C**-U-U
Cascade 8	**C**-U-**C**-U-**C**
Cascade 9 (all gain-clamped)	**C**-**C**-**C**-**C**-**C**

Tab. 5-1: Composition of the different cascades. U refers to an unclamped DFRA and C to a GC-DFRA.

We consider a 64-channel system spaced by 50 GHz where the corresponding wavelength range extends from 1562.5 nm to 1588.2 nm. To simulate drop and addition operations, 63 of the 64 signals are cut (at t = 50 μs) and subsequently added (at t = 1 ms) to the first amplifier of the cascade, and we analyze the transient response for different surviving channel wavelengths, i.e. at the shortest wavelength (λ_s = 1562.5 nm), at midband (λ_m = 1575.2 nm), and at the longest wavelength (λ_l = 1588.2 nm). The different cascades are operated in the small-signal regime and in the critical minus 3 dB regime. Figure 5-2 shows a typical plot of gain as a function of per signal input power for a channel located at midband for the GC-DFRA. Using Fig. 5-2, we fix the critical per signal input power at -17.9 dBm. Thus, for the small-signal regime, the per signal input power chosen at the input to the cascade is -30 dBm, and for the critical minus 3 dB regime, the per signal input power is -20.9 dBm.

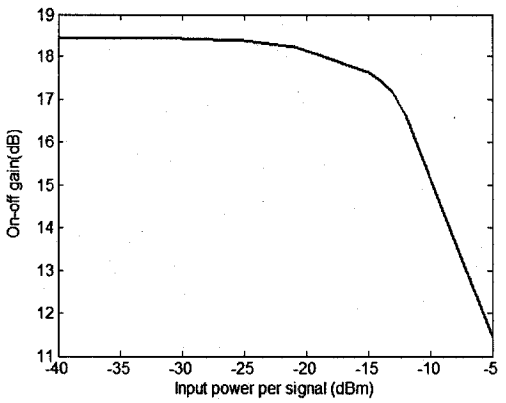

Fig. 5-2: On-off gain of the GC-DFRA as a function of per signal input power (λ_m = 1575.2 nm) at the output of the amplifier before the gain-flattering filter.

5.2.3 Framework of the simulations

One of our main objectives is to determine if each amplifier in the cascade must be gain-controlled to mitigate the transients. Thus, we compare the dynamic responses of the different cascades using the same parameters as those defined in Chapter 3: peak gain excursions (i.e. overshoot and undershoot), rise time following an undershoot, fall time following an overshoot, and steady-state gain variation ΔG, see Fig. 3-2 for an illustration of these parameters. The peak gain excursion is defined as the difference (in dB) between the gain at the peak following the drop (overshoot) or the addition (undershoot) of channels and the gain of the next steady-state. The rise and fall times represent the time taken to pass between the 10% and 90% values of the gain excursions that follow the drop or addition of channels. The steady-state gain variation ΔG is the difference between the gain of the surviving channel in the case where all channels are input to the cascade and the case where the surviving channel is the only input signal.

We set Cascade 1 (all unclamped DFRAs) and Cascade 9 (all GC-DFRAs) as the reference cascades. Cascade 1 represents the case of a cascade with no gain control where the steady-state gain variations will be

the largest and Cascade 9 represents the cascade with the maximum control in terms of steady-state gain variation. We compare the cascades comprising 1, 2, or 3 GC-DFRAs to the reference cascades to determine whether or not each amplifier needs to be gain-clamped in order to control the transients within a specific tolerance. In the present study, we define the tolerance of the maximum steady-state gain variation and of the over or undershoot that occur in a cascade of mixed amplifiers to be 1 dB and 0.25 dB respectively.

5.3 Simulations results

We begin by examining the transients for a surviving channel located at midband (λ_m = 1575.2 nm). Next, we analyze the influence of the surviving channel location on the transient characteristics. Finally, we consider the evolution of the fall and rise times after each DFRA in a cascade.

5.3.1 Study of cascades comprising 1 GC-DFRA: Cascades 2 and 3

In this section, we investigate cascades comprising only one GC-DFRA located either at the beginning (Cascade 3) or at the end (Cascade 2).

In the small-signal regime

Figure 5-3 (a) shows the time evolution of the surviving channel gain variation at the output of amplifier cascades for operation in the small-signal regime. After the cut of channels (t = 50 µs), the surviving channel experiences a steady-state gain variation (due to the increase in available pump power) which can be reduced by introducing gain-clamping. However, this reduction is not without consequence: as soon as one amplifier of the cascade is gain-clamped, an overshoot following the cut of channels appears. The addition of channels (t = 1 ms) is always

accompanied by an undershoot, though the surviving channel will eventually recover its original gain ($\Delta G = 0$). Note that the evolution of the gain variations for Cascades 2 and 3 are practically superimposed, showing that the location of the gain-clamped amplifier is not relevant in determining the dynamic response.

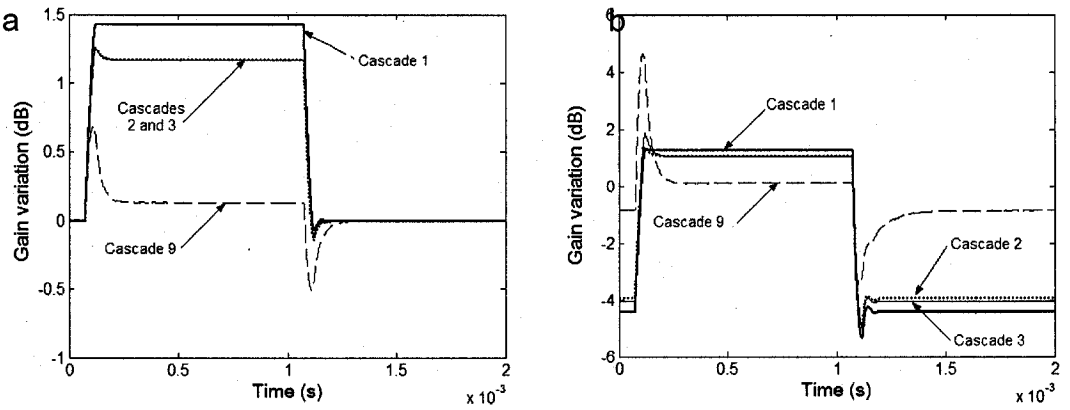

Fig. 5-3: Gain evolution of the surviving channel (λ_m = 1575.2 nm) at the output of the cascade 1, 2, 3, and 9 during the addition and cut of 63 channels in the small-signal (a) and the critical minus 3 dB (b) regimes.

Table 5-2 presents the transient characteristics of the surviving channel for these four cascades. Obviously, the largest steady-state gain variation occurs for Cascade 1 when none of the DFRAs are gain-clamped (ΔG = 1.42 dB) while the smallest variation occurs for Cascade 9 when all of the amplifiers are gain-clamped (ΔG = 0.13 dB). However, as remarked earlier, gain-clamping will result in an overshoot which, in turn, increases the fall time necessary to reach the next steady-state (from 23.6 µs for Cascade 1 to 58.6 µs for Cascade 9). A similar behaviour is observed concerning the rise time following the addition of channels (from 18.1 µs for Cascade 1 up to 73.4 µs for Cascade 9). Introducing a single gain-clamped amplifier in the cascade reduces the steady-state gain variation after the cut of channels from 1.42 to 1.16 dB. Although this reduction is not as good as that of Cascade 9, Cascades 2 and 3 have significantly smaller over and undershoots as well as a faster rise time. The over and

undershoots of these two cascades are within the specified tolerance of 0.25 dB. The fall times are only marginally longer. Thus overall, Cascades 2 and 3 have a performance that is intermediary between the reference cascades. Moreover, other than the rise times, they exhibit similar performance.

	After the cut of channels			After the addition of channels		
Cascade Configuration	Overshoot (dB)	Fall time (μs)	ΔG (dB)	Undershoot (dB)	Rise time (μs)	ΔG (dB)
Cascade 1	0.002	23.6	1.42	0.08	18.1	0
Cascade 2	0.09	59.0	1.16	0.14	37.4	0
Cascade 3	0.09	60.0	1.16	0.12	31.0	0
Cascade 4	0.19	59.1	0.91	0.22	59.2	0
Cascade 5	0.19	59.1	0.91	0.18	57.7	0
Cascade 6	0.30	59.0	0.65	0.30	65.5	0
Cascade 7	0.30	59.1	0.65	0.26	65.1	0
Cascade 8	0.30	59.0	0.65	0.28	65.3	0
Cascade 9	0.55	58.6	0.13	0.51	73.4	0

Tab.5-2: Transient characteristics of the surviving channel (λ_m = 1575.2 nm) for the cascades in the small-signal regime.

In the critical minus 3 dB regime

Figure 5-3 (b) presents the gain variation in time when the four cascades are operated in the critical minus 3 dB regime. We notice that at t = 0 s, the gain variation is not equal to 0 as in the small-signal case because the gain of each amplifier is not strong enough to compensate for the losses coming from the attenuator located between two successive DFRAs. Taking the example of Cascade 9, we notice a surviving channel gain variation of -0.88 dB at t = 0 s. This non-zero gain variation is due to the fact that the on-off gain at 1575.2 nm in the critical minus 3 dB regime is 0.18 dB smaller than that in small-signal regime (see Fig. 4-1). So, the amplifier cannot compensate for the 16 dB attenuator losses and it results

in a negative gain variation at the output of Cascade 9. As before, Cascade 9 is effective for reducing the steady-state gain variations. However, the drawbacks are even more pronounced as there are significant over and undershoots as well as a considerably longer rise time (which is required for the lasing signal to stabilize given the higher power of the WDM channels). Again, by gain-clamping one amplifier in the cascade, we can reduce the steady-state gain variations compared to Cascade 1, though these reductions are still small compared to those achieved with Cascade 9. Except for the fall times, which are even longer than that in Cascade 9, Cascades 2 and 3 offer intermediary performances between the reference cascades.

In this operational regime, the differences between Cascades 2 and 3 are more pronounced (see Table 5-3). While both offer similar steady-state gain variations following the cut or addition of channels, the over and undershoots, as well as fall and rise times are significantly different. Cascade 2 offers better characteristics after the cut of channels: a smaller overshoot (0.33 dB compared 0.82 dB) and slightly faster fall time. On the other hand, Cascade 3 is better following the addition of channels: a smaller undershoot (1 dB compared to 0.86 dB) and a much faster rise time (53 μs compared to 31 μs).

	After the cut of channels			After the addition of channels		
Cascade Configuration	Overshoot (dB)	Fall time (μs)	ΔG (dB)	Undershoot (dB)	Rise time (μs)	ΔG (dB)
Cascade 1	0.04	23.4	1.24	0.91	36.2	-4.43
Cascade 2	0.33	56.2	1.02	1.00	53.6	-3.95
Cascade 3	0.82	57.2	1.02	0.86	31.0	-4.03
Cascade 4	0.75	57.7	0.80	1.17	64.9	-3.38
Cascade 5	1.65	56.5	0.80	0.92	66.0	-3.53
Cascade 6	1.38	57.4	0.57	1.46	80.1	-2.70
Cascade 7	2.53	54.8	0.57	1.16	111.5	-2.89
Cascade 8	1.91	56.3	0.57	1.32	99.6	-2.79
Cascade 9	4.51	51.8	0.11	2.60	176.6	-0.87

Tab. 5-3: Transient characteristics of the surviving channel (λ_m = 1575.2 nm) for the cascades in the critical minus 3 dB regime.

Figure 5-4 presents the lasing signal in time at the output of the first DFRA of cascade 3 under the small-signal and the critical minus 3 dB regimes. The time evolution of the lasing signal has the same behaviour than that of the surviving channel. The lasing signal power increases after the cut of channels as more pump power is available and it comes back to its initial value when the channels are added. The cut and the addition of channels are followed by oscillations for the lasing signal power. These oscillations increase in time and in amplitude with the operational regime which leads to longer rise and fall-times for the surviving channel.

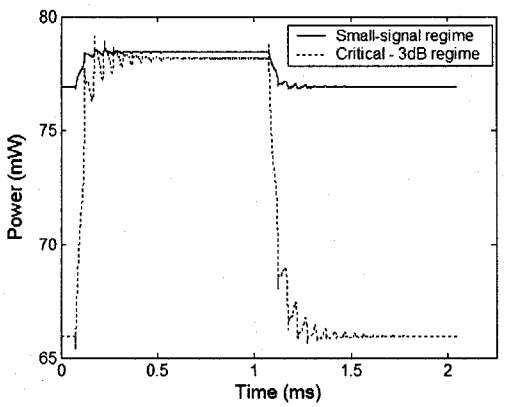

Fig. 5-4: Time evolution of the lasing signal at the output of the first DFRA of Cascade 3.

5.3.2 Study of cascades comprising 2 GC-DFRAs: Cascades 4 and 5

We now investigate cascades comprising two GC-DFRAs. The gain-clamped amplifiers are located either at the last two positions in the cascade (Cascade 4) or at the first two positions at the beginning of the cascade (Cascade 5).

In the small-signal regime

Figure 5-5 (a) presents the gain variations in time for Cascades 1, 4, 5, and 9 in the small-signal regime. As before, the mixed cascades have performances somewhere between those of the reference cascades. By using two gain-clamped amplifiers in the cascade, we can obtain even better control of the steady-state gain variation after the cut of channels, which is now below 1 dB and represents a reduction of 0.25 dB compared to using only one gain-clamped amplifier. While the over and undershoots and the rise time are now greater, they are still better than for Cascade 9. However, the over and undershoots are still within our specified limits.

As deduced from Table 5-2, Cascades 4 and 5 have the same transient performances after the cut of channels: an overshoot of 0.19 dB, fall times of 59.1 µs, and steady-state gain variations of 0.91 dB. However, after the

addition of channels, Cascade 5 in which the GC-DFRAs are placed at the beginning, offers a lower undershoot (0.18 dB) and the shorter rise time (57.7 μs). This trend is similar to that observed for cascades comprising one gain-clamped amplifier.

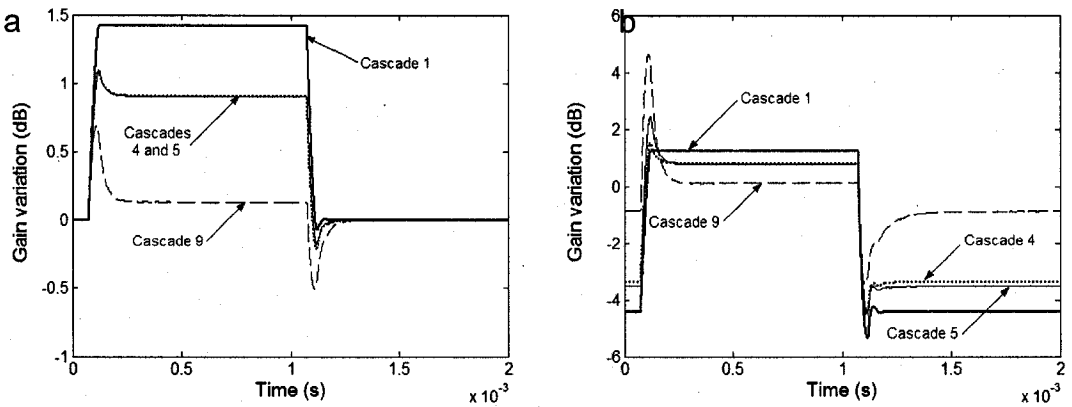

Fig. 5-5: Gain evolution of the surviving channel (λ_m = 1575.2 nm) at the output of the cascade 1, 4, 5 and 9 during the addition and cut of 63 channels in the small-signal (a) and the critical minus 3 dB (b) regimes.

In the critical minus 3 dB regime:

Cascades 4 and 5 offer the same steady-state gain variation after the drop of channels (0.80 dB) and also exhibit similar rise and fall times, see Fig. 5-5 (b). Cascade 4 offers a lower overshoot of 0.75 dB compared to 1.65 dB in the case of Cascade 5. However, this situation is reversed after the addition of channels where Cascade 5 has an undershoot of 0.92 dB compared to 1.17 dB for Cascade 4. Since the rise and fall times are comparable, the best control of the gain variation is achieved when the gain-clamped amplifiers are located at the end of the cascade, i.e. Cascade 4.

Table 5-3 shows that the steady-state gain variations for Cascades 4 and 5 are smaller compared to Cascades 2 and 3. However, while ΔG is less than 1 dB after the cut of channels, it is still too large following the addition

of channels (-3.38 dB and -3.53 dB for Cascades 4 and 5, respectively). Nevertheless, in terms of over and undershoots, they are superior to what is obtained in Cascade 9. With respect to the fall times, those of Cascades 4 and 5 are slightly longer than Cascade 9 but the rise times are significantly shorter (65 µs compared to 176.6 µs).

5.3.3 Study of cascades comprising 3 GC-DFRAs: Cascades 6, 7 and 8

In this section, we examine the performances of Cascades 6, 7 and 8 that comprise three GC-DFRAs located at different positions. In Cascade 6, the gain-controlled amplifiers are located at the beginning of the cascade while they are located at the end in Cascade 7. In Cascade 8, they are distributed uniformly along the cascade (they are located at positions 1, 3, and 5).

In the small-signal regime:

As in the previous cases for the small-signal regime, it is impossible to distinguish the curves corresponding to the gain variations in time for the different mixed cascades, see Fig. 5-6 (a). From Table 5-2, the three mixed cascades offer the same characteristics after the cut of channels: an overshoot of 0.30 dB, fall times of 59.0 µs, and steady-state gain variations of 0.65 dB. After the addition of channels, the results are only slightly different with Cascade 7 providing the lowest undershoot and fastest rise time.

Compared to Cascades 1 – 5, as expected, the presence of three GC-DFRAs enables us to decrease the steady-state gain variation even further at the expense of larger overshoots and longer fall times. The over and undershoots now exceed the maximum tolerable limit of 0.25 dB.

However, compared to Cascade 9, the over and undershoots are smaller and the rise times are shorter. The fall times are still longer.

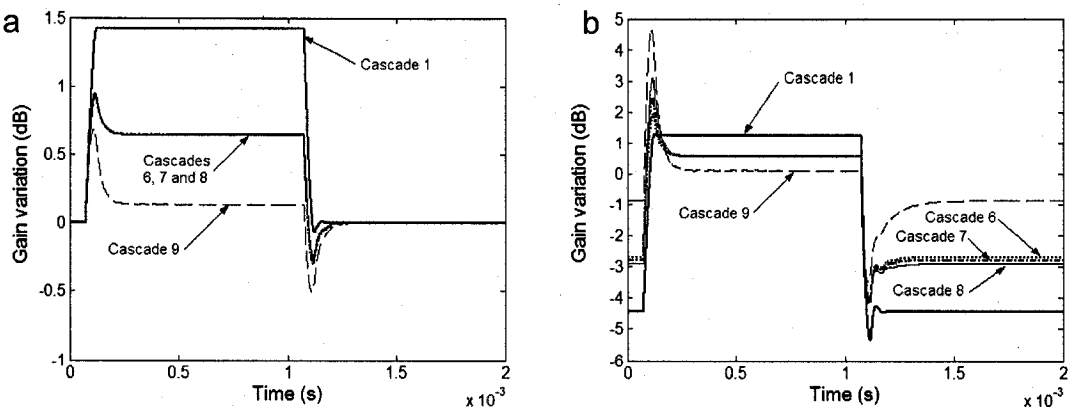

Fig. 5-6: Gain evolution of the surviving change (λ_m = 1575.2 nm) at the output of the cascade 1, 6, 7, 8 and 9 during the addition and cut of 63 channels in the small-signal (a) and the critical minus 3 dB (b) regimes.

In the critical minus 3 dB regime:

In this regime, the three mixed cascades present the exact same steady-state gain variation (0.57 dB) after the cut of channels and very similar fall times of ≈ 56 µs. The main difference is the overshoot. The largest overshoot (2.53 dB) is obtained with Cascade 7 while the smallest one (1.38 dB) is achieved with Cascade 6, see Fig. 5-6 (b). After the addition of channels, the best results are shared between Cascade 6 (rise time of 80.1 µs and steady-state gain variation of -2.70 dB) and Cascade 7 (undershoot of 1.16 dB). Cascade 8 presents intermediary transient characteristics. These mixed cascades have steady-state gain variations after the cut of channels that are smaller than cascades with less than two gain-clamped amplifiers; however, the values are still high compared to Cascade 9 (though well within our 1 dB tolerance limit). The over and undershoots are considerably smaller than those of Cascade 9. As in the case of the other mixed cascades, the fall times are longer than Cascade 9 while the rise times are intermediary between those of Cascades 1 and 9.

5.3.4 Analysis

In a dynamic network, the key point is to mitigate the overshoots, undershoots, and steady-state gain variations, or at least control them within tolerable limits. To obtain the least variation, it is preferable to gain-clamp each amplifier of the cascade but in so doing, we introduce huge over and undershoots, especially in the critical minus 3 dB regime. In the small-signal regime, gain-clamping only two amplifiers of the cascade allows us to maintain the gain variation below 1 dB; moreover, the over and undershoot remain below 0.25 dB. The use of a mixed cascade does not affect the fall time, which is approximately the same as that of a cascade of all gain-controlled DFRAs, but the rise time increases with the number of gain-clamped amplifiers. Depending on the network requirements, the use of a mixed cascade can be interesting as it reduces the over and undershoots.

In the small-signal regime, the location of the gain-clamped amplifiers in a mixed cascade does not influence the steady-state gain variation. However, placing the gain-controlled amplifiers at the beginning of the cascade allows us to reduce the undershoot and the rise time after the addition of channels. On the contrary, in the critical minus 3 dB regime, the steady-state gain variation after the addition of channels is smaller when the GC-DFRAs are located at the end.

5.3.5 Influence of the surviving channel location

We are also interested in the influence of the surviving channel location on the steady-state gain variation and on the transient characteristics. Tables 5-4 and 5-5 present the transient characteristics when the surviving

channel is located at the shortest wavelength (λ_s = 1562.5 nm), midband (λ_m = 1575.2 nm), and at the longest wavelength (λ_l = 1588.2 nm) for Cascade 9 operated in the small-signal and the critical minus 3 dB regimes, respectively.

	After the cut of channels		After the addition of channels	
Surviving channel location	Overshoot (dB)	Fall time (μs)	Undershoot (dB)	Rise time (μs)
λ_s = 1562.5 nm	0.70	56.9	0.67	74.1
λ_m = 1575.2 nm	0.55	58.1	0.51	73.4
λ_l = 1588.2 nm	0.74	58.6	0.69	74.6

Tab. 5-4: Transient characteristics at the output of a gain-clamped cascade (Cascade 9) operated in the small signal regime when the location of the surviving channel varies.

In both operational regimes, the transients are worse if the surviving channel is at either extreme of the amplification bandwidth. On the other hand, when the surviving channel is located at midband, the transients are less important because the power it receives from the shorter wavelength channels is compensated by the power it gives to the longer wavelength channels.

	After the cut of channels		After the addition of channels	
Surviving channel location	Overshoot (dB)	Fall time (μs)	Undershoot (dB)	Rise time (μs)
λ_s = 1562.5 nm	5.57	54.2	4.22	188.1
λ_m = 1575.2 nm	4.51	51.8	2.60	176.6
λ_l = 1588.2 nm	5.89	52.1	3.92	184.9

Tab. 5-5: Transient characteristics at the output of a gain-clamped cascade (Cascade 9) operated in the critical minus 3 dB regime when the location of the surviving channel varies.

5.3.6 Evolution of the rise and fall times along the cascades

Cascade of homogenous amplifiers

In this section, we follow the evolution of the fall and rise times at the output of each amplifier in a homogenous cascade. Tables 5-6 and 5-7 present the results for Cascades 1 and 9 respectively, when operated in the critical minus 3 dB regime.

Amplifier location	Fall time (μs)	Rise time (μs)
Amplifier 1	24.3	23.1
Amplifier 2	23.8	32.9
Amplifier 3	23.6	34.1
Amplifier 4	23.5	35.6
Amplifier 5	23.4	36.2

Tab. 5-6: Fall and rise times of the surviving channel (λ_m = 1575.2 nm) at the output of each amplifier of an all unclamped DFRAs cascade (Cascade 1) operated in the critical minus 3 dB regime.

Amplifier location	Fall time (μs)	Rise time (μs)
Amplifier 1	59.7	109.3
Amplifier 2	57.7	124.9
Amplifier 3	55.5	140.8
Amplifier 4	53.4	164.6
Amplifier 5	51.8	176.6

Tab. 5-7: Fall and rise times of the surviving channel (λ_m = 1575.2 nm) at the output of each amplifier of an all GC-DFRAs cascade (Cascade 9) operated in the critical minus 3 dB regime.

Both cascades exhibit the same behaviour concerning the evolution of the fall and rise times as function of the number of amplifiers: the fall time

decreases and the rise time increase as the number of amplifiers in the cascade increases. We notice that the fall and rise times are much more important in Cascade 9 because the lasing signal requires time to stabilize following channel addition and drop. We also remark that the rate at which the fall times decrease is higher for Cascade 9 than for Cascade 1 while the rates at which the rise times increase are comparable for both cascades.

Cascade of mixed amplifiers

Introducing gain-clamping changes radically the evolution of the fall and rise times. Tables 5-8 and 5-9 present the results in the critical minus 3 dB regime for Cascades 5 and 6.

When we replace the last three amplifiers of Cascade 9 by three unclamped amplifiers (i.e. Cascade 5), the evolution of the fall and rise times changes dramatically. Starting from Amplifier 3, the fall time decreases slower compared to Cascade 9 and the rise time decreases instead of increasing so that transient characteristics appear to be governed by the unclamped amplifiers. As a result, the fall and rise times tend towards the values associated Cascade 1. For this reason, the rise time, that has a huge value (124.9 μs) after the second amplifier compared to that in Cascade 1 (32.9 μs), decreases until 66 μs trying to reach the value of 36.3 μs obtained with Cascade 1.

Amplifier location	Fall time (μs)	Rise time (μs)
Amplifier 1	59.7	109.3
Amplifier 2	57.7	124.9
Amplifier 3	57.0	112.6
Amplifier 4	56.7	77.3
Amplifier 5	56.5	66.0

Tab. 5-8: Fall and rise times of the surviving channel (λ_m = 1575.2 nm) at the output of each amplifier of Cascade 5 (C-C-U-U-U) operated in the critical minus 3 dB regime.

A similar behaviour is observed for the transient characteristics of Cascade 6. In this case, the last three amplifiers of an unclamped cascade are replaced by three gain-clamped amplifiers. Starting from Amplifier 3, the fall and rise times will tend towards the values associated with an all gain-clamped cascade. As a result, the fall and rise times which present low values after the second amplifiers increase significantly as they go towards the high values of Cascade 9.

Amplifier location	Fall time (μs)	Rise time (μs)
Amplifier 1	24.3	23.1
Amplifier 2	23.8	32.9
Amplifier 3	58.6	62.1
Amplifier 4	58.1	72.3
Amplifier 5	57.4	80.1

Tab. 5-9: Fall and rise times of the surviving channel (λ_m = 1575.2 nm) at the output of each amplifier of Cascade 6 (U-U-C-C-C) operated in the critical minus 3 dB regime.

5.4 Conclusions

In this chapter, we analyzed the power transients of cascades of DFRAs in the worst possible case of transients. We considered cascades comprising

both unclamped and gain-clamped amplifiers in the worst-case scenario where all the channels except one were cut and added to the first amplifier of the cascade. We took into account the operational regime of the amplifiers, the location of the GC-DFRAs in cascades of mixed amplifiers, and the location of the surviving channel. Our results show that Cascades 2 – 8 have a performance in between those of Cascades 1 and 9 as expected, and that it is possible to maintain the steady-state gain variation and the over and undershoots within predefined tolerance limits (in our case, 1 dB and 0.25 dB respectively) by gain-clamping only two amplifiers in a cascade of 5 DFRAs. This approach enables a reduction of 0.69 W for the total pump power compared to a cascade of all GC-DFRAs which implies a cost reduction and it also presents the advantage of reducing the over and undershoots compared to those observed in the case of a cascade of all GC-DFRAs. We also found that the location of the surviving channel is of importance. In particular, the transients are less important for channels located at midband than for the channels at the extremities. Finally, concerning cascades of mixed amplifiers, we established that locating the gain-clamped amplifiers at the end of the cascade allows us to reduce the steady-state gain-variation after the addition of channels. The evolution of the fall and rise times along the mixed cascade can present different behaviours and the fall and rise times tend to reach the value of a homogenous cascade constituted of the type of amplifier located at the end of the mixed cascade. These results should be useful in determining the requirements of DFRAs for use in AAPNs.

Chapter 6: Transient characteristics of hybrid amplifiers

6.1 Introduction

A hybrid amplifier is defined as the association of at least two amplifiers using different amplification technologies. A wide diversity exists in terms of hybrid amplifiers and numerous combinations are possible such as hybrid EDFA/Brillouin amplifier [76], EDFA/fiber optical parametric amplifier (FOPA) [77], EDFA/Thulium-doped fiber amplifier (TDFA) [78-79], EDFA/Ytterbium-doped fiber amplifier (YDFA) [80], FRA/FOPA [81-83], FRA/SOA [84], FRA/TDFA [85-87] and EDFA/FRA. Such associations between different amplification technologies have been studied in order to increase the amplification bandwidth, the amplification gain or to improve the noise performances.

Hybrid FRAs/EDFAs are an enabling and promising technology for future DWDM multi-terabit systems as it has been shown in recent publications [88-91]. They were studied so as to improve their noise performances [92-93], to maximize their gain profile [94-97] or to increase the maximum reachable distance [98]. They have also been used to compensate for dispersion [99]. The gain transients occurring FRAs/EDFAs were analyzed in a few studies [100-105]. In this thesis, we define a hybrid fiber amplifier (HFA) as a cascade of in-line amplifiers based on different technologies, for example a cascade of one DFRA and one EDFA.

In this chapter, we propose to investigate the gain transients that occur in HFAs in the worst-case scenario of channel addition and drop. Contrary to our previous studies that involved 32 or 64 WDM channels, in this case, we only consider a system involving 4 WDM channels for computational

reasons. In particular, we analyze the possibility of mitigating the gain transients by the use of the AOGC technique. In our study, we take into account the number of gain-clamped amplifiers in the HFA and their location. We also consider the impact of the surviving channel location in the amplification band on the transient characteristics. Figure 6-1 presents the set-up of the numerically simulated HFAs and the framework of the simulations.

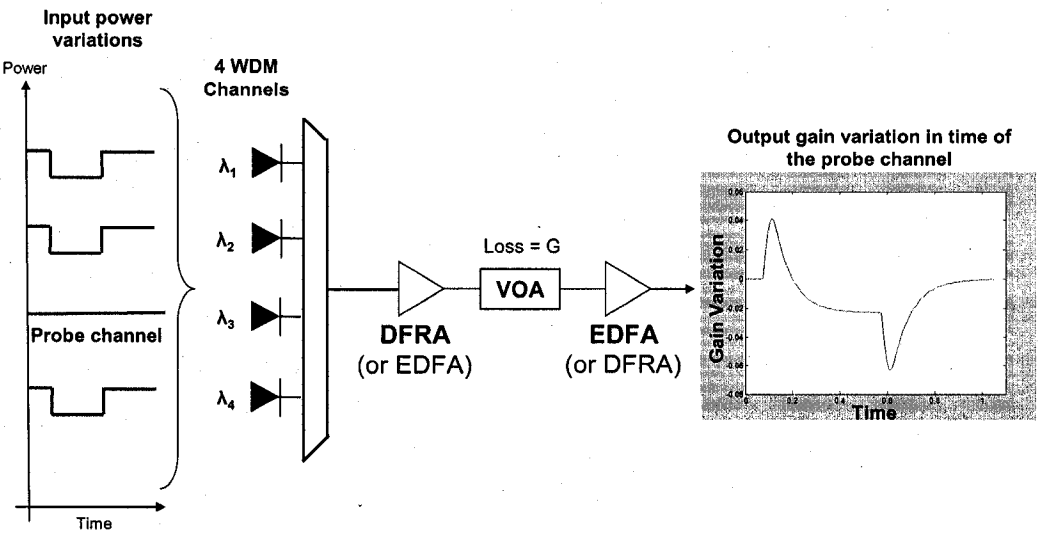

Fig. 6-1: Set-up of numerically simulated HFA. Each amplifier can be either unclamped or gain-clamped.

6.2 Simulations conditions

6.2.1 Conditions on the amplifiers

Each HFA is constituted of an EDFA and a DFRA. The DFRA comprises 5 km of HNLF and is backward pumped (to avoid any polarization dependence of Raman gain) using one pump at 1450.5 nm. The EDFA is pumped at 980 nm and comprises 20.6 m of Erbium-doped fiber (EDF) which has the following characteristics:

- Erbium metastable lifetime: 10 ms;

- numerical aperture: 0.25;
- Erbium ion density: 4×10^{-24} m^{-3};
- core radius: 1.5 μm;
- Erbium doping radius: 1.4 μm.

To induce the least gain tilt relative to the unclamped case, the lasing signal is located at 1669.5 nm for the GC-DFRA and at 1530 nm for the GC-EDFA. The standing-wave AOGC technique is applied to both GC-EDFAs and GC-DFRAs. We consider a 4-channel system spaced by 400 GHz where the corresponding wavelength range extends from 1550 nm to 1559.7 nm in the C-band. OptiSystem® of Optiwave was used to simulate the dynamic behaviour of EDFAs.

In order to carry out a fair study of the different HFAs, the unclamped and gain-clamped EDFAs and DFRAs in the HFAs must offer similar on-off gain spectra in the small-signal regime. We also decided to design the gain-clamped amplifiers so that the GC-EDFAS and GC-DFRAs have the same critical power. In addition to these particular design criteria, we decided to fix the lengths of the HNLF and of the EDF, the lasing signal wavelengths and the pump wavelengths. By adjusting the pumps power and the FBGs reflection coefficients, it is possible to obtain a GC-DFRA and a GC-EDFA that present the same on-off gain in the small-signal regime and the same critical power. We target a 16 dB gain in the small-signal regime. This is achieved by setting the pump at 0.25 W and both FBG reflection coefficients at 44.3 % for the DFRA and the pump at 27.5 mW and both FBG reflection coefficients at 31 % for the EDFA. Figure 6-2 shows the on-off gain of the GC-DFRA and the GC-EDFA as function of the per channel input power after a gain flattening filter for the WDM channel located at 1553.2 nm. We notice that both amplifiers offer a 15.5 dB gain for a per channel input power of -11.2 dBm (the per-channel critical power). As the per channel increases, we note that the GC-DFRA

gain decreases smoothly contrary to that of the GC-EDFA. As a result, less input power is necessary to saturate the GC-EDFA in comparison to the GC-DFRA.

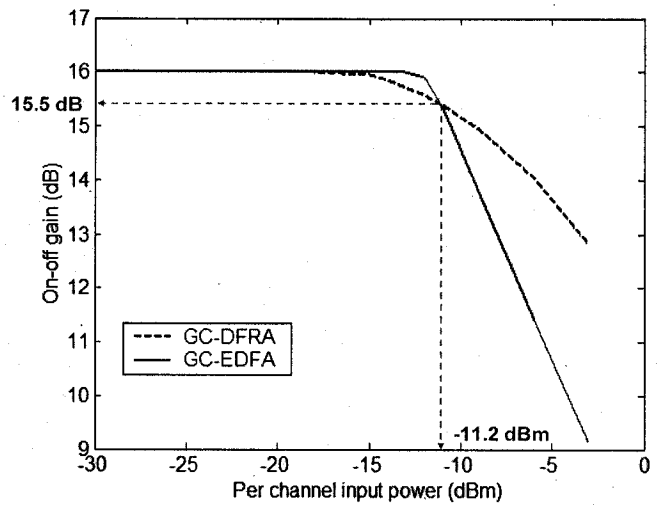

Fig. 6-2: On-off gain of the GC-DFRA and the GC-EDFA as function of the per channel input power after a gain flattening filter for the WDM channel located at 1553.2 nm.

Keeping the same amplifier lengths and pump wavelengths, by adjusting the pumps powers, we can achieve a 16 dB gain in the small-signal regime for both unclamped EDFA and DFRA. The pump power is set at 0.245 W for the unclamped DFRA and at 7.36 mW for the unclamped EDFA. Figure 6-3 presents the on-off gain of the unclamped DFRA and the unclamped EDFA as function of the per channel input power after a gain flattening filter for the WDM channel located at 1553.2 nm. We notice that the gain decreases much more with the per channel input power in the case of the unclamped EDFA rather than in the case of the unclamped DFRA.

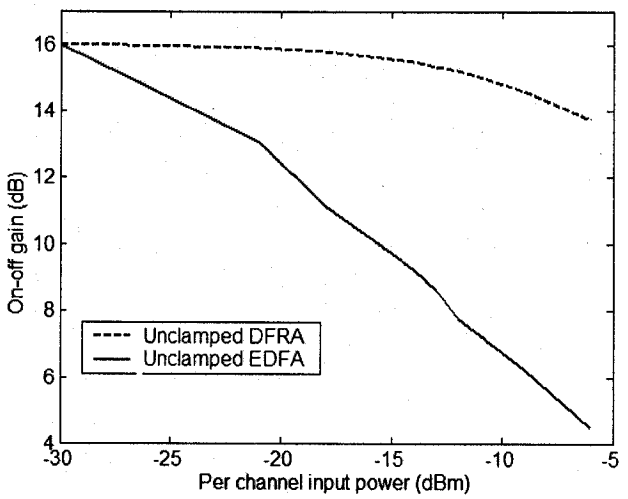

Fig. 6-3: on-off gain of the unclamped DFRA and the unclamped EDFA as function of the per channel input power after a gain flattening filter for the WDM channel located at 1553.2 nm.

6.2.2 Framework of the simulations

Each HFA comprises one EDFA and one DFRA and each amplifier can be either unclamped or gain-clamped (see Fig. 6-1). We place a variable optical attenuator between the two amplifiers to ensure the same per channel input power in the small-signal regime. In our case, the attenuation is set to 16 dB, which corresponds to the loss of 80 km of single mode fiber with a typical loss coefficient of 0.2 dB/km (all WDM channels are assumed to have the same loss coefficient).

Since we want to determine the impact of gain-clamping in a HFA, we vary the number, the location and the type of the gain-clamped amplifiers. The different configurations are summarized in Table 6-1.

We consider a 4-channel system spaced by 400 GHz where the corresponding wavelengths are 1550, 1553.2, 1556.4 and 1559.7 nm. To simulate drop and addition operations, 3 of the 4 signals are cut at t = 50 μs and subsequently added at t = 4.05 ms in the small-signal regime and

at t = 14.05 ms in the critical minus 3 dB regime, to the first amplifier of the HFA, and we analyze the transient response for the four surviving channel wavelengths. Note that the times for dropping and adding channels are different than those considered in previous chapters. The time at which the channels are added varies from a study to another one. Before adding the channels, we have to wait until the amplifier reaches its steady-state following the cut of channels. Depending on the type of amplifier, the operational regime and the use AOGC, the time it takes for the surviving channel to reach its steady-state after the cut of channels varies.

Name	Description and order of amplifiers
HFA 1 (all unclamped)	unclamped EDFA + unclamped DFRA
HFA 2 (all unclamped)	unclamped DFRA + unclamped EDFA
HFA 3	unclamped EDFA + GC-DFRA
HFA 4	GC-DFRA + unclamped EDFA
HFA 5	GC-EDFA + unclamped DFRA
HFA 6	unclamped DFRA + GC-EDFA
HFA 7 (all gain-clamped)	GC-EDFA + GC-DFRA
HFA 8 (all gain-clamped)	GC-EDFA + GC-DFRA

Tab. 6-1: Composition of the different HFAs.

The different HFAs are operated in the small-signal regime and in the critical minus 3 dB regime. The per signal input power is set at -30 dBm in the small-signal regime and at -14.2 dBm in the critical minus 3 dB regime. Figure 6-4 shows the on-off gain of the unclamped and gain-clamped EDFAs and DFRAs before the gain equalizing filter in those two operational regimes. We notice that the gain of the unclamped EDFA collapses when the amplifier is operated in the critical minus 3 dB regime [Fig. 6-4 (c)]. In comparison, the unclamped DFRA gain only decreases by around 0.5 dB between the small-signal and the critical minus 3 dB regimes [Fig. 6-4 (a)]. Increasing the operational mode implies a decrease

of around 0.2 dB in the GC-DFRA gain [Fig. 6-4 (b)] and has no impact on the GC-EDFA gain [Fig. 6-4 (d)].

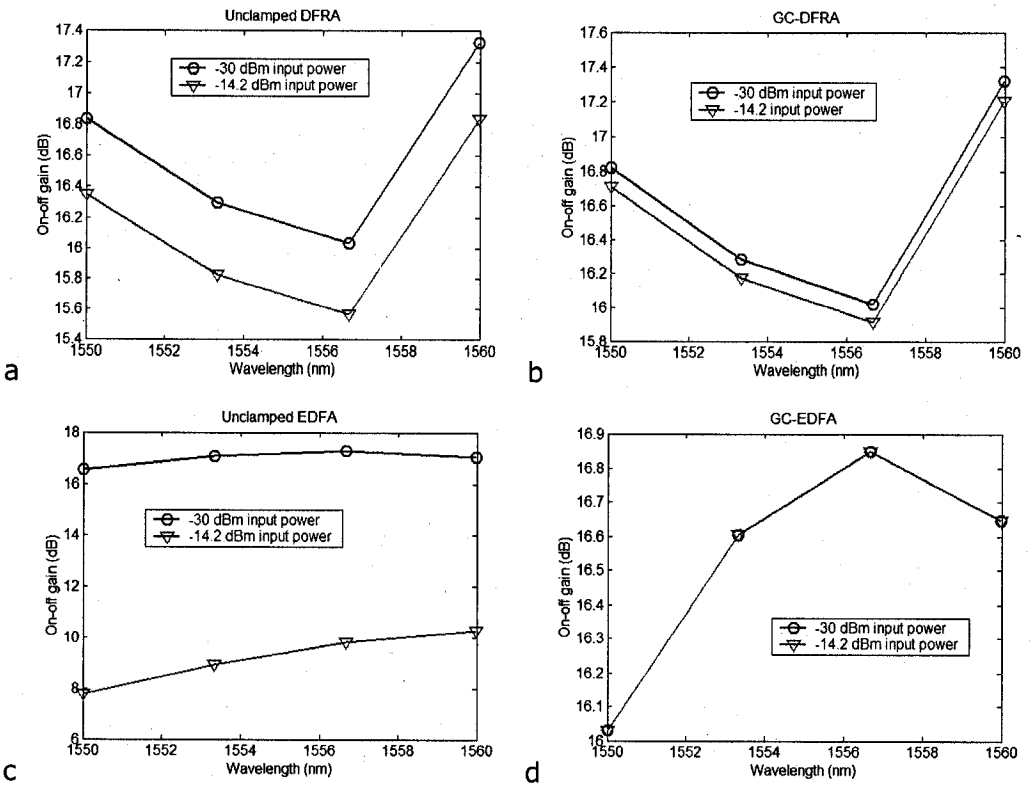

Fig. 6-4: On-off gain of the unclamped (a) and gain-clamped (b) DFRA and of the unclamped (c) and gain-clamped (d) EDFA in the small-signal and the critical minus 3 dB regimes.

6.3 Simulations results

We begin by examining the transients for a surviving channel located at λ = 1553.2 nm. We vary the number, the location and the type of the gain-clamped amplifiers within the HFAs. Finally, we analyze the influence of the surviving channel location on the transient characteristics.

6.3.1 Study of HFAs comprising no gain-clamped amplifiers: HFA 1 and 2

In this section, we investigate HFAs comprising two unclamped amplifiers. The unclamped EDFA can be located either at the first position (HFA 1) or at the second position (HFA 2).

In the small-signal regime

Figure 6-5 shows the time evolution of the surviving channel gain variation at the output of HFAs 1 and 2 for operation in the small-signal regime. After the cut of channels (t = 50 µs), the surviving channel will experience a steady-state gain variation (due to the increase in available pump power). The addition of channels (t = 4.05 ms) is also accompanied by a steady-state gain variation, though the surviving channel recovers its original gain ($\Delta G = 0$).

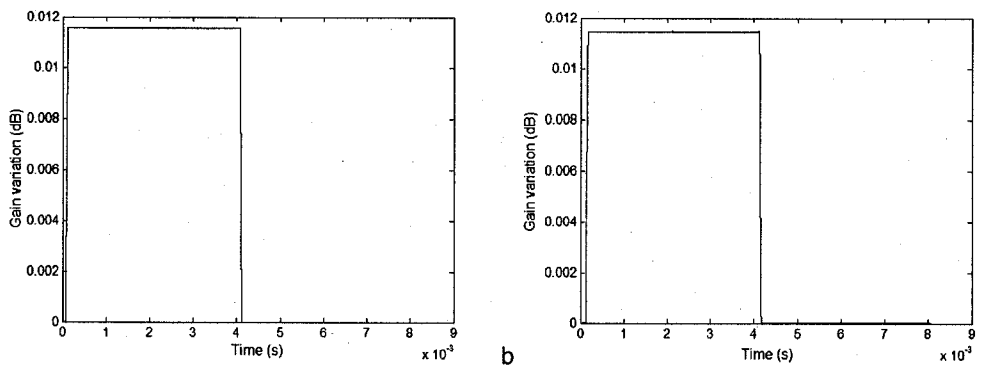

Fig. 6-5: Gain evolution of the surviving channel (λ = 1553.2 nm) at the output of the HFA 1 (a) and 2 (b) during the addition and cut of 3 channels in the small-signal regime.

Table 6-2 presents the transient characteristics of the surviving channel for the all HFAs under study in small-signal regime. We note that there is no gain transient following the addition and drop of channels, which is illustrated by over- and undershoots, and fall and rise times all equal to zero. We also notice HFAs 1 and 2 offer the same gain evolution of the

surviving channel in small-signal regime with ΔG equal to 11.6×10^{-3} dB for HFA 1 and 11.5×10^{-3} dB for HFA 2.

	After the cut of channels			After the addition of channels		
HFA Configuration	Overshoot (10^{-3} dB)	Fall time (μs)	ΔG (10^{-3} dB)	Undershoot (10^{-3} dB)	Rise time (μs)	ΔG (dB)
HFA 1	0	0	11.6	0	0	0
HFA 2	0	0	11.5	0	0	0
HFA 3	11.2	1782	0.2	10.9	1960	0
HFA 4	11.0	1696	0.3	11.0	1897	0
HFA 5	1.2	411	11.1	1.4	570	0
HFA 6	1.3	524	11.2	1.4	576	0
HFA 7	12.0	1493	-0.2	12.1	1865	0
HFA 8	12.2	1765	-0.3	12.2	1857	0

Tab.6-2: Transient characteristics of the surviving channel (λ = 1575.2 nm) for the HFAs in the small-signal regime.

In the critical minus 3 dB regime

Figure 6-6 presents the gain variation in time when the two HFAs are operated in the critical minus 3 dB regime. We notice that at t = 0 s, the gain variation is not equal to 0 as in the small-signal case because the gain of each amplifier is not strong enough to compensate for the losses coming from the attenuator located between the two amplifiers constituting the HFA. Taking the example of HFA1, we notice a surviving channel gain variation of -8.207 dB at t = 0 s. This non-zero gain variation is due to the fact that the on-off gain at 1553.2 nm in the critical minus 3 dB regime is smaller than that in the small-signal regime for both the DFRA and the EDFA (see Fig. 6-4). So, the amplifier cannot compensate for the 16 dB attenuator losses and it results in a negative gain variation at the output of HFA 1. As in the small-signal regime, HFAs 1 and 2 suffer from no over- and undershoots following the drop and addition of channels, respectively.

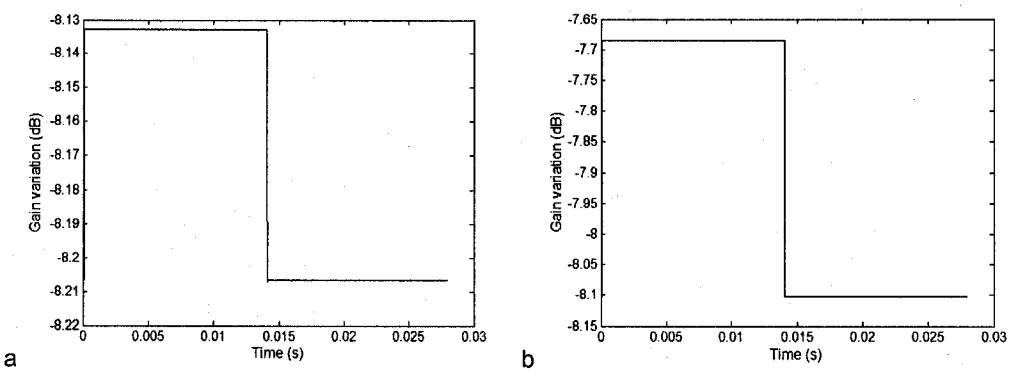

Fig. 6-6: Gain evolution of the surviving channel (λ = 1553.2 nm) at the output of the HFA 1 (a) and 2 (b) during the addition and cut of 3 channels in the critical minus 3dB regime.

In this operational regime, the differences between HFAs 1 and 2 are more pronounced (see Table 6-3). We note that ΔG is around 6 times larger when the EDFA is second (HFA 2) compared to that when it is located first (HFA 1). This difference is due to the fact that the unclamped EDFA saturates much faster with the total input power than the unclamped DFRA (see Fig. 6-3). When the channels are cut, the total input power decreases at the entry of the first amplifier, which results in a higher gain for the surviving channel. When the EDFA is first (HFA 1), the gain variation that follows the cut of channels is important because the EDFA saturates strongly with the input power, but the DFRA is able to mitigate this gain variation because it saturates slowly. When the EDFA is second (HFA 2), the gain variation produced by the unclamped DFRA is worsened by that created by the EDFA. As a result, ΔG is higher when the unclamped EDFA is located second.

	After the cut of channels			After the addition of channels		
HFA Configuration	Overshoot (dB)	Fall time (ms)	ΔG (dB)	Undershoot (dB)	Rise time (ms)	ΔG (dB)
HFA 1	0	0	0.074	0	0	-8.207
HFA 2	0	0	0.418	0	0	-8.103
HFA 3	0.08	2100	0.001	0.07	2300	-8.123
HFA 4	0.29	5433	0.116	0.26	3649	-8.279
HFA 5	0.10	484	0.370	0.09	700	-0.479
HFA 6	0.12	484	0.367	0.08	528	-0.514
HFA 7	0.38	8035	0.120	0.34	3000	-0.115
HFA 8	0.37	8028	0.115	0.33	3150	-0.151

Tab.6-3: Transient characteristics of the surviving channel (λ = 1575.2 nm) for the HFAs in the critical minus 3 dB regime.

6.3.2 Study of HFAs comprising one GC-DFRA: HFA 3 and 4

We now investigate HFAs comprising one GC-DFRA. The gain-clamped amplifier is located either at the first position in the HFA (HFA 4) or at the last position in the HFA (HFA 3).

In the small-signal regime

Figure 6-7 presents the gain variations in time for HFAs 3 and 4 in the small-signal regime. The cut of signals (t = 50 µs) is followed by an overshoot and a steady-state gain variation. The addition of channels (t = 4.05 ms) is always accompanied by an undershoot, though the surviving channel recovers its original gain (ΔG = 0). The evolution of the gain variations in time for HFAs 3 and 4 are practically superimposed, showing that the location of the gain-clamped amplifier is not relevant in determining the dynamic response.

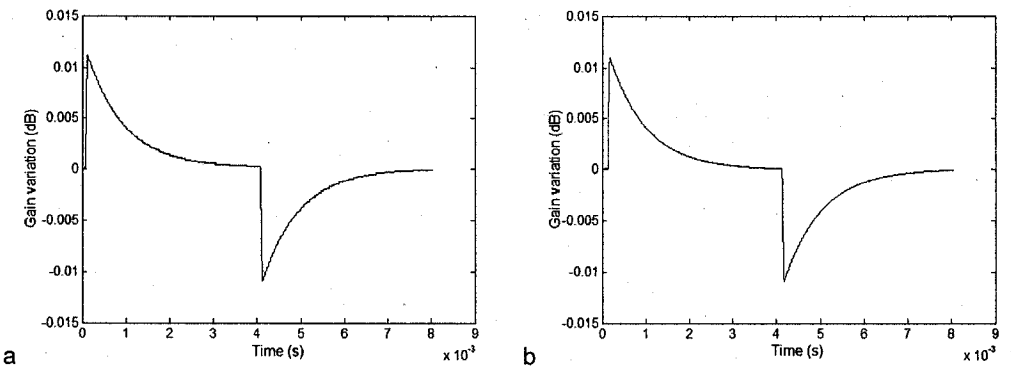

Fig. 6-7: Gain evolution of the surviving channel (λ = 1553.2 nm) at the output of the HFA 3 (a) and 4 (b) during the addition and cut of 3 channels in the small-signal regime.

From Table 6-2, we notice that HFA 3 (GC-DFRA as second amplifier) presents the worst transient performances even if all of the parameters are close between HFAs 3 and 4. However, as the difference between both configurations is slight, we cannot conclude that one HFA is superior to the other one.

In the critical minus 3 dB regime

Figure 6-8 shows the gain evolution in time of the surviving channel for HFAs 3 and 4 in the critical minus 3 dB regime. We note a difference in the behaviour of both amplifiers. HFA 3 presents a typical response of a gain-clamped amplifier and HFA 4 offers the behaviour of an amplifier in which gain-clamping is not in effect.

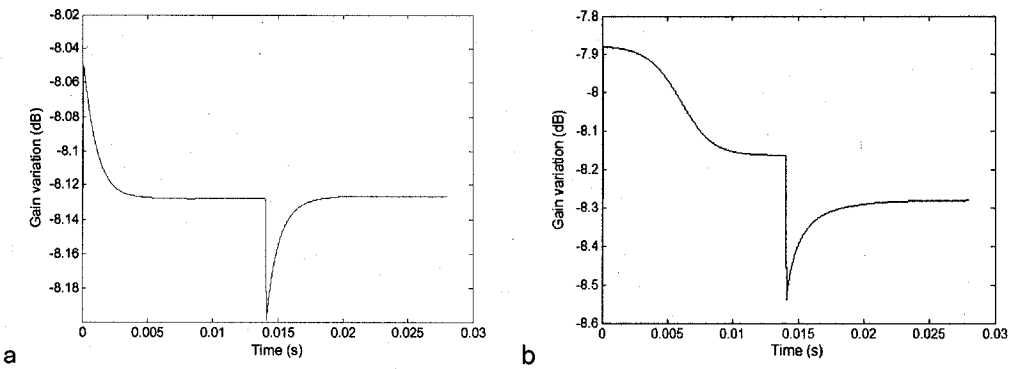

Fig. 6-8: Gain evolution of the surviving channel (λ = 1553.2 nm) at the output of the HFA 3 (a) and 4 (b) during the addition and cut of 3 channels in the critical minus 3 dB regime.

The previous observation is confirmed by the transient characteristics presented in Table 6-3. HFA 4 presents over- and undershoots 3.5 times higher than HFA 3. This important difference in overshoot comes from the fact that only HFA 3 presents a gain-clamping in effect. When HFA 4 is operated in this regime and when all channels are loaded in the amplifier, there is not enough pump power to create the lasing signal. After the cut of channels, there is now enough pump power to create the lasing signal but this process takes time. During that time, the surviving channel experiences an important overshoot. The difference in ΔG following the cut of signals is particularly notable: 0.0116 dB for HFA 4 compared 0.001 dB for HFA 3. This difference can be explained by the fact that the input power at the entry of the GC-DFRA in HFA 3 is lower than that in HFA 4 because of the saturation of the unclamped EDFA in HFA 3.

6.3.3 Study of HFAs comprising one GC-EDFA: HFA 5 and 6

We now consider HFAs comprising one GC-EDFA. The gain-clamped amplifier is located either at the first position in the HFA (HFA 5) or at the last position in the HFA (HFA 6).

In the small-signal regime

Figure 6-9 presents the gain variations in time for HFAs 5 and 6 in the small-signal regime. We obtain similar gain evolution for both configurations. We observe that the gain-clamping is in effect and that oscillations follow the cut and the addition of signals, which are due to the lasing signal in the GC-EDFA.

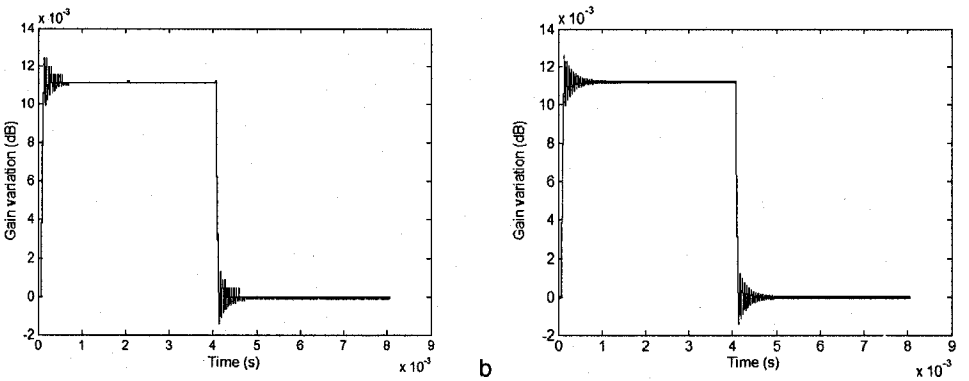

Fig. 6-9: Gain evolution of the surviving channel (λ = 1553.2 nm) at the output of the HFA 5 (a) and 6 (b) during the addition and cut of 3 channels in the small-signal regime.

From Table 6-2, we notice that ΔG following the drop of signals for HFAs 5 and 6 is close to that of HFAs 1 and 2 contrary to HFA 3 and 4 for which ΔG was much smaller then that of the unclamped HFAs. This proves that gain-clamping the EDFA is less efficient in controlling the steady-state gain variation than gain-clamping the DFRA. However, HFAs 5 and 6 present better gain transient performances in term of over- and undershoots, and of fall and rise times in comparison to HFAs 3 and 4: the over- and undershoots are reduced by one order of magnitude and the fall and rise times by 4 times. Amongst HFAs 5 and 6, HFA 5 presents the best performances except for the fall time following the addition of signals.

In the critical minus 3 dB regime

Figure 6-10 shows the gain variations in time for HFAs 5 and 6 in the critical minus 3 dB regime. We obtain similar behaviour than in the small-signal regime with larger transient characteristics.

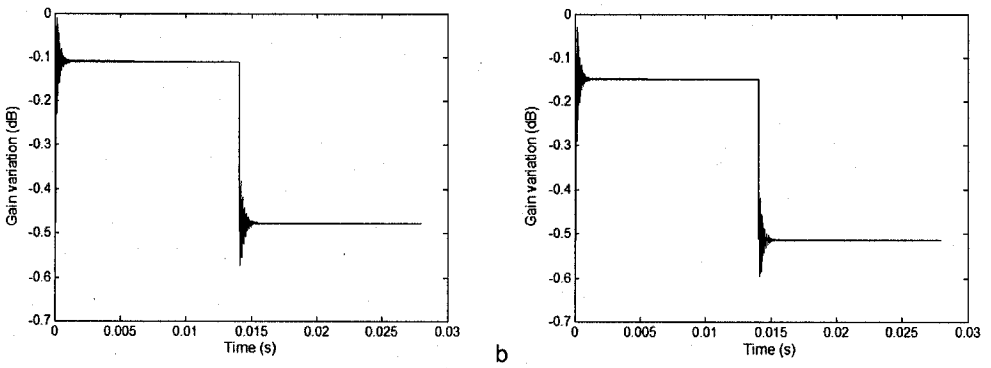

Fig. 6-10: Gain evolution of the surviving channel (λ = 1553.2 nm) at the output of the HFA 5 (a) and 6 (b) during the addition and cut of 3 channels in the critical minus 3 dB regime.

From Table 6-3, we note that HFAs 5 and 6 (presenting one GC-EDFA) are not anymore more efficient than HFAs presenting one GC-DFRA as in the small-signal regime. In fact, HFA 4 presents better transient characteristics rather than HFA 5 and 6, except for the fall and rise times (gain-clamping is not in effect in HFA3). Amongst HFAs 5 and 6, the best performances are shared between both configurations.

6.3.4 Study of HFAs comprising two gain-clamped amplifiers: HFA 7 and 8

We finally consider HFAs comprising two gain-clamped amplifiers. The GC-EDFA is located either at the first position in the HFA (HFA 5) or at the last position in the HFA (HFA 6).

In the small-signal regime

Figure 6-11 presents the gain variations in time for HFAs 7 and 8 in the small-signal regime. We see that the gain-clamping is in effect in both amplifiers.

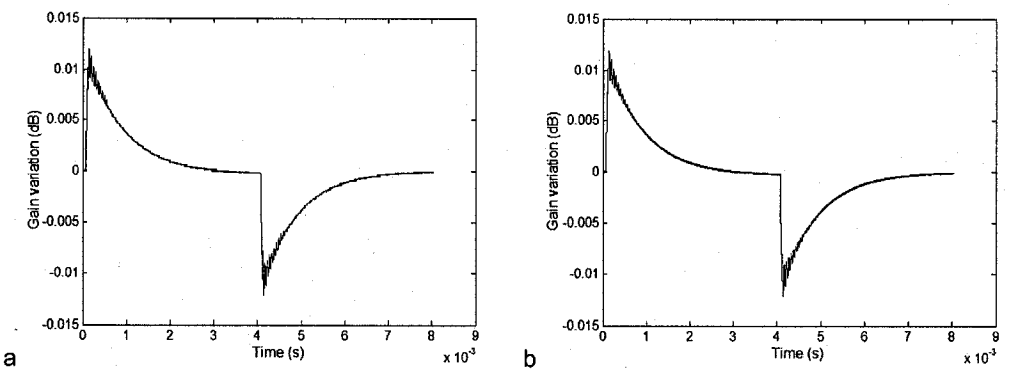

Fig. 6-11: Gain evolution of the surviving channel (λ = 1553.2 nm) at the output of the HFA 7 (a) and 8 (b) during the addition and cut of 3 channels in the small-signal regime.

HFAs 7 and 8 have similar behaviour in the small-signal regime as we can see with the transient characteristics given in Table 6-2. Even if both configurations present similar transient parameters, we note that HFA 7 (having the GC-EDFA as first amplifier) present better performances except for the rise time.

In the critical minus 3 dB regime

Figure 6-12 shows the gain evolution in time of the surviving channel for HFAs 7 and 8 in the critical minus 3 dB regime. We note that the gain-clamping is not in effect in both amplifiers.

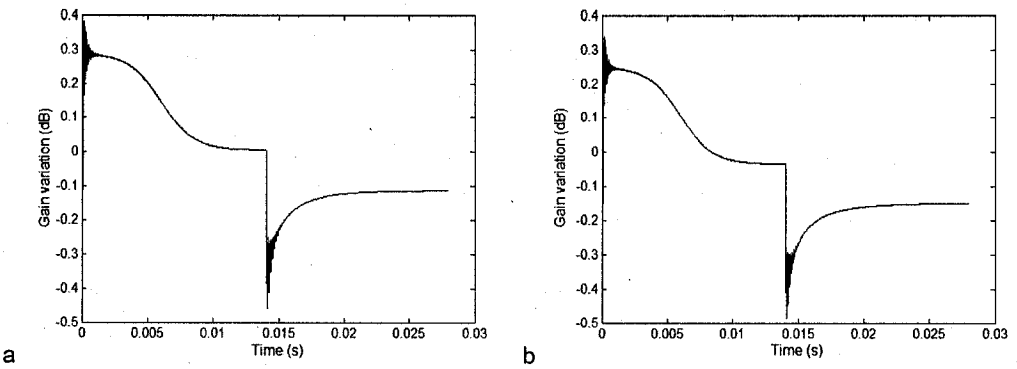

Fig. 6-12: Gain evolution of the surviving channel (λ = 1553.2 nm) at the output of the HFA 7 (a) and 8 (b) during the addition and cut of 3 channels in the critical minus 3 dB regime.

The failure of the gain-clamping is confirmed by the very long fall and rise times (see Table 6-3).

6.3.5 Analysis

The target point is to mitigate the overshoots, undershoots, and steady-state gain variations, or at least control them within tolerable limits. In the small-signal regime, each HFA presenting at least one gain-clamped amplifier is able to mitigate the gain transient of the surviving channel. The gain-clamped HFAs present better transient performances (except the rise time) when the EDFA is located at the first place. This is due to the fact that gain-clamping is more efficient in the EDFA rather than in the DFRA (see Fig. 6-2). In this regime, the HFAs 5 and 6 (presenting one GC-EDFA) offer the lowest over- and undershoots, and fall and rise times to the detriment of ΔG. However, as ΔG is low ($\approx 10^{-2}$ dB), we can conclude that only gain-clamping the EDFA is the best configuration to mitigate the transient.

In the critical minus 3 dB regime, gain-clamping is in effect in only three configurations: HFAs 3, 5 and 6. HFA 4 is unable to control the gain

transients because the gain-clamping in the GC-DFRA under the critical minus 3 dB regime is not in effect. When the GC-DFRA is located as second amplifier (HFA 3), gain-clamping is in effect. This is due to the saturation of the EDFA located at first position. As the unclamped EDFA saturates in this regime, it offers a lower gain to the signals, which result in a lower input power at the entry of the GC-DFRA. As the DFRA is operated in a lower regime than the critical minus 3 dB regime, there is now enough pump power to create the lasing signal when all of the channels are loaded in the GC-DFRA. Thus, the gain-clamping is in effect in HFA 3 and not in HFA 4.

We note that both configurations having 2 gain-clamped amplifiers fail to control the gain transients because gain-clamping is not in effect in the GC-DFRA. Contrary to HFA 3 in which the unclamped EDFA permits to reduce the input power at the entry of the GC-DFRA, the GC-EDFA located at the first position in HFA 7 keeps high the amount of input power at the entry of the GC-DFRA and gain-clamping is not in effect in the presence of the 4 channels.

The best performances are shared between the HFAs having one GC-EDFA (HFAs 5 and 6) and the HFA having one GC-DFRA as second amplifier (HFA 3). As HFAs 5 and 6 offer the lowest fall and rise times, and ΔG after the addition of channels, HFA 3 presents the lowest over- and undershoots, and ΔG after the cut of signals. Amongst HFAs 5 and 6, it is preferable to place the EDFA in first position as in the small-signal regime.

6.3.6 Influence of the surviving channel location

We are also interested in the influence of the surviving channel location on the steady-state gain variation and on the transient characteristics. Tables

6-4 and 6-5 present the transient characteristics when the surviving channel is located at the following wavelength: λ = 1550, 1553.2, 1556.4 and 1559.7 nm for HFA 3 and 5 operated in the small-signal regime.

	After the cut of channels		After the addition of channels	
Surviving channel location	Overshoot (10^{-3} dB)	Fall time (µs)	Undershoot (10^{-3} dB)	Rise time (µs)
λ = 1550.0 nm	11.1	1742	11.0	1881
λ = 1553.2 nm	11.2	1782	10.9	1960
λ = 1556.4 nm	11.0	1768	10.9	1898
λ = 1559.7 nm	10.6	1786	10.4	1896

Tab. 6-4: Transient characteristics at the output of HFA 3 operated in the small signal regime when the location of the surviving channel varies.

We notice that no surviving channel location offers the lowest transient characteristics. The best performances are shared randomly between the different wavelengths contrary to DFRAs in which the transients are less important when the surviving channel is located at midband. In DFRAs, WDM channels exchange power through SRS. A WDM channel located in the middle of the amplification band receives power from WDM channels located at the shorter wavelengths and gives power to WDM channels located at the higher wavelengths. This power exchange between WDM channels does not exist in EDFAs in which the best transient performances are randomly shared between the different surviving channel locations. As a result, the location of the surviving channel is not of importance in HFAs.

	After the cut of channels		After the addition of channels	
Surviving channel location	Overshoot (10^{-3} dB)	Fall time (μs)	Undershoot (10^{-3} dB)	Rise time (μs)
λ = 1550.0 nm	1.29	402	1.64	501
λ = 1553.2 nm	1.24	411	1.45	570
λ = 1556.4 nm	1.24	409	1.31	543
λ = 1559.7 nm	1.19	404	1.20	503

Tab. 6-5: Transient characteristics at the output of HFA 5 operated in the small-signal regime when the location of the surviving channel varies.

6.4 Conclusions

In this chapter, we analyze the power transients of HFAs in the worst possible case of transient. We consider HFAs comprising both unclamped or gain-clamped EDFAs and DFRAs in the worst-case scenario where all the channels except one were cut and added to the first amplifier of the cascade. We take into account the operational regime of the amplifiers, the location, the number and the type of the gain-clamped amplifiers in HFAs, and the location of the surviving channel. In the small-signal regime, our results show that all of the HFAs presenting at least one gain-clamped amplifier can mitigate the gain transients and that HFA 5 (presenting one GC-EDFA in first position) represent the best trade-off. In the critical minus 3 dB regime, only three HFAs enable the gain-clamping to be efficient: HFAs 4, 5 and 6. However, it was impossible to determine which HFA is the best, as the best transient characteristics are shared between the three configurations. Finally, we find that the location of the surviving channel is not relevant as it was impossible to find a location where the gain transients are less important, contrary to cascades of DFRAs.

Chapter 7: Conclusion

In this thesis, we studied the dynamic behaviour of DFRAs for their use in dynamic networks such as AAPN. In particular, a design achieving optical feedback through the use of FBGs has been investigated to mitigate the gain transients that occur when an amplifier is faced with a dynamic traffic.

We first explored the dynamic behaviour of single DFRAs in the context of addition and drop of all of the WDM channels except one and also in the context of multi-channel packet traffic. In the first study, we analyzed the performances of two AOGC configurations. We took into account the operational regime of the amplifiers, the location of the surviving channel in the amplification band and the feedback level of the lasing signal. We demonstrated that a GC-DFRA has to be operated in a regime below the critical regime to ensure the gain-clamping technique to be fully in effect and the gain transients are less significant when the surviving channel is located at midband, because the power it receives from the lower wavelength channels is compensated by the power it gives to the higher wavelength channels.

Concerning the second study of single DFRAs, we examined the behaviour of DFRAs fed by multi-channel packet traffic. In particular, we considered the influence of the packet duration, the operational mode of the amplifier, and the input power distribution on the performance of both unclamped and gain-clamped amplifiers. We concluded that the efficiency of the gain-clamping technique is dependent on the operational regime and on the packet duration. As the gain-clamping technique is efficient to reduce the gain transients in the small-signal regime for any packet duration, this technique is not in effect in higher operational regime for short packet durations. However, even when the gain-clamping technique

enables the mitigation of the gain transients, its use is not necessary as the gain variations of the unclamped DFRA are small enough to be neglected. Such a conclusion is true for a single DFRA, however, in-line fiber amplifiers are usually used in cascades, which amplifies the gain transients. Thus, we expect that the gain transients caused by multi-channel packet traffic will increase with the number of amplifiers in a cascade and will require some form of gain control. In the future, a thorough study of cascades of DFRAs fed by multi-channel packet traffic could tell if the gain control is necessary or not.

The second part of this thesis focuses on multiple amplifiers: Chapter 5 considers cascades of DFRAs while Chapter 6 examines the dynamic behaviour of HFAs. In the case of cascaded DFRAs, we considered cascades comprising 5 DFRAs that could be either unclamped or gain-clamped amplifiers in the worst-case scenario of channels addition and drop. We took into account the operational regime of the amplifiers, the location of the GC-DFRAs in cascades of mixed amplifiers, and the location of the surviving channel. We demonstrated that it is possible to maintain the steady-state gain variation and the over and undershoots within predefined tolerance limits by gain-clamping only two amplifiers in the cascade. Concerning cascades of mixed amplifiers, we established that locating the gain-clamped amplifiers at the end of the cascade allows us to reduce the steady-state gain variation after the addition of channels. In a cascade of mixed DFRAs, the fall and rise times tend to reach the value of a homogenous cascade constituted of the type of amplifier located at the end of the mixed cascade.

In Chapter 6, we analyzed the power transients of HFAs in the worst possible case of transients. We considered HFAs comprising both unclamped or gain-clamped EDFAs and DFRAs in the worst-case scenario where all the channels except one were cut and added to the first

amplifier of the cascade. We take into account the operational regime of the amplifiers, the location, the number and the type of the gain-clamped amplifiers in HFAs, and the location of the surviving channel. In the small-signal regime, our study showed that gain-clamping at least one amplifier of the HFA is enough to control the gain transients. In the critical minus 3 dB regime, only a few configurations enable the gain-clamping to be fully in effect and the best transient characteristics are shared between those configurations. Finally, contrary to single and cascaded DFRAs, the location of the surviving channel is not relevant as it was impossible to find a location where the gain transients are less important.

Our work demonstrates that it is possible to control the gain transients in DFRAs using the AOGC technique. This technique presents the advantage of being cost effective and simple and makes DFRAs suitable for dynamic networks, such as AAPN. However, the role that DFRAs could play in such networks has to be defined. DFRAs can be used as pre-amplifier, in-line amplifier or booster. As it is clear that FRAs will not replace EDFAs in the traditional C- and L- bands, the future of DFRAs probably lies in the use of new telecommunications band, such as the S-band, where doped-fiber amplifiers are inefficient.

The development of photonic crystal fibers will probably influence the future of FRAs. Such fibers have the capacity of presenting very high Raman gain coefficients, which will permit to reduce the fiber length of the amplifiers. The transient times occurring FRAs will be reduced as they are directly related to the amplifier length.

Bibliography

[1] G. R. Ash, "Dynamic network evolution, with examples from AT&T's evolving dynamic network," *IEEE Communications Magazine*, vol. 33, no. 7, pp. 26-39, 1995.

[2] K. Struyve and P. Demeester, "Dynamic routing of protected optical paths in wavelength routed and wavelength translated networks," *Integrated Optics and and Optical Fiber Communications*, vol. 2, pp. 151-154, 1997.

[3] R. Ramamurthy, Z. Bogdanowicz, S. Samieian, D. Saha, B. Rajagopalan, S. Sengupta, S. Chaudhuri, *and* K. Bala, "Capacity performance of dynamic provisioning in optical networks," *IEEE/OSA Journal of Lightwave Technology*, vol. 19, no. 1, pp. 40-48, 2001.

[4] M. Duser, and P. Bayvel, "Analysis of wavelength-routes optical burst-switched network performance," *IEEE/OSA Journal of Lightwave Technology*, vol. 20, no. 4, pp. 574-585, 2002.

[5] G. v. Bochmann, T. Hall, O. Yang, M. J. Coates, L. Masson, and R. Vickers, "The Agile All-Photonic Network: an architectural outline," *Queen's University 22nd Biennial Symposium on Communications*, pp. 217-219, 2004.

[6] L. Mason, A. Vinokurov, N. Zhao, and D. Plant, "Topological design and dimensioning of Agile All Photonic Networks," *Computer Networks*, vol. 50, pp 268-287, 2006.

[7] E. Desurvire, "Analysis of transient gain saturation and recovery in Erbium-doped fiber amplifiers," *IEEE Photonics Technology Letters*, vol. 1, no. 8, pp. 196-199, 1989.

[8] A. K. Srivastava, Y. Sun, J. L. Zyskind, and J. W. Zulhoff, "EDFA transient response to channel loss in WDM transmission system," *IEEE Photonics Technology Letters*, vol. 9, no. 3, pp. 386-388, 1997.

[9] K. Motoshima, L. M. Leba, D. N. Chen, M. M. Downs, T. Li, and E. Desurvire, "Dynamic compansation of transient gain saturation in Erbium-doped fiber amplifiers by pump feedback control," *IEEE Photonics Technology Letters*, vol. 5, no. 12, pp. 1423-1426, 1993.

[10] K. Motoshima, L. M. Leba, D. N. Chen, M. M. Downs, T. Li, and E. Desurvire, "Dynamic compensation of transient gain saturation in Erbium-Doped Fiber Amplifiers by pump feedback control," *IEEE Photonics Technology Letters*, vol. 5, no. 12, pp. 1423-1426, 1993.

[11] H. S. Chung, H. H. Lee, J. C. Lee, M. J. Chu, and J. H. Lee, "Reduction of relaxation oscillations in optical automatic gain clamped EDFA using fast electronic feedforward," *IEE Electronics Letters*, vol. 38, no. 5, pp. 215-217, 2001.

[12] F. Shehadeh, R. S. Vodhanel, C. Gibbons, and M. Ali, "Comparison of gain control techniques to stabilize EDFAs for WDM networks," *Optical Fiber Communication Conference*, pp 190-191, 1996.

[13] J. Chung, S. Y. Kim, and C. J. Chae, "All-optical gain-clamped EDFAs with different feedback wavelengths for use in multiwavelength optical networks," *IEE Electronics Letters*, vol. 32, no. 23, pp. 2159-2161, 1996.

[14] M. A. Mahdi, F. R. Mahamd, P. Poopalan, S. Selvakennedy, W. Y. Chan, and H. Ahmad, "Gain-clamped fibre amplifier using an ASE and reflector," *Optics Communications*, vol. 177, no. 1, pp. 195-199, 2000.

[15] Y. Liu, and M. F. Krol, "Transient Gain Control in EDFA's by Dual-Cavity Optical Automatic Gain Control," *IEEE Photonics Technology Letters*, vol. 11, no. 11, pp. 1381-1383, 1999.

[16] B. Xia, D. Pudo, and L. R. Chen, "Comparison of the static and dynamic properties of single- and double-pass partially gain-clamped two-stage L-band EDFAs," *IEEE Photonics Technology Letters*, vol. 15, no. 4, pp. 519-521, 2003.

[17] S. Yamashia, and M. Nishihara, "L-band Erbium-doped fiber amplifier incorporating an inline fiber grating laser," *IEEE Journal of Selected Topics in Quantum Electronics*, vol. 07, no. 1, pp. 44-48, 2001.

[18] J. Bryce, Y. Zhao, and R. Minasian, "Modeling and optimization of add-drop dynamics in gain-clamped fiber amplifiers," *Applied Optics*, vol. 39, no. 24, pp. 4270-4277.

[19] K. Song, M. Premaratne, and R. D. T. Lauder, "An analytical formulation of the transient response of gain-clamped EDFA's," *IEEE Photonics Technology Letters*, vol. 11, no. 11, pp. 1378-1380, 1999.

[20] M. I. Hayee, and A. E. Willner "Transmission penalties due to EDFA gain transients in add-drop multiplexed WDM netrworks," *IEEE Photonics Technology Letters*, vol. 11, no. 7, pp. 889-891, 1999.

[21] A. Bononi, and L. A. Rusch, "Doped-fiber amplifier dynamics: a system perspective," *IEEE/OSA Journal of Lightwave Technology*, vol. 15, no. 5 pp. 945-956, 1998.

[22] M. Karásek, "Optical amplifiers in dynamic networks with all-optical routing" *International Conference on Transparent Optical Networks*, vol. 1, Mo. C. 3, pp. 57-61, 2002.

[23] D. H. Richards, J. L. Jackel, and M. A. Ali, "A theoretical investigation of dynamic all-optical automatic gain control in multichannel EDFA's and EDFA cascades," *IEEE Journal of Selected Topics in Quantum Electronics*, vol. 3, no. 4, pp. 1027-1035, 1997.

[24] Q. Yu, and C. Fan, "Simple dynamic model of all-optical gain-clamped Erbium-doped fiber amplifiers," *IEEE/OSA Journal of Lightwave Technology*, vol. 17, no. 7, pp. 1166-1171, 1999.

[25] M. Nissov, C. R. Davidson, K. Rottwitt, R. Menges, P. C. Corbett, D. Innis, and N. S. Bergano, "100 Gb/s (10 × 10 Gb/s) WDM transmission over 7200 km using distributed Raman amplification," *European Conference Optical Communication*, Postdeadline Paper, pp. 9–12, 1997.

[26] T. Terahara, T. Hoshida, J. Kumasako, and H. Onaka, "128 × 10.66 Gbit/s transmission over 840-km standard SMF with 140-km optical repeater spacing (30.4-dB loss) employing dual-band distributed Raman amplification," *Optical Fiber Communication Conference*, vol. 4, pp. 251-253, 2000.

[27] N. Shimojoh, T. Tanaka, T. Naito, H. Nakamoto, I. Yokota, A. Sugiyama, T. Ueki, and M. Suyama, "1.22 Tbit/s WDM transmission over 7,221 km with 38 nm bandwidth expanded by distributed Raman amplifier and EDFA," *Optical Fiber Communication Conference*, vol. 3, pp. 9-12, 2000.

[28] T. N. Nielsen, A. J. Stents, K. Rottwitt, D. S. Vengsarkar, Z. J. Chen, P. B. Hansen, J. H. Park, K. S. Feder, S. Cabot, S. Stulz, D. W. Peckham, L. Hsu, C. K. Kan, A. F. Judy, S. Y. Park, L. E. Nelson, and L. Grüner-Nielsen, "3.28-Tb/s transmission over 3 × 100 km of nonzero-dispersion fiber using dual C- and L-band distributed Raman amplification," *IEEE Photonics Technology Letters*, vol. 12, no. 8, pp. 10-79-1081, 2000.

[29] H. Suzuki, J. Kani, H. Masuda, N. Takachio, K. Iwatsuki, Y. Tada, and M. Sumida, "25 GHz-spaced, 1 Tb/s (100 ×10 Gb/s) super dense-WDM transmission in the C-band over a dispersion-shifted fiber cable employing distributed Raman amplification," *European Conference Optical Communication*, vol. 4, pp. 30-31, 1999.

[30] E. Schulze, R. Freund, M. Malach, and F. Raub, "10 Gb/s NRZ transmission over 1800 km multiple pumped distributed Raman amplified

transmission link without lumped amplifiers," *European Conference Optical Communication*, vol. 2, pp. 160-161, 2001.

[31] S. Namiki, and Y. Emori, "Ultrabroad-band Raman amplifiers pumped and gain-equalized by wavelength-division-multiplexed high-power laser diodes," *IEEE Journal on Selected Topics in Quantum Electronics*, vol. 7, no. 1, pp. 3-16, 2001.

[32] P.C. Reeves-Hall, D.A. Chestnut, C.J.S. De Matos, and J.R. Taylor, "Dual wavelength pumped L- and U-band Raman amplifier," *IEE Electronics Letters*, vol. 37, no. 14, pp. 883-884, July 2001.

[33] Y. Emori, and S. Namiki, "100 nm bandwidth flat gain Raman amplifiers pumped and gain-equalized by 12-wavelength-channel WDM high power laser diodes," *Optical Fiber Communication Conference*, vol. suppl., PD19/1-PD19/3, 1999.

[34] H. Kidorf, K. Rottwitt, M. Nissov, M. Ma, and E. Rabarijaona, "Pump interactions in a 100-nm bandwidth Raman amplifier," *IEEE Photonics Technology Letters*, vol. 11, no. 5, May 1999.

[35] T. Miyamoto, T. Tsuzaki, T. Okuno, M. Kakui, M. Hirano, M. Onishi, and M. Shigematsu, "Raman amplification over 100 nm-bandwidth with dispersion and dispersion slope compensation for conventional single mode fiber," *Optical Fiber Communication Conference*, pp 66-68, 2002.

[36] S. A. E. Lewis, S. V. Chernikov, and J. R. Taylor, "Triple wavelength pumped silica-fibre Raman amplifiers with 114 nm bandwidth," *IEE Electronic Letters*, vol. 35, pp. 1761–1762, 1999.

[37] M. Yan, J. Chen, W. Jiang, J. Li, J. Chen, and X. Li, "Pump depletion induced noise and crosstalk in distributed optical fiber Raman amplifiers," *IEEE Photonics Technology Letters*, vol. 13, no. 7, July 2001.

[38] P. Ebrahimi, M.C. Hauer, Q. Yu, R. Khosravani, D. Gurkan, D.W. Kim, D.W. Lee, and A.E. Willner, "Statistics of polarization dependant gain in Raman fiber amplifiers due to PMD," *Conference on Lasers and Electro-Optics*, pp. 143-144, 2001.

[39] S. Popov, and E. Vanin, "Polarization dependence of Raman gain on propagation direction of pump and probe signal in optical fibers," *Conference on Lasers and Electro-Optics*, pp. 146-147, 2001.

[40] P. B. Hansen and L. Eskildsen, "Rayleigh scattering limitations in distributed Raman pre-amplifiers," *IEEE Photonics Technology Letters*, vol. 10, no. 1, pp. 159-161, 1998.

[41] A. J. Stentz, T. Nielsen, S. G. Grubb, T. A. Strasser, and J. R. Pedrazzani, "Raman ring amplifier at 1.3 μm with analog-grade performance and an output power of 23 dBm," *Optical Fiber Communication Conference*, pp. 16-17, 1996.

[42] S.A.E. Lewis, S.V. Chernikov, and J.R. Taylor, "Characterization of double Rayleigh scatter noise in Raman amplifiers," *IEEE Photonics Technology Letters*, vol. 12, no. 5, pp. 528-530, 2000.

[43] A. B. Puc, M. W. Chbat, J. D. Henrie, N. A. Weaver, H. Kim, A. Kaminski, A. Rahman, and H. A. Fevrier, "Long-haul WDM NRZ transmission at 10.7 Gb/s in S-band using cascade of lumped Raman amplifiers," *Optical Fiber Communication Conference*, vol. 4, PD39-1 PD39-3, 2001.

[44] V. Dominic, E. Mao, J. Zhang, B. Fidric, S. Sanders, and D. Mehuys, "Distributed Raman amplification with co-propagating pump light," *Optical Amplifiers and Their Applications*, 2001.

[45] C. R. S. Fludger and V. Henderek, "Fundamental noise limits in broadband Raman amplifiers," *Optical Fiber Communication Conference*, vol. 1, MA5-1 MA5-3, 2001.

[46] S. A. Lewis, S. V. Chernikov, and J. R. Taylor, "Temperature-dependent gain and noise in fiber Raman amplifiers," *Optics Letters*, vol. 24, no. 24, pp. 1823-1825, 1999.

[47] C-J. Chen and W. S. Wong, "Transient effects in saturated Raman amplifiers," *IEE Electronic Letters*, vol. 37, no. 6, pp. 371-373, 2001.

[48] L. L. Wang, B. C. Hwang, and L. M. Yang, "Gain transients in copumped and counterpumped Raman amplifiers," *IEEE Photonics Technology Letters*, vol. 15, no. 5, pp. 664-666, 2003.

[49] Z. Tong, H. Wei, and S. Jian, "Transient responses to slowly varying input waveforms in backward pumped Raman amplifiers," *Optics Communications*, vol. 218, no. 1-3, pp. 105-111, 2003.

[50] C-J. Chen, J. Ye, W. S. Wong, Y.-W. Lu, M.-C. Ho, Y. Cao, M.J. Gassner, J.S. Pease, H.-S. Tsai, H.K. Lee, S. Cabot, and Y. Sun, "Control of transient effects in distributed and lumped Raman amplifiers," *IEE Electronic Letters*, vol. 37, no. 21, pp. 1304-1305, 2001.

[51] C-J. Chen and M-C. Ho, "Time-domain characterization of transient effects and double Rayleigh backscattering noise in Raman amplifiers," *Optical Fiber Communication Conference*, pp 634-636, 2002.

[52] M. Karásek and M. Menif, "Protection of surviving channels in pump-controlled gain-locked Raman fibre amplifier," *Optics Communications*, Vol. 210, no. 1-2, pp. 57-65, 2002.

[53] M. Karásek, J. Kaňka, P. Honzátko, and P. Peterka, "Modelling of a pump-power-controlled gain-locking system for multi-pump wideband Raman fibre amplifiers," *IEE Proceedings-Optoelectronics*, vol. 151, no. 2, pp. 74-80, 2004.

[54] X. Zhou, M. Feuer, and M. Birk, "Submicrosecond transient control for a forward-pumped Raman fiber amplifier," *IEEE Photonics Technology Letters*, vol. 17, no. 10, pp. 2059-2061, 2005.

[55] X. Zhou, M. Feuer, and M. Birk, "A simple feed-forward control algorithm for fast dynamic profile control in a multiwavelength forward-pumped Raman fiber amplifiers," *IEEE Photonics Technology Letters*, vol. 18, no. 9, pp. 1004-1006, 2006.

[56] S. H. Chang, H. S. Chung, K. Kim, and J. S Ko, "Automatic gain control in Raman amplifier with multi-wavelength pumps," *Optics Communications*, vol. 266, no. 2, pp 521-526, 2006.

[57] A. Ahmad, M. I. M. Ali, A. K. Zamzuri, and M. A. Mahdi, "Gain-control Raman fiber amplifier incorporating ring cavity," *IEEE International Conference on Communications*, vol. 1, no. 16, pp. 77-79, 2005.

[58] X. Zhou, H. H. M. Shalaby, C. H. Lu, P. Shum, and T. Cheng, "Theoretical investigation of fiber Raman amplifier with dynamic gain control," *Optical Fiber Communication Conference*, vol. 3, pp. WDD17-1 - WDD17-3, 2001.

[59] M. Karásek, J. Kaňka, P. Honzátko, and J. Radil, "Protection of surviving channels in pump-controlled gain-locked Raman fibre amplifiers," *Optics Communications*, vol. 210, no. 1-2, pp. 309-317, 2002.

[60] S. S.-H. Tam, M. E. Marhic, Y. Akasaka, and L. G. Kazovsky, "Gain-clamped S-band discrete Raman amplifier," *Optics Letters*, vol. 29, no. 7, pp. 757-759, 2004.

[61] M. Tang, Y. D. Gong, and P. Shum, "Dynamic properties of double-pass discrete Raman amplifier with FBG-based all-optical clamping techniques," *IEEE Photonics Technology Letters*, vol. 16, no. 3, pp. 768-770, 2004.

[62] L. Zhang, S. Wang, and C. Fan, "Transient analysis in discrete fiber Raman amplifiers," *Optics Communications*, vol. 197, no. 4-6, pp. 469-465, 2001.

[63] G. Bolognini and F. Di Pasquale, "Transient effects in gain-clamped discrete Raman amplifier cascades," *IEEE Photonics Technology Letters*, vol. 16, no. 1, pp. 66-68, 2004.

[64] G. Bolognini, S. Faralli, S. Sugliani, G. Sacchi, and F. Di Pasquale, "Theoretical study of dynamics in gain-clamped Raman amplifier cascades," *Optical Fiber Communication Conference*, pp 244-245, 2003.

[65] M. Karásek, J. Kaňka, and J. Radil, "Analysis of channel addition/removal response in all-optical gain-clamped cascade of lumped Raman fiber amplifiers," *IEEE/OSA Journal of Lightwave Technology*, vol. 22, no. 10, pp. 530-532, 2004.

[66] M. Karásek and M. Menif , "Channel Addition/Removal Response in Raman Fiber Amplifiers: Modeling and Experimentation," *IEEE/OSA Journal of Lightwave Technology*, vol. 20, no.9, pp. 1680-1687, 2002.

[67] W. H. Press, B. P. Flannery, S. A. Teukolsky, and W. T. Vetterling, Numerical recipies in C: the art of scientific computing, "Integration of Ordinary Differential Equations," *Cambridge University Press*, 2nd edition, pp. 710-714, January 1993.

[68] T. G. Hodgkinson, "Average power analysis technique for erbium-doped fiber amplifiers," *IEEE Photonics Technology Letters*, vol. 3, no. 12 pp. 1082–1084, 1991.

[69] T. G. Hodgkinson, "Improved average power analysis technique for erbium-doped fiber amplifiers," *IEEE Photonics Technology Letters*, vol. 4, no. 11, pp. 1273–1275, 1992.

[70] B. Min, W. J. Lee, and N. Park, "Efficient formulation of Raman amplifier propagation equations with average power analysis," *IEEE Photonics Technology Letters*, vol. 12, no. 11, pp. 1486-1488, November 2000.

[71] M. Karásek, J. Kaňka, P. Honzátko, and P. Peterka, "Time-domain simulation of power transients in Raman fiber amplifiers," *International Journal of Numerical Modeling: Electronic Networks, Devices and Fields*, vol. 17, pp. 165-176, 2004.

[72] T. Zambelis, N. Gryspolakis, and L. R. Chen," Design of all-optical gain-clamped discrete fiber Raman amplifiers," *Lasers and Electro-Optics Society*, vol. 2, no. 27-28, pp. 1050-1051, 2003.

[73] L. Tančevski, A. Bononi, and L. A. Rusch, "Output power and SNR swings in cascades of EDFAs for circuit- and packet switched optical networks," *IEEE/OSA Journal of Lightwave Technology*, vol. 17, no. 5, pp. 733-742, 1999.

[74] M. Karásek, A. Bononi, L. A. Rusch, and M. Menif, "Gain stabilization in gain clamped EDFA cascades fed by WDM burst-mode packet traffic," *IEEE/OSA Journal of Lightwave Technology*, vol.18, no. 3, pp. 308-313, 2000.

[75] M. Karásek, M. Menif, and L. A. Rusch, "Output power excursions in a cascade of EDFAs fed by multichannel burst-mode packet traffic: experimentation and modeling," *IEEE/OSA Journal of Lightwave Technology*, vol. 19, no. 7, pp. 933-940, 2001.

[76] S. J. Strutz, K. J. Williams, and R. D. Esman, "Polarization-maintaining hybrid Erbium–Brillouin amplifier for high-power low-noise sources," *IEEE Photonics Technology Letters*, vol. 13, no. 9, pp. 936-938, 2001.

[77] A. Guimarles, J. M. Chavez Boggio, J. D. Marconi, F. A. Callegari, and H. L. Fragnito, "High performance hybrid EDFA-FOPA pre-amplifier for 40 Gb/s transmission," *Conference on Lasers & Electro-Optics*, pp. 989-991, 2005.

[78] T. Sakamoto, S. Aozasa, M. Yamada, and M. Shimizu, "High-gain hybrid amplifier consisting of cascaded fluoride-based TDFA and silica-based EDFA in 1458-1540 nm wavelength region," *IEE Electronics Letters*, vol. 39, no. 7, pp. 597-599, 2003.

[79] T. Sakamoto, S.i Aozasa, M. Yamada, and M. Shimizu, "Hybrid fiber amplifiers consisting of cascaded TDFA and EDFA for WDM signals," *IEEE/OSA Journal of Lightwave Technology*, vol. 24, no. 6, pp. 2287-2295, 2006.

[80] P. Even, N. Tallaron, A. Monteville, B. Metayer, R. Ossikovski, and D.Pureur, "A +24 dBm two stage hybrid Er doped - Er/Yb co-doped double clad fiber amplifier for the C-band," *European Conference on Optical Communications*, vol. 3, pp. 1-2, 2003.

[81] M.-C. Ho, K. Uesaka, M. Marhic, Y. Akasaka, and L. G. Kazovsky, "200-nm-bandwidth fiber optical amplifier combining parametric and

Raman gain," *IEEE/OSA Journal of Lightwave Technology*, vol. 19, no. 7, pp. 977-981, 2001.

[82] S. Sugliani, G. Sacchi, G. Bolognini, S. Faralli, and F. Di Pasquale, "Effective suppression of penalties induced by parametric nonlinear interaction in distributed Raman amplifiers based on NZ-DS fibers," *IEEE Photonics Technology Letters*, vol. 16, no. 1, pp. 81-83, 2004.

[83] L. Marazzi, P. Parolari, S. Seghizzi, and M. Martinelli, "Raman-generated pump impact on optical parametric amplification," *IEEE Photonics Technology Letters*, vol. 16, no.1, pp. 78-80, 2004.

[84] K. C. Reichmann, P. P. Iannone, X. Zhou, N. J. Frigo, and B. R. Hemenway, "240-km CWDM transmission using cascaded SOA Raman hybrid amplifiers with 70-nm bandwidth," *IEEE Photonics Technology Letters*, vol. 18, no. 2, pp. 328-330, 2006.

[85] Y. Miyamoto, H. Masuda, A. Hirano, S. Kuwahara, Y. Kisaka, H. Kawakami, M. Tomirawa, *Y.* Tada, and S. Aozasa, "S-band WDM coherent transmission of 40 x 43-Gbit/s CS-RZ DPSK signals over 400 km DSF using hybrid GS-TDFAs/Raman amplifiers," *IEE Electronics Letters*, vol. 38, no. 24, pp. 1569-1570, 2002.

[86] S. R. Lüthi, M. B. Costa e Silva, C. J. A. Bastos-Filho, J. F. Martins-Filho and A. S. L. Gomes, "TDFA/Raman hybrid amplifiers covering the entire S-band pumped by a single laser," *IEEE Photonics Technology Letters*, vol. 17, no. 10, pp. 2050-2052, 2005.

[87] H. Masuda, S. Aozasa, and M. Shimizu, "Ultra-wide-band hybrid amplifier consisting of two dispersion-compensating fibres for Raman amplification and thulium-doped fibre," *IEE Electronics Letters*, vol. 38, no. 11, pp. 500-502, 2002.

[88] B. Zhu, L. Leng, L.E. Nelson, Y. Qian, L. Cowsar, S. Slulz, *C.* Doerr, L. Stulz, S. Chandrasekhar, S. Radic, D. Vengsarkar. *Z.* Chen, J. Park, K.S. Feder, H. Thiele, J. Bromage, L. Gruner-Nielsen, and S. Kiiudsen, "3.08Tbit/s (77 x 42.7 Gbit/s) WDM transmission over 1200 km fibre with 100 km repeater spacing using dual C- and L-band hybrid Raman/erbium-doped inline amplifiers," *IEE Electronics Letters*, vol. 37, no. 13, pp. 844-845, 2001.

[89] H. Masuda, H. Kawakami, S. Kuwahara, A. Hirano, K. Sato, and Y. Miyamoto, "1.28 Tbit/s (32×43 Gbit/s) field trial over 528km (6×88 km) DSF using L-band remotely-pumped EDF/distributed Raman hybrid inline amplifiers," *IEE Electronics Letters*, vol. 39, no. 33, pp. 1668-1670, 2003.

[90] T. Matsuda, T. Kotanigawa, T. Kataoka, and A. Naka, "54×42.7 Gbit/s L- and U-band WDM signal transmission experiments with in-line hybrid optical amplifiers," *IEE Electronics Letters*, vol. 40, no. 6, pp. 380-381, 2004.

[91] I. Morita, K. Tanaka, and N. Edagawa, "Benefit of Raman amplification in ultra-long-distance 40 Gbits/s-based WDM transmission using dispersion-flattened fibre span," *IEE Electronics Letters*, vol. 37, no. 8, pp. 508-510, 2001.

[92] H. Masuda, S. Kawai, K.-I. Suzuki, and K. Aida, "Wide-band and low noise amplification using distributed Raman amplifiers and Erbiium-doped fiber amplifiers," *European Conference on Optical Comuunications*, pp. 51-52, 1998.

[93] Zhaohui Li, Chun-Liu Zhao, Yang Jing Wen, Chao Lu, Yixin Wang, and Jian Chen, "Optimization of a Raman/EDFA hybrid amplifier based on dual-order stimulated Raman scattering using a single-pump," *Optics Communications*, vol. 265, no. 2, pp. 655-658, 2006.

[94] H. Masuda and S. Kawai, "Wide-band and gain-flattened hybrid fiber amplifier consisting of an EDFA and a multiwavelength pumped Raman amplifier," *IEEE Photonics Technology Letters*, vol. 11, no. 6, pp. 647-649, 1999.

[95] H. Masuda, "Review of wideband hybrid amplifiers," *Optical Fiber Communication Conference*, vol. 1, pp. 2-4, 2000.

[96] M.Karásek, M.Menif, and A.Bellemare, "Design of wideband hybrid amplifiers for local area networks," *IEE Proceedings-Optoelectronics*, vol. 148, no. 3, pp. 150-155, 2001.

[97] G. E. Tudury, J. Hu, B. S. Marks, A. S. Lenihan, C. R. Menyuk, and G. M. Carter, "Gain characteristics of a 210 km hybrid Raman/Erbium-doped fiber amplified loop," *Optics Communications*, vol. 261, no. 1, pp. 152-157, 2006.

[98] A. Carena, V. Curri, and P. Poggiolini, "On the optimization of hybrid Raman/Erbium-doped fiber amplifiers," *IEEE Photonics Technology Letters*, vol. 13, no. 11, pp. 1170-1172, 2001.

[99] J. H. Lee, Y. M. Chang, Y.-G. Han, S. H. Kim, H. Chung, and S. B. Lee, "Dispersion-compensating Raman/EDFA hybrid amplifier recycling residual Raman pump for efficiency enhancement," *IEEE Photonics Technology Letters*, vol. 17, no. 1, pp. 43-45, 2005.

[100] J. H. Lee, Y. M. Chang, Y.-G. Han, S. H. Kim, H. Chung, and S. B. Lee, "A detailed experimental study on single-pump Raman/EDFA hybrid amplifiers: static, dynamic and system performance comparison," *IEEE/OSA Journal of Lightwave Technology*, vol. 23, no. 11, pp. 3484-3493, 2005.

[101] S. H. Chang, J. S. Han, H. S. Chung, K. Kim, and J. S. Ko, "Characteristics of low noise hybrid fiber amplifier," *Optics Communications*, vol. 261, no. 2, pp. 269-275, 2006.

[102] J. H. Lee, Y. M. Chang, Y.-G. Han, S. H. Kim, and S. B. Lee, "Dynamic properties of single pump, dispersion-compensating Raman/EDFA hybrid amplifier recycling residual Raman pump," *Optics Express*, vol. 12, no. 26, pp. 6594-6599, 2004.

[103] S. Su. H. Chang, H. S. Chung, H. J. Lee, and K. Kim, "Suppression of Transient Phenomena in Hybrid Raman/EDF Amplifier," *IEEE Photonics Technology Letters*, vol. 17, no. 5, pp.1004-1006, 2005.

[104] S. H. Chang, S. K. Kim, H. S. Chung, and M.-J. Chu, "Transient effects and gain-control method in low-noise dispersion-compensating hybrid fiber amplifier," *IEEE Photonics Technology Letters*, vol. 15, no. 7, pp. 906-908, 2003.

[105] S. Chang, S. Kim, H. Chung, M. Chu, and J. Lee, "Transient effects in low-noise dispersion-compensating hybrid fiber amplifier," *Optical Fiber Communications Conference*, vol. 2, pp. 438-439, 2003.

APPENDIX A: HNLF parameters

This section presents the attenuation coefficient α and effective Raman gain parameter g_R / A_{eff}.

Effective Raman gain parameter g_R / A_{eff}:

Figure A-1 presents the effective Raman gain parameter used in the simulations has a peak value of approximately 6 [$km^{-1} \cdot W^{-1}$] which is similar to that of commercially HNLF.

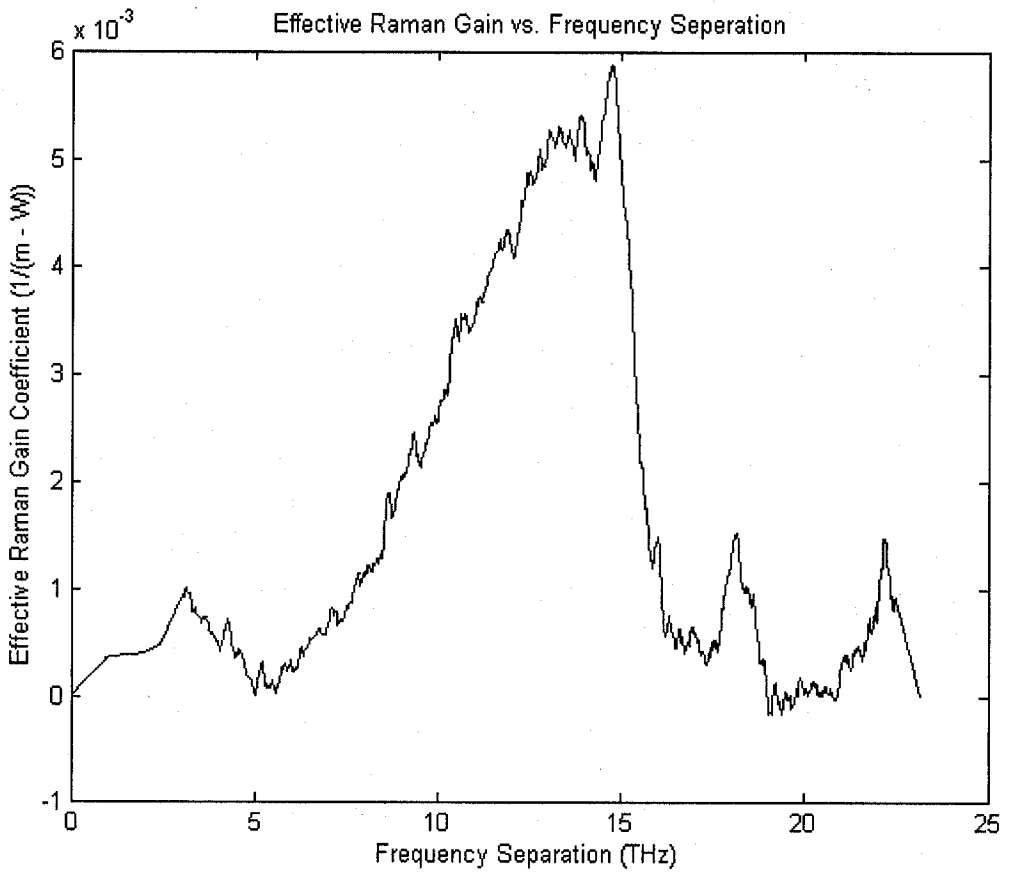

Fig. A-1: Effective Raman gain of the HNLF.

Attenuation Coefficient α:

The attenuation coefficient shown in Fig. A-2 was used, which roughly corresponds to the loss in certain HNLF.

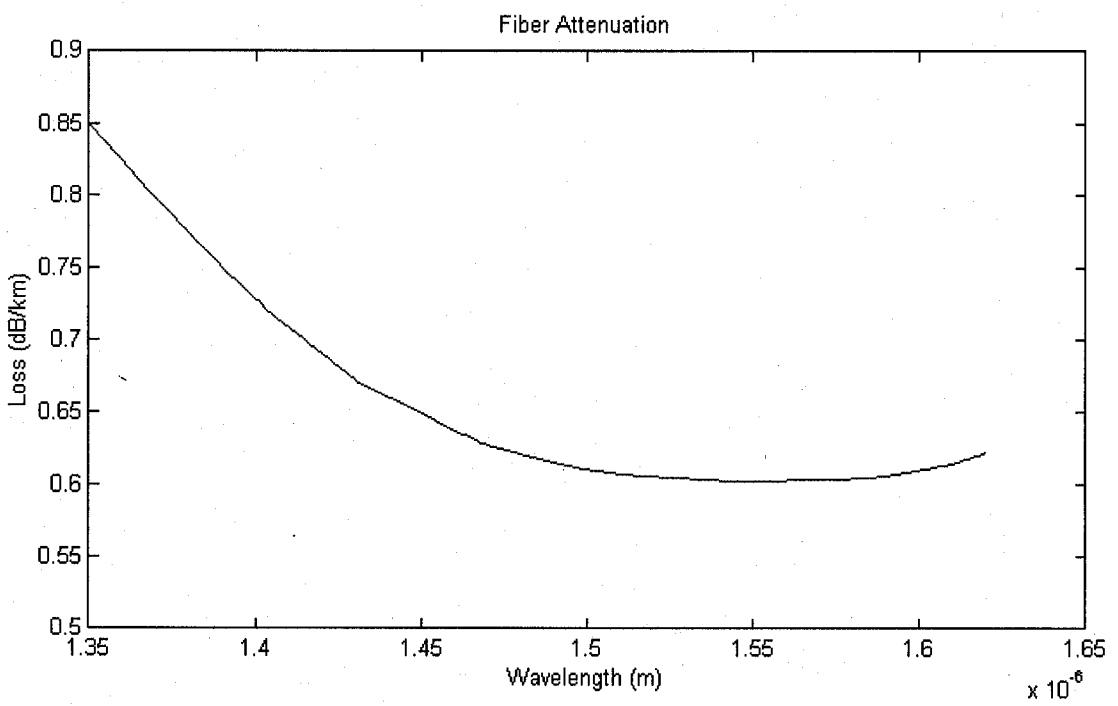

Fig. A-2: Attenuation coefficient of the HNLF

APPENDIX B: Average power analysis

Following [18] but not taking into account the ASE or the Rayleigh scattering, we start from Eq. (2.5) and first reorganize the equations by defining the following terms $A(z,t,\nu)$ and $B(z,t,\nu)$:

$$A(z,t,\nu) = P^{\pm}(z,t,\nu)\sum_{\mu>\nu}\frac{g_R(\nu-\mu)}{K_{eff}A_{eff}}\left[P^{\pm}(z,t,\mu)+P^{\mp}(z,t,\mu)\right]$$

$$B(z,t,\nu) = P^{\pm}(z,t,\nu)\sum_{\mu<\nu}\frac{\nu}{\mu}\frac{g_R(\mu-\nu)}{K_{eff}A_{eff}}\left[P^{\pm}(z,t,\mu)+P^{\mp}(z,t,\mu)\right] \qquad \textbf{Equation B.1}$$

The propagation equations then become

$$\frac{\partial P^{\pm}(z,t,\nu)}{\partial z} \mp \frac{1}{\upsilon_g(\nu)}\frac{\partial P^{\pm}(z,t,\nu)}{\partial t} \qquad \textbf{Equation B.2}$$
$$= \left[\mp\alpha(\nu)+A(z,t,\nu)-B(z,t,\nu)\right]P^{\pm}(z,t,\nu)$$

After dividing the fiber length into N sections of equal size Δz, we split the DFRA round trip into a concatenation of N segments of size Δt, where Δz and Δt are related through $\Delta z = \Delta t \cdot \upsilon_g$. Provided the time step is small enough, a steady-state power distribution can be assumed in Δt as well as in Δz, so that optical powers in each space and time step match the following relations:

$$P^{+}(z_{m+1},t_{n+1},\nu) = P^{+}(z_m,t_n,\nu).G(z_m,t_n,\nu)$$
$$P^{-}(z_{m+1},t_{n+1},\nu) = P^{-}(z_m,t_n,\nu)/G(z_m,t_n,\nu) \qquad \textbf{Equation B.3}$$

where subscripts m and n denote the m^{th} and n^{th} sections of distance and time, respectively, and $G(z_m,t_n,\nu)$ is the step gain within $[z_m, z_{m+1}]$:

$$G(z_m,t_n,\nu) = \exp\left[\left(A(z_m,t_n,\nu) - B(z_m,t_n,\nu) - \alpha(\nu)\right)\Delta z\right] \quad \textbf{Equation B.4}$$

Since we know the power of all the signals at each z at the initial time $t = 0$, we calculate all the powers at the next time step $t = \Delta t$ using equations B.3 and B.4).

At this point, we use the average power analysis to reduce the error implied by the above simple solving method. The first step is to calculate the average powers $\langle P(\nu)\rangle = P_{in}^{\pm}(\nu)(G(\nu)-1)/\ln G(\nu)$ using the powers and the gains obtained for $t = \Delta t$ where $P_{in}^{\pm}(\nu)$ represents the sum of the co-propagative and counter-propagative powers at frequency ν. The second step is to determine the average gain defined as $\overline{G}(\nu)$ by calculating the coefficients $A(z,t,\nu)$ and $B(z,t,\nu)$ using the average powers $\langle P(\nu)\rangle$. We repeat these two steps until the convergence of $\overline{G}(\nu)$. Replacing $G(\nu)$ by $\overline{G}(\nu)$ and using Eq.B.3, we obtain all powers at $t = \Delta t$ for each z. Finally, we integrate from $t = \Delta t$ to $t = 2.\Delta t$ and begin the process over.

Our developed time-domain average power method reduces the calculation time by more than one order of magnitude compared with a RK4 method and the results are within 2%.